

$$\frac{\delta E_{xc}[S]}{\delta S(\vec{r})} = \vartheta_{xc}[S](\vec{r}) \quad F[S] = \min_{\phi \rightarrow S} \langle \phi | \hat{T} + \hat{V}_{ee} | \phi \rangle \quad \frac{\delta E[S]}{\delta S(\vec{r})} = \frac{\delta F[S]}{\delta S(\vec{r})} + \vartheta[S](\vec{r}) = \mu \quad \hat{H}\phi = E\phi \quad E[S] = F[S] + \int d\vec{r} \vartheta(\vec{r}) S(\vec{r}) \quad E_o[\phi] \leq E_o[\tilde{\phi}] = \min_{\tilde{\phi}} \frac{\langle \tilde{\phi} | \hat{H} | \tilde{\phi} \rangle}{\langle \tilde{\phi} | \tilde{\phi} \rangle}$$

This monograph comprises:

- ① An introduction to the electronic structure problem, focused on DFT
- ② An introduction to the strictly correlated electrons concept
- ③ Discussion of functional approximations by interpolations on the *local* energy density
"Energy densities in the strong-interaction limit of density functional theory"
A. Mirtschink, M. Seidl and P. Gori-Giorgi, J. Chem. Theory Comput. **8**, 3097 (2012)
- ④ An Introduction to the KS-SCE method and pilot applications to model quantum wires and model chemical systems
"Kohn-Sham density functional theory for quantum wires in arbitrary correlation regimes"
F. Malet, A. Mirtschink et al., Phys. Rev. B **87**, 115146 (2013)
- ⑤ "Exchange-correlation functionals from the strongly interacting limit of DFT: Applications to model chemical systems"
F. Malet, A. Mirtschink et al., Phys. Chem. Chem. Phys. **16**, 14551 (2014)
- ⑥ Investigations on the derivative discontinuity of the SCE functional
"The derivative discontinuity in the strong-interaction limit of density functional theory"
A. Mirtschink, M. Seidl and P. Gori-Giorgi, Phys. Rev. Lett. **111**, 126402 (2013)
- ⑦ Pilot applications of the SCE functional to the Hydrogen anion
"Energy density functionals from the strong-coupling limit applied to the anions of the He isoelectronic series"
A. Mirtschink, C.J. Umrigar, J.D. Moragan III and P. Gori-Giorgi, J. Chem. Phys. **140**, 18A532 (2014)

Energy Density Functionals From the Strong-Interaction Limit of DFT

André Mirtschink

Energy Density Functionals From the Strong-Interaction Limit of Density Functional Theory

Dissertation Thesis

$$\omega_{\infty}[S](\vec{r}) = \frac{1}{Z} \sum_{k=2}^N \frac{1}{|\vec{r} - \vec{f}_k(\vec{r})|} - \vartheta_H(\vec{r}) \quad E_{xc}[S] = \int_0^1 d\lambda \langle \phi_\lambda[S] | \hat{V}_{ee} | \phi_\lambda[S] \rangle - U[S]$$

$$F[S] \approx V_{ee}^{SCE}[S] \left[-\frac{1}{Z} \nabla_r^2 - \frac{z-N+1}{r} + O\left(\frac{1}{r^4}\right) \right] \sqrt{S(r)} = 0 \quad E_{xc}[S] = \int_0^1 d\lambda \int d\vec{r} S(\vec{r}) \omega_\lambda[S](\vec{r})$$

$$\sum_i^{\text{occ}} |\psi_i(\vec{r})|^2 \quad E_{xc}[S] = \frac{1}{Z} \iint d\vec{r}_1 d\vec{r}_2 \frac{S(\vec{r}_1) \hat{V}_{xc}(\vec{r}_1, \vec{r}_2)}{|\vec{r}_1 - \vec{r}_2|}$$

$$\min_{\phi \rightarrow S} \langle \phi | \hat{T} + \hat{V}_{ee} | \phi \rangle \approx \min_{\phi \rightarrow S} \langle \phi | \hat{T} | \phi \rangle + \min_{\phi \rightarrow S} \langle \phi | \hat{V}_{ee} | \phi \rangle$$

$$F[S] = T_S[S] + U[S] + E_{xc}[S] \quad F_\lambda[S] = \min_{\phi \rightarrow S} \langle \phi | \hat{T} + \lambda \hat{V}_{ee} | \phi \rangle \quad \forall \lambda \in \mathbb{R}$$

$$\frac{\delta V_{ee}^{SCE}[S]}{\delta S(\vec{r})} = \tilde{\vartheta}_{SCE}[S](\vec{r}) \quad \omega_\infty^b(\vec{r}) = \frac{1}{N} \sum_i^N \omega_\infty^a(\vec{f}_i(\vec{r})) \quad \hat{H} = -\frac{1}{2} \nabla_r^2 - \frac{1}{Z} \nabla_r^2 - \frac{z}{r_1} - \frac{z}{r_2} + \frac{1}{r_{12}}$$

$$f_i(r) = \begin{cases} N_e^{-1} [N_e(r) + 2i - Z] & i < \tilde{a}_{N+\eta-2i+2} \\ N_e^{-1} [N_e(r) - 2N + 2i - 4] & i > \tilde{a}_{N-\eta-2i+4} \\ \infty & \text{else} \end{cases}$$

$$\nabla \tilde{\vartheta}_{SCE}(\vec{r}) = \sum_{i=1}^N \frac{\vec{r} - \vec{f}_i(\vec{r})}{|\vec{r} - \vec{f}_i(\vec{r})|^3}$$

$$-\frac{1}{2} \nabla_r^2 + \omega_{ext}(\vec{r}) + \tilde{\vartheta}_{SCE}[S](\vec{r}) \quad \psi_i(\vec{r}) = E_i \psi_i(\vec{r})$$

$$E_{Hxc}[S] \approx V_{ee}^{SCE}[S] + 2 V_{ee}^{ZPE}[S]$$

$$\omega_{CT}^{SCE} \approx -E_{HOMO}^H + E_{HOMO}^{H,SCE} - \frac{1}{R}$$

Energy Density Functionals From the Strong-Interaction Limit of Density Functional Theory

André Měrćink

Dissertation Thesis

ISBN: 978-94-6259-503-3

DOI: 10.6084/m9.figshare.1254927

Printed copies are available on request at the Department of Theoretical Chemistry,
VU University Amsterdam.

This work was carried out in the Department of Theoretical Chemistry at the VU University Amsterdam, De Boelelaan 1083, 1081 HV Amsterdam. Financial support was provided by the Council for Chemical Sciences of the Netherlands Organization for Scientific Research (CW-NWO).



④ Anti-Copyright! Reprint freely, in any manner desired, even without naming the source (well, but please support my citation record if you publish in scientific journals).

Printed 2014, by PrintPartners Ipskamp, Enschede.

VRIJE UNIVERSITEIT

Energy Density Functionals From the Strong-Interaction Limit of Density Functional Theory

ACADEMISCH PROEFSCHRIFT

ter verkrijging van de graad Doctor aan
de Vrije Universiteit Amsterdam,
op gezag van de rector magnificus
prof.dr. F.A. van der Duyn Schouten,
in het openbaar te verdedigen
ten overstaan van de promotiecommissie
van de Faculteit der Exacte Wetenschappen
op donderdag 29 januari 2015 om 15.45 uur
in de aula van de universiteit,
De Boelelaan 1105

door

André Peter Mirtschink
geboren te Räckelwitz, Duitsland

Promotor: prof.dr. E.J. Baerends
Copromotor: dr. P. Gori-Giorgi
Beoordelingscommissie: prof.dr. T. Helgaker
dr. A. Savin
prof.dr. A. Rubio
prof.dr. L. Visscher
prof.dr. R. van Leeuwen
prof.dr. K. Pernal

to everyone supporting me

Contents

1	Introduction	1
2	Electronic Structure Problem	5
2.1	Basic concepts	5
2.1.1	Quantum mechanical description of atomic matter	5
2.1.2	Approximate wavefunction methods	6
2.1.3	Energy functionals for density matrices	7
2.2	Density functional theory	8
2.2.1	Formulation of Hohenberg and Kohn	8
2.2.2	Kohn-Sham non-interacting reference system	9
2.2.3	Adiabatic connection	11
2.2.4	Traditional exchange-correlation approximations	13
2.2.5	Spin-density functional theory	14
2.2.6	Deficiencies of density functional approximations	15
2.2.7	Approximate functionals from the adiabatic connection	17
3	Strong-Interaction Limit of Density Functional Theory	19
3.1	Strictly correlated electrons	19
3.2	Co-motion functions for quasi-one-dimensional densities	24
3.3	Models for the strong-interaction limit	27
4	Energy Densities in the Strong-Interaction Limit of Density Functional Theory	31
<i>A. Mirtschink, M. Seidl and P. Gori-Giorgi, J. Chem. Theory Comput. 8, 3097 (2012)</i>		
4.1	An overview	31
4.2	Energy density: definitions	33
4.3	Energy densities for atoms	36
4.4	Energy densities for Hooke's atom	36
4.5	Local assessment of the point-charge-plus-continuum model in atoms .	40
4.6	Examination of the local Lieb-Oxford bound	43
4.7	Conclusions	46

5 Kohn-Sham Density Functional Theory With Exchange-Correlation Functionals From the Strong-Interaction Limit	47
<i>F. Malet, A. Mirtschink et al., Phys. Rev. B</i> 87 , 115146 (2013)	
<i>F. Malet, A. Mirtschink et al., Phys. Chem. Chem. Phys.</i> 16 , 14551 (2014)	
5.1 Kohn-Sham density functional theory with the strictly correlated electrons functional	47
5.2 Higher-order corrections to zeroth-order KS-SCE	51
5.3 Strong correlation in one-dimensional model quantum wires	52
5.3.1 An overview	52
5.3.2 A quantum wire model in one dimension	54
5.3.3 Supplemental computational approaches	54
5.3.4 KS-SCE treatment of one-dimensional model quantum wires . .	55
5.3.5 Conclusions	62
5.4 Strong correlation in one-dimensional models for elementary chemistry	63
5.4.1 An overview	63
5.4.2 Chemistry models in one dimension	63
5.4.3 Supplemental computational approaches	64
5.4.4 KS-SCE treatment of one-dimensional atoms and ions	64
5.4.5 KS-SCE treatment of the one-dimensional H ₂ molecule	65
5.4.6 Conclusions	69
6 The Derivative Discontinuity in the Strong-Interaction Limit of Density Functional Theory	71
<i>A. Mirtschink, M. Seidl and P. Gori-Giorgi, Phys. Rev. Lett.</i> 111 , 126402 (2013)	
6.1 An overview	71
6.2 Fractional particle numbers in KS-DFT	73
6.3 Extension of the SCE formalism to fractional electron numbers . .	73
6.4 The derivative discontinuity in harmonic external potentials	78
6.5 Conclusions	80
7 Energy Density Functionals From the Strong-Coupling Limit Applied to the Anions of the Helium Isoelectronic Series	81
<i>A. Mirtschink et al., J. Chem. Phys.</i> 140 , 18A532 (2014)	
7.1 An overview	81
7.2 The SCE functional for two electrons	82
7.3 Quantitative corrections to the SCE functional	83
7.4 Accurate results for the anions of the He isoelectronic series . .	85
7.5 SCE functionals for the anions of the He isoelectronic series .	89
7.6 The derivative discontinuity in the Hydrogen nuclear field	95
7.7 Conclusions	97
8 Summary and Outlook	99

Appendix

A PC Cell and Exchange-Correlation Hole for the Homogeneous Electron Gas	103
B KS-SCE Total Energies for Hooke's Atom	105
Samenvatting	107
Acknowledgment	109
List of Publications	111
Bibliography	113

Chapter 1

Introduction

Quantum mechanics plays a significant role in the accurate description of atomic matter. It adequately captures the delicate interplay of electronic quantum effects and particle-particle interactions, decisive for the properties of compounds from atomic scale up to advanced materials. Algorithmic implementations of the many-body Schrödinger equation face the problem that an accurate ground state computation is limited by the overwhelming computational cost inherent to such implementations, and an accurate treatment can only be achieved for systems with electron numbers in the order of hundreds.

A computationally efficient approach that allows for an accurate modeling of compounds with sizeable electron numbers is provided by density functional theory (DFT). A proof that an exact DFT formulation of the electronic structure problem exists was given by Hohenberg and Kohn [1], and present-day approximate implementations have demonstrated their applicability to systems with as much as millions of atoms [2]. Approximations are necessary because of the commonly employed Kohn-Sham (KS) reference system [3] in which non-interacting electrons are used to model the physical system, and all the complicated many-body effects are contained in the effective one-body KS potential. Closed form expressions for the exact potential do not lead to efficient algorithmic solutions, but a huge amount of approximations exists covering many properties of interest.

Strongly correlated systems are notoriously difficult to describe by means of the non-interacting reference system. Drastic corrections in the effective KS potential are needed to accurately account for the dominance of electronic correlation. Traditional approximations do not capture the subtle physics of strong electronic correlation, and issues, *e.g.*, in the correct description of bond-breaking processes and the prediction of conductance properties of Mott insulators arise. Though some remedy is found in the extension of DFT to spin-densities, with spin-density functional theory itself being in principle exact [4], its approximate realization still leads to a false characterization of, *e.g.*, magnetic properties.

In this thesis we follow a rigorous approach to construct the required corrections in the KS potential for the case of strong correlation. After a brief review on the electronic structure problem and its treatment by wavefunction and density matrix

methods in chapter 2, DFT will be considered in more detail. Traditional functional approximations for the exchange and correlation contributions are discussed, along with strategies for the development of improved approximations. This strategies emerge from the *adiabatic connection* of DFT, which provides an exact expression for the exchange-correlation energy in terms of the coupling-constant integrand $W_\lambda[\rho]$. Approximate functionals are obtained from interaction-strength interpolations (ISIs) of the coupling-constant integrand $W_\lambda[\rho]$, which can incorporate the KS system as reference.

Another useful reference system for the ISI is the one of strictly correlated electrons (SCE), which is the strong-interaction analogue of the KS non-interacting reference system. We will present the SCE formulation of the physical problem in chapter 3. In this reference system the electronic interaction dominates over the kinetic energy, and a description of the electrons as point charges is suitable as long as the electronic positions are chosen according to well defined equilibrium conditions that account for the quantum mechanical density. The electrostatic energy of the electrons is then readily computed and can be used as foundation for a new generation of functional approximations. Models for the strong-interaction limit will be discussed in the same chapter, in particular the point-charge plus continuum (PC) model.

A continuation of the ISI idea is introduced in chapter 4. We first review the already available ISI approximations targeting the coupling-constant integrand $W_\lambda[\rho]$ of the adiabatic connection as whole, thus *globally*. We discuss then the size-consistency issues of these functionals, which arise because of the non-linear interpolation models that were employed in their construction, and we devise a *local* strategy to overcome this problems. The main attention of our work is devoted to the study of the quantities that serve as basic input for improved functional approximations, the *local energy densities*. Next to specifying the energy densities of the non-interacting and physical systems, the energy density of the strong-interaction limit is derived, and implications for local ISI models are drawn by evaluating energy densities in different correlation regimes for atoms and quantum dots (Hooke's atoms). Additionally, the local PC model is compared to the SCE reference for an assessment. We also analyze the local version of the Lieb-Oxford bound, which is a condition widely used in the construction of approximate exchange-correlation functionals.

The KS-SCE method that uses a simple linear model for the coupling-constant integrand $W_\lambda[\rho]$ is considered in chapter 5. As was demonstrated in ref. [5], this method is able to capture strong-correlation effects within the single-determinantal KS-DFT without symmetry breaking, thus in a *spin-restricted* formalism. Here we will extend the studies of Malet *et al.* [5] and give a first assessment on the quantitative accuracy of the method. Applications to model quantum wires, where strong correlation plays a significant role, will be presented, and first conclusions on the relevance of the KS-SCE method for chemistry will be drawn from applications to one-dimensional models for atoms, ions and the H₂ bond dissociation. For an improved accuracy of the KS-SCE method in the intermediate-correlation regime curved ISI models are considered at a post-functional level.

In chapter 6 we demonstrate that the KS-SCE approximation correctly exhibits the derivative discontinuity, which is a crucial feature of the exact exchange-correlation functional derived by rigorous arguments, but is missed in traditional functional

approximations. The SCE formalism is extended to fractional particle numbers, and strongly correlated one-dimensional model quantum wires will be studied as well as the three-dimensional low-density Hooke's atom. A correct resemblance of the exact eigenvalue step structure is observed upon continuous variation of the particle number, which is a clear signature of the derivative discontinuity in the SCE functional.

Results for atomic systems will be reported in chapter 7. Though not very extensive – only the Hydrogen anion is considered – the presented analysis serves as first quantitative benchmark for the accuracy of the KS-SCE method in chemical systems, and addresses simultaneously the challenging problem of anion binding in DFT, as traditional functional approximations usually fail to bind the additional electron. Further attention will be payed to corrected SCE functionals that improve the significant underestimation of the total energy of the KS-SCE method in the intermediate-correlation regime. In the corrections the SCE functional is complemented by a local density approximation, and, because of the formal simplicity of the correction, a self-consistent solution of the KS equations is still feasible. To investigate the challenging case of anion binding in approximate DFT in more detail, we examine the phase transition from a bound to an unbound two-electron system by allowing for non-integer nuclear charges. A critical value $Z_{crit} < 1$ is found, which is estimated by very precise wavefunction calculations at $Z_{crit} \approx 0.911029$, and can be compared to predictions of functional approximations.

Chapter 8 summarizes our findings and gives an outlook.

Chapter 2

Electronic Structure Problem

2.1 Basic concepts

2.1.1 Quantum mechanical description of atomic matter

A system of N electrons with velocities well below the speed of light, *i.e.* *non-relativistic*, evolving in the electric field of resting nuclei is accurately described by solutions to the stationary Schrödinger equation

$$\hat{H}\Phi = E\Phi \quad (2.1)$$

that give the energies E and electronic wavefunctions Φ for the ground and excited states of a given system. The Hamiltonian¹ is set by the position and charge of the M nuclei and the number of electrons

$$\begin{aligned} \hat{H} &= \hat{T} + \hat{V}_{ee} + \hat{V}_{en} \\ &= -\sum_i^N \frac{1}{2} \nabla_i^2 + \frac{1}{2} \sum_{j \neq i}^N \frac{1}{|\mathbf{r}_i - \mathbf{r}_j|} - \sum_{a,i}^{M,N} \frac{Z_a}{|\mathbf{R}_a - \mathbf{r}_i|} \end{aligned} \quad (2.2)$$

Because the nuclear positions \mathbf{R} are taken to be fixed (*Born-Oppenheimer approximation*) the electronic wavefunction is a variable of the electronic positions alone $\Phi(\mathbf{r}_1 \dots \mathbf{r}_N)$. To account for the fermionic nature of the electrons an additional *spin* degree of freedom is introduced in the electronic coordinate

$$\Phi(\mathbf{r}_1 \dots \mathbf{r}_N) \rightarrow \Phi(\mathbf{r}_1 \sigma_1 \dots \mathbf{r}_N \sigma_N) \equiv \Phi(\mathbf{x}_1 \dots \mathbf{x}_N) \quad (2.3)$$

such that the wavefunction becomes antisymmetric under coordinate interchange of particles

$$\Phi(\dots \mathbf{x}_i \dots \mathbf{x}_j \dots) = -\Phi(\dots \mathbf{x}_j \dots \mathbf{x}_i \dots) \quad (2.4)$$

¹In Hartree atomic units (a.u.).

2.1.2 Approximate wavefunction methods

In practice, solutions to the Schrödinger equation for many-electron systems ($N \geq 2$) with Hamiltonian (2.2) can only be found approximately. A space of trial wavefunctions is scanned to find an approximate *ground state* wavefunction $\tilde{\Phi}_0$ and energy $E_0[\tilde{\Phi}]$, by minimization of the total energy expression

$$E[\tilde{\Phi}] \equiv \frac{\langle \tilde{\Phi} | \hat{H} | \tilde{\Phi} \rangle}{\langle \tilde{\Phi} | \tilde{\Phi} \rangle} \quad (2.5)$$

and an upper bound to the true ground state energy $E_0[\Phi]$ is obtained

$$E_0[\Phi] \leq E_0[\tilde{\Phi}] = \min_{\tilde{\Phi}} \frac{\langle \tilde{\Phi} | \hat{H} | \tilde{\Phi} \rangle}{\langle \tilde{\Phi} | \tilde{\Phi} \rangle} \quad (2.6)$$

Trial wavefunctions can be as simple as antisymmetrized products of one-particle wavefunctions (*Slater determinant*)

$$\Psi(\mathbf{x}_1, \mathbf{x}_2 \dots \mathbf{x}_N) = \frac{1}{\sqrt{N!}} \begin{vmatrix} \varphi_1(\mathbf{x}_1) & \varphi_2(\mathbf{x}_1) & \dots & \varphi_N(\mathbf{x}_1) \\ \varphi_1(\mathbf{x}_2) & \varphi_2(\mathbf{x}_2) & \dots & \varphi_N(\mathbf{x}_2) \\ \vdots & \vdots & \ddots & \vdots \\ \varphi_1(\mathbf{x}_N) & \varphi_2(\mathbf{x}_N) & \dots & \varphi_N(\mathbf{x}_N) \end{vmatrix} \quad (2.7)$$

with the orbitals $\varphi_i(\mathbf{x}) \equiv \varphi_i(\mathbf{r})\chi_i(\sigma)$ chosen according to the Aufbau principle from the *self-consistent* solution of the effective one-particle Hartree-Fock (HF) equations

$$\left[-\frac{1}{2}\nabla^2 + v_H(\mathbf{r}) + \hat{v}_x(\mathbf{x}) + v_{ext}(\mathbf{r}) \right] \varphi_i(\mathbf{x}) = \varepsilon_i \varphi_i(\mathbf{x}) \quad (2.8)$$

In this equation the effective potential acting on an electron is the sum of the Hartree potential $v_H(\mathbf{r}) = \int d\mathbf{r}' \frac{\rho(\mathbf{r}')}{|\mathbf{r}-\mathbf{r}'|}$, the HF exchange potential defined by its action on an orbital $\hat{v}_x(\mathbf{x})\varphi_i(\mathbf{x}) = -\sum_j^N \delta_{ij}^{\sigma} \int d\mathbf{r}' \frac{\varphi_i^*(\mathbf{r}')\varphi_j(\mathbf{r}')}{|\mathbf{r}-\mathbf{r}'|} \varphi_j(\mathbf{r})$, and the Coulombic external potential exerted by the nuclei $v_{ext}(\mathbf{r}) = -\sum_a^M \frac{Z_a}{|\mathbf{R}_a - \mathbf{r}|}$.

The Slater determinant that minimizes $\langle \Psi | \hat{H} | \Psi \rangle$ yields the HF energy E_{HF} , which is composed of the kinetic energy T , Hartree energy U , exchange energy E_x and electron-nuclear attraction energy E_{en} ²

$$\begin{aligned} E_{HF} &\equiv T + U + E_x + E_{en} \\ &= \sum_i^N \left[-\frac{1}{2} \int d\mathbf{r} \varphi_i^*(\mathbf{r}) \nabla^2 \varphi_i(\mathbf{r}) + \frac{1}{2} \int d\mathbf{r} \varphi_i^*(\mathbf{r}) v_H(\mathbf{r}) \varphi_i(\mathbf{r}) \right. \\ &\quad \left. + \int d\mathbf{x} \varphi_i^*(\mathbf{r}, \sigma) \hat{v}_x(\mathbf{r}, \sigma) \varphi_i(\mathbf{r}, \sigma) + \int d\mathbf{r} \varphi_i^*(\mathbf{r}) v_{ext}(\mathbf{r}) \varphi_i(\mathbf{r}) \right] \end{aligned} \quad (2.9)$$

² $\int d\mathbf{x}$ indicates the integration over spin- and spatial coordinates $\sum_{\sigma} \int d\mathbf{r}$.

A Slater determinant is the formal solution to a Hamiltonian with *non-interacting* electrons. If employed together with the interacting Hamiltonian (2.2), the approximate energy will be in error by the correlation energy, which is defined as the difference of the HF energy with the true ground state energy

$$E_c \equiv E_0[\Phi] - E_{HF}[\Psi] \quad (2.10)$$

Several methods have been developed to capture correlation by the use of trial wavefunctions of increasing complexity. We give an overview with some references to recent reviews on the most relevant methods. For an extensive review see *ref.* [6].

Many-body perturbation theory approaches [7, 8] build up on a perturbation expansion of the exact energy in terms of the ground state of some trial wavefunction and higher order corrections to it. In the configuration-interaction method [9, 10] the true wavefunction is written as a linear combination of the HF ground state Slater determinant and excited determinants, which are obtained from the ground state after one or more occupied HF orbitals have been replaced with unoccupied ones. It can be formally shown that, if all possible excitations are taken into account, the true ground state energy can be reached by variation of the coefficients in the linear combination. This approach, however, is practically cumbersome and the space of excited determinants is truncated. Improved convergence with less excited determinants is achieved by the multi-configuration self-consistent field method [10], where the HF orbitals are optimized along with the coefficients of the configuration-interaction wavefunction. Multi-reference methods [10, 11] are given if next to the ground state Slater determinant as reference for the construction of the excited determinants other references are considered, *e.g.* energetically nearly degenerate states to the ground state.

Because the space of excited determinants in the linear combination of the three former methods is truncated, artifacts arise in the approximate solutions, such as the violation of *size extensivity* [7]. The coupled-cluster methods [12, 13] avoid this problem by expressing the linear combination coefficients of multiple excited determinants in terms of coefficients of less excited determinants. To the methods computational disadvantage a non-variational scheme is obtained.

Explicitly correlated methods [14, 15] differ from the orbital based methods in introducing inter-electronic distances as variables for the electronic wavefunction. Very accurate ground state estimates can be obtained for the cost of solving computationally demanding integrals. Quantum Monte Carlo methods build up on a stochastic sampling of the many-body Schrödinger equation and many different flavors of this method exist, each with their own pros and cons. For a review the reader is referred to *ref.* [16]. Another approach worth mentioning is the density matrix renormalization group method [17, 18].

2.1.3 Energy functionals for density matrices

The energy of a given system can also be written in terms of the two-body reduced density matrix (2-RDM)

$$\gamma_2(\mathbf{x}_1\mathbf{x}_2, \mathbf{x}'_1\mathbf{x}'_2) = N(N-1) \int d\mathbf{x}_3 \dots d\mathbf{x}_N \Phi^*(\mathbf{x}_1 \dots \mathbf{x}_N) \Phi(\mathbf{x}_1 \dots \mathbf{x}_N) \quad (2.11)$$

This is possible because there are at most two-body operators in the Hamiltonian (2.2), and the energy reads

$$E[\gamma_2] = -\frac{1}{2} \int d\mathbf{x} \nabla_{\mathbf{x}'}^2 \gamma_1(\mathbf{x}, \mathbf{x}') \Big|_{\mathbf{x}=\mathbf{x}'} + \frac{1}{2} \iint d\mathbf{x}_1 d\mathbf{x}_2 \frac{P_2(\mathbf{x}_1 \mathbf{x}_2)}{|\mathbf{r}_1 - \mathbf{r}_2|} + \int d\mathbf{r} \rho(\mathbf{r}) v_{ext}(\mathbf{r}) \quad (2.12)$$

where the pair density P_2 , the one-body reduced density matrix (1-RDM) γ_1 , and the electronic density ρ were used, which are related to the 2-RDM

$$\begin{aligned} P_2(\mathbf{x}_1 \mathbf{x}_2) &= \gamma_2(\mathbf{x}_1 \mathbf{x}_2, \mathbf{x}'_1 \mathbf{x}'_2) \Big|_{\mathbf{x}_1=\mathbf{x}'_1, \mathbf{x}_2=\mathbf{x}'_2} \\ \gamma_1(\mathbf{x}, \mathbf{x}') &= \frac{1}{N-1} \int d\mathbf{x}_2 \gamma_2(\mathbf{x} \mathbf{x}_2, \mathbf{x}' \mathbf{x}'_2) \Big|_{\mathbf{x}_2=\mathbf{x}'_2} \\ \rho(\mathbf{r}) &= \sum_{\sigma} \gamma_1(\mathbf{x}, \mathbf{x}') \Big|_{\mathbf{x}=\mathbf{x}'} \end{aligned} \quad (2.13)$$

With the energy expression as functional of the 2-RDM, the N -variable dependent wavefunction can be avoided in the energy minimization (2.5). Complications however arise for the requirement of the minimizing 2-RDM to stem from an N -electron fermionic wavefunction (*N*-representability [19]). Though the conditions on the 2-RDM for *N*-representability are known [20], their enforcement results in computationally demanding approaches relying on semidefinite programming techniques [21, 22]. As resort methods are developed that avoid the explicit confinement of the 2-RDM by parametrization [23], e.g., to post-HF wavefunctions [24], or impose only a subset of the *N*-representability conditions [25–27].

Other alternatives to the wavefunction methods avoid the 2-RDM and build up on the pair density, the 1-RDM, or the electronic density, at the price of introducing an unknown energy functional that needs to be determined. E.g., in pair-density functional theory [28] the *N*-representability conditions for the pair-density are known [29, 30] but essentially impossible to apply, with the additional complication of determining the kinetic energy functional in terms of the pair density [31, 32]. For one-body reduced density matrix functional theory the *N*-representability conditions on the 1-RDM are known [33] and readily enforced, and approximate energy functionals for the electronic interaction were applied to small molecular systems [34–36] and solids [37].

Finally, in density functional theory (DFT) the *N*-representability conditions on the electronic density are easily imposed and vast amounts of approximate energy functionals have been developed. An overview about this method will be given in the next section. A recent review can be found in ref. [38].

2.2 Density functional theory

2.2.1 Formulation of Hohenberg and Kohn

Hohenberg and Kohn have proven that for *non-degenerate* ground states³ there is a unique mapping between a local external potential $\hat{V} = \sum_i^N v(\mathbf{r}_i)$ and its correspond-

³For a straight forward extension to *degenerate* ground states see, e.g., ref. [39].

ing ground state density. Consequently the density can be used to determine the external potential from which it originates. From the external potential the ground state wavefunction can be calculated, and it shows that all properties of a given system can be found by knowledge on its density alone.

This is in particular true for the energy of a system with given density

$$E[\rho] = F[\rho] + \int d\mathbf{r} \rho(\mathbf{r})v(\mathbf{r}) \quad (2.14)$$

where we have separated the energy contributions of the local external potential from the kinetic and electronic interaction contributions. As the treatment of the kinetic energy and electronic repulsion will be the same for any system, the functional form will be independent of the external potential, and $F[\rho]$ is also called the *universal* functional.

The unique mapping of ground state density and external potential can be established for any electronic interaction. If the electronic interaction is the physical one, the external potential will be just the Coulombic field created by the nuclei. In Levy's constrained search formulation [40] the universal functional then writes

$$F[\rho] = \min_{\Phi \rightarrow \rho} \langle \Phi | \hat{T} + \hat{V}_{ee} | \Phi \rangle \quad (2.15)$$

where the minimization is carried out *w.r.t.* all fermionic wave functions Φ that yield a given density $\rho(\mathbf{r})$ and the constraint $\Phi \rightarrow \rho$ will be realized by suitable choice of the external potential, which therefore can be written as functional of the density $v(\mathbf{r}) \rightarrow v[\rho](\mathbf{r})$.

Because of the variational properties of the functional (2.14) the ground state density results from the solution of the Euler-Lagrange equation

$$\frac{\delta E[\rho]}{\delta \rho(\mathbf{r})} = \frac{\delta F[\rho]}{\delta \rho(\mathbf{r})} + v[\rho](\mathbf{r}) = \mu \quad (2.16)$$

where the Lagrange multiplier μ enters to assure the proper density normalization $\int d\mathbf{r} \rho(\mathbf{r}) = N$.

2.2.2 Kohn-Sham non-interacting reference system

Kohn and Sham [3] were the first to consider the non-interacting reference system for the calculation of the physical ground state density. They define the functional $T_s[\rho]$ as the minimum kinetic energy of non-interacting electrons, whereby the wavefunction is constrained to yield a given density

$$T_s[\rho] \equiv \min_{\Psi \rightarrow \rho} \langle \Psi | \hat{T} | \Psi \rangle \quad (2.17)$$

Here we have considered that, for the case of a non-degenerate ground state, the minimizing wavefunction becomes a Slater determinant $\Phi \rightarrow \Psi$.

According to the HK theorems there exists a unique local potential that will account for the density constraint $\Psi \rightarrow \rho$. This potential will be the effective Kohn-Sham

(KS) potential $v_s[\rho](\mathbf{r})$ that enters the Euler-Lagrange equation for T_s as Lagrange multiplier

$$\frac{\delta E[\rho]}{\delta \rho(\mathbf{r})} = \frac{\delta T_s[\rho]}{\delta \rho(\mathbf{r})} + v_s[\rho](\mathbf{r}) = \mu \quad (2.18)$$

It consists of the external potential v_{ext} , and a complementary contribution to model the electronic interactions of the physical system in the non-interacting reference system

$$v_s(\mathbf{r}) \equiv v_{ext}(\mathbf{r}) + v_{Hxc}[\rho](\mathbf{r}) \equiv v_{ext}(\mathbf{r}) + v_H[\rho](\mathbf{r}) + v_{xc}[\rho](\mathbf{r}) \quad (2.19)$$

The electronic interaction part is commonly referred to as Hartree-exchange-correlation. The Hartree-exchange-correlation energy can be defined as remainder of the universal functional $F[\rho]$ after subtraction of $T_s[\rho]$

$$F[\rho] - T_s[\rho] \equiv E_{Hxc}[\rho] \equiv U[\rho] + E_{xc}[\rho] \quad (2.20)$$

and the exchange-correlation energy will consist of kinetic and interaction contributions

$$E_{xc}[\rho] = \langle \Phi | \hat{T} | \Phi \rangle - \langle \Psi | \hat{T} | \Psi \rangle + \langle \Phi | \hat{V}_{ee} | \Phi \rangle - U[\rho] \quad (2.21)$$

With the definition of the universal functional according to (2.20) the physical ground state energy will be obtained after the electron-nuclei attraction energy is added

$$E[\rho] = T_s[\rho] + E_{Hxc}[\rho] + \int d\mathbf{r} \rho(\mathbf{r}) v_{ext}(\mathbf{r}) \quad (2.22)$$

and the functional derivative of $E_{Hxc}[\rho]$ will be related to the potential $v_{Hxc}[\rho](\mathbf{r})$ as can be seen from (2.16)

$$\frac{\delta E_{Hxc}[\rho]}{\delta \rho(\mathbf{r})} = v_{Hxc}[\rho](\mathbf{r}) \quad (2.23)$$

Because of the Slater determinant that minimizes the non-interacting kinetic energy functional $T_s[\rho]$ (2.17), the N -representability conditions on the density are fulfilled by construction [41]. The electronic density is then simply given by the orbitals

$$\rho(\mathbf{r}) = \sum_i^{occ} |\varphi_i(\mathbf{r})|^2 \quad (2.24)$$

where the orbitals are the solutions to the single-particle KS equations

$$\left[-\frac{1}{2} \nabla^2 + v_s[\rho](\mathbf{r}) \right] \varphi_i(\mathbf{r}) = \varepsilon_i \varphi_i(\mathbf{r}) \quad (2.25)$$

which follow from the total energy (2.22) if variations w.r.t. the orbitals are undertaken with the constraint of ortho-normalized orbitals. As the density depends on the

solutions of the KS equations via the orbitals, and also defines the KS potential that enters the KS equations, solutions to the KS equations are found in a self-consistent procedure.

KS-DFT is in principle an exact theory, mapping the ground state energy and density of an interacting many-electron system into a problem of non-interacting electrons moving in the effective KS potential. In practice, KS-DFT relies on approximations for the exchange-correlation functional.

2.2.3 Adiabatic connection

An exact expression for the KS exchange-correlation functional is provided by the adiabatic connection framework of DFT [42–44]. In the *linear* adiabatic connection an interaction-strength scaled functional is introduced

$$F_\lambda[\rho] = \min_{\Phi \rightarrow \rho} \langle \Phi | \hat{T} + \lambda \hat{V}_{ee} | \Phi \rangle \quad \forall \lambda \in \mathbb{R} \quad (2.26)$$

that yields the universal functional $F[\rho]$ (2.15) at physical interaction strength $\lambda = 1$, and the KS non-interacting functional $T_s[\rho]$ (2.17) in the weak-interaction limit $\lambda = 0$. For the strong-interaction limit $\lambda \rightarrow \infty$ a reference system of *strictly correlated electrons* (SCE) can be established, which will be introduced in the next chapter of this thesis.

As denoted in the general functional (2.26), the minimizing wavefunction $\Phi_\lambda[\rho]$ is constrained at all coupling strengths to the same density, typically the physical one. With such $\Phi_\lambda[\rho]$ for all systems that connect the non-interacting with the physical $0 \leq \lambda \leq 1$, the exact Hartree-exchange-correlation energy is obtained from the coupling-constant integration

$$E_{Hxc}[\rho] = \int_0^1 d\lambda \langle \Phi_\lambda[\rho] | \hat{V}_{ee} | \Phi_\lambda[\rho] \rangle = \int_0^1 d\lambda V_{ee}^\lambda[\rho] \quad (2.27)$$

The exchange-correlation energy alone is given from the indirect part of the electrostatic interaction energy $W_\lambda[\rho]$, because the Hartree energy is the same for every λ

$$E_{xc}[\rho] = \int_0^1 d\lambda \langle \Phi_\lambda[\rho] | \hat{V}_{ee} | \Phi_\lambda[\rho] \rangle - U[\rho] = \int_0^1 d\lambda W_\lambda[\rho] \quad (2.28)$$

A schematic illustration of the above expression is given in figure 2.1.

Approximations to the coupling-strength integrand $W_\lambda[\rho]$ can be attempted for accurate, yet efficient, exchange-correlation functional approximations. A review on approximations that follow this strategy will be given in section 2.2.7. The functional approximations that are presented in this work will also be constructed by the use of the adiabatic connection. Other functional approximations, which do not use the coupling-strength integration explicitly, will be discussed in the next sections. Functional approximations that build up on the adiabatic connection can also be validated, if compared to reference calculations with wavefunction methods [45, 46].

One can relate the rigorous energy expression in terms of the density matrices (2.12) to the exchange-correlation energy $E_{xc}[\rho]$. Therefore define the exchange-correlation hole from the density matrices for all auxiliary systems connecting the

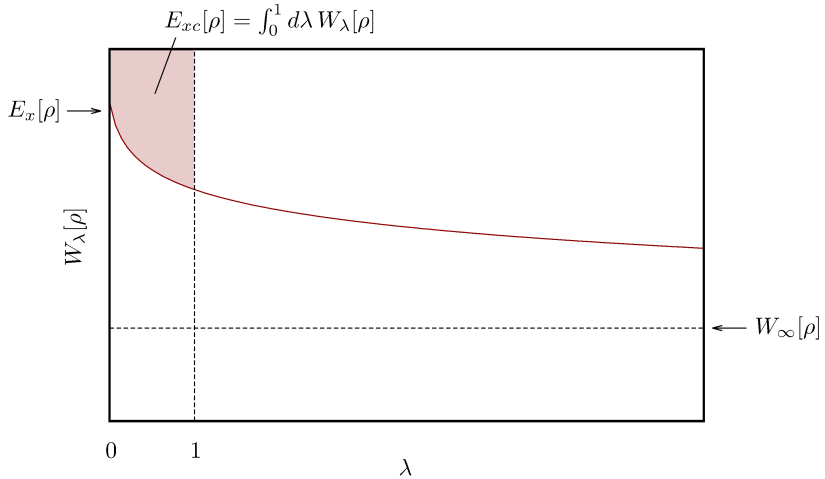


Figure 2.1: Schematic representation of the coupling-constant integration $E_{xc}[\rho] = \int_0^1 d\lambda W_\lambda[\rho]$ for a given density. The exact-exchange energy $E_x[\rho] = \langle \Psi[\rho] | \hat{V}_{ee} | \Psi[\rho] \rangle - U[\rho]$ with the KS orbitals is recovered in the limit $\lambda = 0$, and $W_\infty[\rho] = V_{ee}^{SCE}[\rho] - U[\rho]$ can be obtained from the strong-interacting reference system $\lambda \rightarrow \infty$, cf. chapter 3.1.

non-interacting reference system with the physical system

$$h_{xc}^\lambda(\mathbf{r}_1, \mathbf{r}_2) = \sum_{\sigma_1 \sigma_2} \frac{P_2^\lambda(\mathbf{x}_1 \mathbf{x}_2)}{\rho(\mathbf{r}_1)} - \rho(\mathbf{r}_2) \quad (2.29)$$

Averaging the hole over all auxiliary systems

$$\bar{h}_{xc}(\mathbf{r}_1, \mathbf{r}_2) = \int_0^1 d\lambda h_{xc}^\lambda(\mathbf{r}_1, \mathbf{r}_2) \quad (2.30)$$

yields the exchange-correlation energy in terms of the averaged exchange-correlation hole

$$E_{xc}[\rho] = \frac{1}{2} \iint d\mathbf{r}_1 d\mathbf{r}_2 \frac{\rho(\mathbf{r}_1) \bar{h}_{xc}(\mathbf{r}_1, \mathbf{r}_2)}{|\mathbf{r}_1 - \mathbf{r}_2|} \quad (2.31)$$

The exchange-correlation hole allows for a transparent physical interpretation of the exchange and correlation corrections. Next to the self-interaction correction, which has to be subtracted from the Hartree energy and potential, the Pauli repulsion effects of spin-like electrons are taken into account by creating the exchange hole h_x^λ around a reference electron. Coulomb repulsion effects for opposite-spin electrons beyond the Hartree mean-field description are embodied in the correlation hole h_c^λ . Averaging over the holes of all auxiliary systems gives finally rise to the correlation correction to the non-interacting kinetic energy.

2.2.4 Traditional exchange-correlation approximations

We give an overview of the most established approximate exchange-correlation functionals that do not use the coupling-constant integration explicitly in their construction.

The computationally simplest approximation is given by the local density approximation (LDA) [3]. In the LDA $E_{xc}[\rho]$ is rewritten as integral in space

$$E_{xc}[\rho] = \int d\mathbf{r} \rho(\mathbf{r}) \epsilon_{xc}[\rho](\mathbf{r}) \quad (2.32)$$

with $\epsilon_{xc}[\rho](\mathbf{r})$ a local exchange-correlation energy per particle (energy density) as functional of the overall density. $\epsilon_{xc}[\rho](\mathbf{r})$ is not unique but subject to gauge freedom⁴. Further on, the functional dependence of $\epsilon_{xc}[\rho](\mathbf{r})$ is replaced by the dependence on the local density alone

$$\epsilon_{xc}[\rho](\mathbf{r}) \approx \epsilon_{xc}^{LDA}(\rho(\mathbf{r})) \quad (2.33)$$

An approximate evaluation of the energy density for some, in general inhomogeneous, system is then accomplished by estimating it from the homogeneous electron gas (HEG) of density $\rho_0 = \rho(\mathbf{r})$

$$\epsilon_{xc}^{LDA}(\rho(\mathbf{r})) \approx \epsilon_{xc}^{HEG}(\rho_0)|_{\rho_0=\rho(\mathbf{r})} \quad (2.34)$$

for which analytic expressions can be found [4, 47–50]. The LDA is very successful in the treatment of extended systems as encountered in solid state physics. In chemistry, however, its success is limited as in the finite systems treated here, inhomogeneities in the electronic density prevail.

To account for inhomogeneities, the LDA is refined by recourse to the slowly varying electron gas (SVEG). Analytic expressions for the SVEG energy density are obtained from perturbation expansions for the HEG, and as a result the energy density becomes additionally a function of the local density gradient $\nabla\rho(\mathbf{r})$ for perturbation expansions carried out to second order. The gradient expansion approximation (GEA) $\epsilon_{xc}^{GEA}(\rho(\mathbf{r}), \nabla\rho(\mathbf{r}))$ [51] follows, but an improvement over the LDA is not observed. This can be attributed to the averaged exchange-correlation hole \bar{h}_{xc} . Carrying out a gradient expansion for the exact averaged exchange-correlation hole [52–55] shows that by the GEA an improved sampling of the short range part of the spherically averaged hole $\bar{h}_{xc}(\mathbf{r}, \mathbf{r} + |\mathbf{u}|), |\mathbf{u}| \rightarrow 0$ is achieved, but the long range part $|\mathbf{u}| \rightarrow \infty$ is considerably worsened. As a consequence the sum rule of the exchange-correlation hole is violated $\int d\mathbf{r} \bar{h}_{xc}(\mathbf{r}) \neq 1$. Recently, it has also been realized, that a different gradient expansion applies in classically forbidden regions [56]. Hence, corrections in the long range domain of the energy density are introduced, and the generalized gradient approximation (GGA) is obtained $\epsilon_{xc}^{GGA}(\rho(\mathbf{r}), \nabla\rho(\mathbf{r}))$ [51, 53, 57–63] allowing for an accurate description of a wide variety of chemical systems.

Further accounting of inhomogeneities is achieved by an extension of the SVEG perturbation expansion to fourth order, and a dependence on the local Laplacian of

⁴Adding any functional of the density that integrates to zero will change the energy density locally, but not the integrated value.

the density $\nabla^2\rho(\mathbf{r})$ arises [64, 65]. However, more significant corrections are required for the self-interaction error present in the functional approximations from above. Such error arises, e.g., for one-electron densities where $E_{xc}[\rho]$ is required to yield $-U[\rho]$, as for one-electron systems the electronic interaction contributions should vanish and the kinetic energy is exactly described by T_s – a condition not satisfied by the already presented functionals. One-electron regions in electronic systems can be identified by the use of the local kinetic energy density $\tau(\mathbf{r}) = \sum_i |\nabla\varphi_i(\mathbf{r})|^2$ [66]. Functionals depending on the density Laplacian and/or the kinetic energy density are categorized as metaGGA functionals $\epsilon_{xc}^{metaGGA}(\rho(\mathbf{r}), \nabla\rho(\mathbf{r}), \nabla^2\rho(\mathbf{r}), \tau(\mathbf{r}))$ [67–73].

To complete this brief overview about traditional density functional approximations, we mention that the *non-local* HF exchange can be transformed into a *local* potential via the optimized effective potential method [74–77], yielding the well defined orbital-dependent exact exchange functional [78]. A self-interaction free functional is obtained and solely the correlation components remain to be determined. Correlation in the exact exchange functional can be included via the random phase approximation with the additional complication that unoccupied orbitals have to be taken into account [79, 80]. If HF exchange is combined with GGA or metaGGA exchange and correlation, hybrid functionals are obtained [81–83]. Double hybrids result from additional inclusion of correlation of second-order perturbation theory (and thereby again by inclusion of unoccupied orbitals) [84–87]. As in this hybrids the non-local HF exchange is usually not transformed into a local potential, a generalized KS framework to non-local potentials is invoked [3].

Though successful in very many cases, traditional density functional approximations (DFAs) still have severe deficiencies that hamper their overall usefulness [38, 88, 89]. Some problematic examples will be given in section 2.2.6. A resolution, at least in some respects, can be found by extending the density functionals to spin-densities.

2.2.5 Spin-density functional theory

The universal functional $F[\rho]$ can also be defined by the use of spin densities [4, 90], and, e.g., for the KS reference system one can write

$$F[\rho] = T_s[\rho_\uparrow, \rho_\downarrow] + E_{xc}[\rho_\uparrow, \rho_\downarrow] + U[\rho] \quad (2.35)$$

that in its exact form should clearly yield the same ground state as the spin-independent KS functional (2.22)

$$T_s[\rho_\uparrow, \rho_\downarrow] + E_{xc}[\rho_\uparrow, \rho_\downarrow] = T_s[\rho] + E_{xc}[\rho] \quad (2.36)$$

In the case of approximations the increased variational freedom in the energy minimization can lead to improved ground state estimates.

Practical implementations solve the *unrestricted* KS equations for the KS spin orbitals

$$\left[-\frac{1}{2}\nabla^2 + v_s[\rho_\uparrow, \rho_\downarrow](\mathbf{r}, \sigma) \right] \varphi_i(\mathbf{r}, \sigma) = \varepsilon_{i,\sigma} \varphi_i(\mathbf{r}, \sigma) \quad (2.37)$$

with the spin-dependent KS potential

$$v_s[\rho_\uparrow, \rho_\downarrow](\mathbf{r}, \sigma) = v_{ext}(\mathbf{r}, \sigma) + v_H[\rho](\mathbf{r}) + v_{xc}[\rho_\uparrow, \rho_\downarrow](\mathbf{r}, \sigma) \quad (2.38)$$

and the exchange-correlation potential obtained from the exchange-correlation energy by the derivative w.r.t. the spin density

$$\frac{\delta E_{xc}[\rho_\uparrow, \rho_\downarrow]}{\delta \rho_\sigma(\mathbf{r})} = v_{xc}[\rho_\uparrow, \rho_\downarrow](\mathbf{r}, \sigma) \quad (2.39)$$

The overall density results from the spin densities, that are themselves related to the KS spin orbitals

$$\begin{aligned} \rho(\mathbf{r}) &= \rho_\uparrow(\mathbf{r}) + \rho_\downarrow(\mathbf{r}) \\ &= \sum_i^{N_\uparrow} |\varphi_i(\mathbf{r}, \uparrow)|^2 + \sum_i^{N_\downarrow} |\varphi_i(\mathbf{r}, \downarrow)|^2 \end{aligned} \quad (2.40)$$

To benefit from the increased variational freedom in the approximate case, the approximations have to be extended to spin-densities. Therefore, e.g., in the LDA exchange-correlation functional (2.34) a local approximation can be evaluated from the homogeneous spin-polarized electron gas and the local spin-density approximation (LSDA) is obtained

$$\epsilon_{xc}^{LSDA}(\rho_\uparrow(\mathbf{r}), \rho_\downarrow(\mathbf{r})) \approx \epsilon_{xc}^{HEG}(\rho_{0\uparrow}, \rho_{0\downarrow}) \Big|_{\rho_{0\uparrow}=\rho_\uparrow(\mathbf{r}), \rho_{0\downarrow}=\rho_\downarrow(\mathbf{r})} \quad (2.41)$$

Spin-polarized counterparts of the higher level approximations (GGA, metaGGA) exist as well, and commonly in practice the unrestricted KS equations are solved instead of the restricted ones.

Note that in the external potential $v_{ext}(\mathbf{r}, \sigma)$ of (2.38) a magnetic field can be included, allowing for a variational determination of magnetic properties [91, 92] or the inclusion of relativistic effects [44].

2.2.6 Deficiencies of density functional approximations

As mentioned in section 2.2.4, the intuitive, yet simple, LDA successfully established DFT methods in solid states physics, yielding, e.g., reasonable lattice constants and surface energies for extended systems. When more confined system are considered and inhomogeneities in the electronic density become relevant the LDA falls short, leading to wrong predictions of adsorption energies of molecules on surfaces or overestimation of atomization energies of molecules. The GGA corrections give some improvement, though it has been found that improved adsorption energies come at the price of worse surface energies and vice versa. Similar tendencies are found for atomization energies and equilibrium bond distances, where atomization energies are improved but equilibrium bond distances are underestimated. MetaGGA functionals perform equally well for the mentioned properties, but still show qualitative errors, e.g., for the adsorption sites of CO on Cu, Rh and Pt (111) surfaces [93].

Even more drastic failures arise in the determination of the fundamental conductance gap (being the difference between ionization energy and electron affinity). Though it is well understood that the KS gap between the highest occupied (HOMO) and lowest unoccupied (LUMO) eigenvalues can only be taken as an estimate for the optical gap, the fundamental gap can be accessed within KS-DFT by considering a molecule or large cluster of a material and adding or subtracting electrons to/from it respectively. For the exchange-correlation potential it is then required to be shifted by a constant in the bulk region with otherwise unchanged shape, and the constant shift has to vanish when the bulk region is left [94]. Such a behavior is not covered by traditional functionals, having consequences for the charge transport description in insulators, semiconductor nanostructures and molecular wires. Long-range charge transfer excitations in molecules or dissociating heterogeneous chemical bonds are also notoriously difficult to describe. The constant shift is commonly referred to as derivative discontinuity and will be considered in more detail in chapter 6 of this thesis.

Some remedy is provided in the generalized KS framework when hybrid functionals with some portion of HF exchange are used. *E.g.*, the B3LYP functional [49, 61, 82, 95], being the most popular hybrid functional in the chemistry community, gives striking atomization energies close to chemical accuracy ($\approx 4 \text{ kcal mol}^{-1}$) and good equilibrium geometries, but still lacks the derivative discontinuity. Nevertheless, as due to the inclusion of HF exchange the HOMO-LUMO gap is opened⁵, some improvement might be expected. Though care has to be taken, because a clear distinction between optical and fundamental gap is not possible anymore. Another drawback of the B3LYP functional is its limited scope to molecular systems, as the empirical parameters that define this functionals derive by fitting to a molecular benchmark set and are not transferable to solids. In solids the HSE functional [96] is employed but is unsatisfactory for the adsorption properties as discussed in the first paragraph of this section.

The above considerations show that the DFAs are not universally applicable, but often a specific functional will be appropriate for the property of interest. Strongly correlated systems, in which a degenerate or nearly degenerate ground state occurs, are overall difficult to deal with for any DFA within the single-determinant KS scheme. This is given, *e.g.*, in the case of Mott insulators, which exhibit a vanishing optical gap but finite conductance gap, and issues in the simulation of charge transport arise. Homogeneous bond stretching in such simple molecules as H_2 poses another issue that can be partially dealt with by spin-DFT. However, the usual (semi-)local approximations lead to a wrong characterization of the magnetic properties as the unphysical broken spin-symmetry solution is favored. Rearrangement of electrons in unsaturated *d* and *f* shells, as present in transition metals and Actinides, poses another challenge for present DFAs. Functionals for strongly correlated systems in KS-DFT are yet to be devised. Some attempts towards such improved functionals will be presented in this thesis.

⁵In HF theory in contrast to KS theory, the HOMO-LUMO gap corresponds to the fundamental gap.

2.2.7 Approximate functionals from the adiabatic connection

The coupling-constant integration (2.28) serves as excellent starting point for the systematic development of efficient functional approximations when the coupling constant integrand $W_\lambda[\rho]$ is targeted. We review the functionals that emerge along the lines of the adiabatic connection.

Pioneering attempts towards approximate $W_\lambda[\rho]$ build up on the KS non-interacting reference system, and some traditional density functional approximation for F_λ at some intermediate interaction $0 < \lambda \leq 1$. E.g., Becke introduced the half and half functional [81], in which a model is defined assuming a linear dependence of $W_\lambda[\rho]$ on λ . Setting $W_0[\rho]$ equal to exact exchange and $W_1[\rho]$ to LSDA exchange-correlation results in a functional with 50% exact exchange and 50% LSDA exchange-correlation. Further adjustment of the portion of exact exchange by semi-empirical arguments gives rise to hybrid functionals like B3LYP [49, 61, 82, 95]. The adiabatic connection was subsequently used for the construction of non-empirical hybrids in ref. [97], where a model for $W_\lambda[\rho]$ consisting of two intersected straight lines fixed by exact exchange, GGA exchange and GGA exchange-correlation is defined.

However, linear models for the coupling-constant integrand are generally inappropriate and curved models should be used. Therefore the asymptotic expansion of $W_\lambda[\rho]$ in the $\lambda \rightarrow 0$ limit is useful

$$W_{\lambda \rightarrow 0}[\rho] = E_x[\rho] + 2 \lambda E_c^{GL2}[\rho] + O(\lambda^2) \quad (2.42)$$

where $E_c^{GL2}[\rho]$ is the correlation energy given by second-order Görling-Levy perturbation theory (GL2) [98]. Ernzerhof [99] employed a Padé interpolation for the integrand $W_\lambda[\rho]$, with input from exact exchange and GL2 correlation in the weak interaction limit, and GGA exchange-correlation for $\lambda = 1$.

The mentioned models for the integrand (except for B3LYP) share in common that for the physical situation with $\lambda = 1$ DFAs are used, and for the weak interaction limit exact exchange is used. A DFA for exchange alone would introduce errors, as DFA exchange has to be balanced with correlation for error cancellation. At physical interaction DFA exchange is unproblematic, because it is combined with correlation. As error cancellation in DFA exchange-correlation might not be satisfactory, a continuation of the ansatz of Ernzerhof is possible by taking DFA exchange-correlation at some intermediate λ instead of $\lambda = 1$. This would allow to balance the exchange error with the correlation error. Along this lines Mori-Sánchez, Cohen and Yang [100] constructed their MCY1 functional. A Padé interpolation is performed with exact exchange and meta-GGA exchange input in the weak interaction limit and meta-GGA exchange-correlation for an intermediate λ (chosen semi-empirically).

The discussed models clearly outperform the stand alone DFAs they are based on [81, 97, 99, 100]. Nonetheless, employment of DFA quantities in their construction can lead to serious misbehavior in the curvature of the integrand, as demonstrated in ref. [101] by comparison of the MCY1 approximation with accurate quantities along the adiabatic connection (see, e.g., figure 3 in ref. [101]). In the same paper the authors show that accurate exchange-correlation energies can be recovered from interpolations with accurate full-CI ingredients.

An approach that avoids unfavorable DFA bias is the interaction-strength interpolation (ISI) [102–105]. Exact exchange and GL2 from the weak interaction limit are

used, along with information from the strong interaction limit. The λ dependence of $W_\lambda[\rho]$ is then modeled by an interpolation between the two limits. Next to the $\lambda \rightarrow 0$ expansion (2.42), the $\lambda \rightarrow \infty$ expansion of the coupling-constant integrand is invoked for meaningful interpolations

$$W_{\lambda \rightarrow \infty}[\rho] = W_\infty[\rho] + \frac{W'_\infty[\rho]}{\sqrt{\lambda}} + O(\lambda^{-p}) \quad (2.43)$$

with $p \geq 5/4$ [102]. Exact expressions for the functionals $W_\infty[\rho]$ and $W'_\infty[\rho]$ are available within the *strictly correlated electrons* (SCE) formulation or approximately from the *point-charge-plus-continuum* (PC) model, see next chapter. Approximate functionals along the ISI idea will be reviewed in chapter 4 of this thesis.

A *range-separated* adiabatic connection [106–109] can be used to obtain accurate exchange-correlation energies from combinations of DFT with wavefunction theory [110–115]. Especially when applied with multi-determinant wavefunctions, the DFT-wavefunction hybrids are able to capture long-range static correlation effects, as long as a limited number of determinants is involved. As, however, static correlation at short range is of equal importance, the employed DFAs are still crucial for the success of such scheme and are subject to development [116].

Chapter 3

Strong-Interaction Limit of Density Functional Theory

3.1 Strictly correlated electrons

The strong-interaction limit $\lambda \rightarrow \infty$ of the adiabatic connection functional $F_\lambda[\rho]$ (2.26) has first been studied in the seminal work of Seidl *et al.* [103, 104], and later formalized and evaluated exactly in a rigorous mathematical way by Gori-Giorgi *et al.* [102, 117–120]. We give an introduction to the *strictly correlated electrons* (SCE) concept that applies in this limit. For a detailed derivation see ref. [117].

We wish to compute the coupling-constant integrand $W_\lambda[\rho]$ in the strong-interaction limit $\lambda \rightarrow \infty$

$$W_{\lambda \rightarrow \infty}[\rho] = \langle \Phi_\infty[\rho] | \hat{V}_{ee} | \Phi_\infty[\rho] \rangle \equiv V_{ee}^{SCE}[\rho] \quad (3.1)$$

which serves as useful ingredient for interaction-strength interpolations. Therefore we need the minimizing wavefunction $\Phi_\infty[\rho]$ of the general functional $F_\lambda[\rho]$ (2.26)

$$F_\lambda[\rho] = \min_{\Phi_\lambda \rightarrow \rho} \langle \Phi_\lambda | \hat{T} + \lambda \hat{V}_{ee} | \Phi_\lambda \rangle \quad (3.2)$$

where in the $\lambda \rightarrow \infty$ limit the electrostatic energy enters to leading order $\mathcal{O}(\lambda)$ and the kinetic energy to order $\mathcal{O}(\sqrt{\lambda})$ [117]. Hence, the general functional $F_\lambda[\rho]$ in the $\lambda \rightarrow \infty$ limit can be written as

$$F_{\lambda \rightarrow \infty}[\rho] = \min_{\Phi_\lambda \rightarrow \rho} \langle \Phi_\lambda | \lambda \hat{V}_{ee} | \Phi_\lambda \rangle = \lambda \min_{\Phi_\lambda \rightarrow \rho} \langle \Phi_\lambda | \hat{V}_{ee} | \Phi_\lambda \rangle \quad (3.3)$$

In the first minimization of the above equation the external potential $\hat{V}_\lambda = \sum_i^N v_\lambda(\mathbf{r}_i)$ that will compensate for the strong electronic repulsion to account for the density constraint $\Phi \rightarrow \rho$ is to leading order determined by electrostatic contributions similar to the electronic energy, *i.e.* we expect

$$\lim_{\lambda \rightarrow \infty} \frac{v_\lambda[\rho](\mathbf{r})}{\lambda} \equiv v_{SCE}[\rho](\mathbf{r}) \quad (3.4)$$

with $v_{SCE}[\rho](\mathbf{r})$ being a continuous and finite local one-body potential. This allows for a computation of the wavefunction $\Phi_\infty[\rho]$ from the unconstrained minimization problem

$$\min_{\Phi} \langle \Phi | \hat{V}_{ee} + \sum_i^N v_{SCE}[\rho](\mathbf{r}_i) | \Phi \rangle \quad (3.5)$$

which is also equivalent to

$$\min_{\Phi} \int d\mathbf{r}_1 \dots d\mathbf{r}_N |\Phi(\mathbf{r}_1 \dots \mathbf{r}_N)|^2 E_{pot}[\rho](\mathbf{r}_1 \dots \mathbf{r}_N) \quad (3.6)$$

where $|\Phi|^2$ is the N -electron density, and the total potential energy¹ writes

$$\begin{aligned} E_{pot}[\rho](\mathbf{r}_1 \dots \mathbf{r}_N) &\equiv V_{ee} + \sum_i^N v_{SCE}[\rho](\mathbf{r}_i) \\ &= \sum_{j>i}^N \frac{1}{|\mathbf{r}_i - \mathbf{r}_j|} + \sum_i^N v_{SCE}[\rho](\mathbf{r}_i) \end{aligned} \quad (3.7)$$

The minimizing N -electron density $|\Phi_\infty[\rho]|^2$ in (3.6) will be a distribution that is zero everywhere except for positions where $E_{pot}[\rho](\mathbf{r}_1 \dots \mathbf{r}_N)$ reaches its global minimum $(\mathbf{r}_1 \dots \mathbf{r}_N) \in M$, whereby the set of admissible positions is solely determined by the local SCE potential $v_{SCE}[\rho](\mathbf{r})$, $M = M[v_{SCE}]$.

For a quantum mechanical density that is typically smooth the potential v_{SCE} has to be chosen such that the set $M[v_{SCE}]$ is continuous in (at least) three dimensions, i.e. the absolute minimum of the $3N$ -dimensional function E_{pot} needs to be degenerate over an (at least) three dimensional subspace of the total R^{3N} space. This can be written as

$$M = \{[\mathbf{r}, \mathbf{f}_2(\mathbf{r}) \dots \mathbf{f}_N(\mathbf{r})] : \mathbf{r} \in P\} \quad (3.8)$$

with $P \subseteq R^3$ the region where $\rho(\mathbf{r}) \neq 0$. The distribution $|\Phi_\infty|^2$ is correspondingly constructed such that a reference position $\mathbf{r} = \mathbf{r}_1$ can be freely chosen in the space P , and all the positions of the other $N - 1$ electrons are then fixed by the reference positions via the *co-motion* functions

$$\mathbf{r}_i \equiv \mathbf{f}_i[\rho](\mathbf{r}) \quad \forall i \in \{2 \dots N\} \quad (3.9)$$

This defines the strictly correlated electrons (SCE) state $|\Phi_{SCE}|^2$ that is obtained as a superposition of the electronic configurations in $M[v_{SCE}]$

$$\begin{aligned} |\Phi_{SCE}(\mathbf{r}_1 \dots \mathbf{r}_N)|^2 &= \frac{1}{N!} \sum_{\wp} \int d\mathbf{r} \frac{\rho(\mathbf{r})}{N} \delta(\mathbf{r}_1 - \mathbf{f}_{\wp(1)}(\mathbf{r})) \\ &\quad \times \delta(\mathbf{r}_2 - \mathbf{f}_{\wp(2)}(\mathbf{r})) \dots \delta(\mathbf{r}_N - \mathbf{f}_{\wp(N)}(\mathbf{r})) \end{aligned} \quad (3.10)$$

¹It shows that the potential energy (3.7) remains unchanged upon permutation of particles. Hence, the minimizing energy (3.6) is independent of the spin state of the wavefunction and a minimization w.r.t. $|\Phi|^2$ is sufficient to determine the ground state. The spin eigenstate of the wavefunction is readily constructed from the anti-symmetry requirement on the wavefunction [117].

where \wp denotes a permutation of $1 \dots N$. As we will see later the co-motion functions must satisfy special properties to account for the wavefunction constraint $\Phi \rightarrow \rho$. Overall the SCE state can be visualized as “floating Wigner crystal” describing the density ρ .

As mentioned earlier, the local potential $v_{SCE}[\rho](\mathbf{r})$ must compensate the electronic repulsion energy when the electrons are at their respective positions $\mathbf{r}, \mathbf{f}_2(\mathbf{r}) \dots \mathbf{f}_N(\mathbf{r})$. The potential energy E_{pot} of (3.7) will then be minimized

$$\begin{aligned}\nabla_{\mathbf{r}_1} E_{pot}[\rho](\mathbf{r}_1 \dots \mathbf{r}_N)|_{\mathbf{r}_1=\mathbf{r}, \mathbf{r}_2=\mathbf{f}_2(\mathbf{r}) \dots} &= 0 \\ \nabla_{\mathbf{r}_2} E_{pot}[\rho](\mathbf{r}_1 \dots \mathbf{r}_N)|_{\mathbf{r}_1=\mathbf{r}, \mathbf{r}_2=\mathbf{f}_2(\mathbf{r}) \dots} &= 0 \\ &\vdots\end{aligned}\tag{3.11}$$

and from this equilibrium conditions the SCE potential $v_{SCE}[\rho](\mathbf{r})$ follows

$$\begin{aligned}\nabla_{\mathbf{r}_1} v_{SCE}(\mathbf{r}_1)|_{\mathbf{r}_1=\mathbf{r}, \mathbf{r}_2=\mathbf{f}_2(\mathbf{r}) \dots} &= - \sum_{i \neq 1}^N \frac{\mathbf{r} - \mathbf{f}_i(\mathbf{r})}{|\mathbf{r} - \mathbf{f}_i(\mathbf{r})|^3} \\ \nabla_{\mathbf{r}_2} v_{SCE}(\mathbf{r}_2)|_{\mathbf{r}_1=\mathbf{r}, \mathbf{r}_2=\mathbf{f}_2(\mathbf{r}) \dots} &= - \sum_{i \neq 2}^N \frac{\mathbf{f}_2(\mathbf{r}) - \mathbf{f}_i(\mathbf{r})}{|\mathbf{f}_2(\mathbf{r}) - \mathbf{f}_i(\mathbf{r})|^3} \\ &\vdots\end{aligned}\tag{3.12}$$

showing that v_{SCE} also accounts for the compensation of the net Coulombic force on one electron exerted by the other $N - 1$ electrons when all the particles are at their respective positions.

Equations (3.12) are N different equations for the computation of the potential v_{SCE} . We see that they all become equivalent if the co-motion functions obey the group properties

$$\begin{aligned}\mathbf{f}_1(\mathbf{r}) &\equiv \mathbf{r} \\ \mathbf{f}_2(\mathbf{r}) &= \mathbf{f}(\mathbf{r}) \\ \mathbf{f}_3(\mathbf{r}) &= \mathbf{f}(\mathbf{f}(\mathbf{r})) \\ \mathbf{f}_4(\mathbf{r}) &= \mathbf{f}(\mathbf{f}(\mathbf{f}(\mathbf{r}))) \\ &\vdots \\ \underbrace{\mathbf{f}(\mathbf{f}(\dots \mathbf{f}(\mathbf{f}(\mathbf{r}))))}_{N \text{ times}} &= \mathbf{r}\end{aligned}\tag{3.13}$$

which also guarantee the indistinguishability of the electrons.

Eventually, the co-motion functions $\mathbf{f}_i(\mathbf{r})$ within the density constraint have to be specified. Therefore the quantum mechanical interpretation of the density is invoked by demanding that the probability of finding the reference electron at position \mathbf{r} in volume element $d\mathbf{r}$ is equal to finding an other electron at position $\mathbf{f}_i(\mathbf{r})$ in the volume element $d\mathbf{f}_i(\mathbf{r})$

$$\rho(\mathbf{r}) d\mathbf{r} = \rho(\mathbf{f}_i(\mathbf{r})) d\mathbf{f}_i(\mathbf{r}) \quad \forall i \in 2 \dots N\tag{3.14}$$

thus ensuring the invariance of ρ under the coordinate transform $\mathbf{r} \rightarrow \mathbf{f}_i(\mathbf{r})$. If the differential equation (3.7) and the group properties (3.13) are fulfilled, it is easy to verify that SCE N particle density (3.10) yields the required density ρ .

With the SCE state (3.10) the functional $V_{ee}^{SCE}[\rho]$ evaluates according to

$$V_{ee}^{SCE}[\rho] = \int d\mathbf{r} \frac{\rho(\mathbf{r})}{N} \sum_{j>i}^N \frac{1}{|\mathbf{f}_i(\mathbf{r}) - \mathbf{f}_j(\mathbf{r})|} \quad (3.15)$$

It is given in terms of the co-motion functions \mathbf{f}_i , analogous to the Kohn-Sham orbitals φ_i that give $T_s[\rho]$. We see that the possibility of all electrons on top of each other $\mathbf{r} = \mathbf{f}_i(\mathbf{r})$, which is also a solution to the differential equation (3.14) and obeys the group properties (3.13), is excluded, as this would not minimize the energy functional (3.15). Hence, a continuous potential v_{SCE} will be obtained as the first derivative of the potential (3.12) remains finite everywhere in space. An alternative expression for $V_{ee}^{SCE}[\rho]$ will be derived in chapter 4 of this thesis.

With the SCE potential $v_{SCE}[\rho](\mathbf{r})$ obtained by integration from (3.12), we will have that the potential energy (3.7) is minimum when the electronic positions $\mathbf{r}_i \in M[v_{SCE}]$, or, equivalently, when the associated density at each point is equal to $\rho(\mathbf{r})$. This follows by defining an energy density functional for the SCE reference system with potential $v_{SCE}[\rho](\mathbf{r})$, which for an arbitrary density $\tilde{\rho}$ writes

$$E_{tot}^{SCE}[\tilde{\rho}] = V_{ee}^{SCE}[\tilde{\rho}] + \int d\mathbf{r} \tilde{\rho}(\mathbf{r}) v_{SCE}[\rho](\mathbf{r}) \quad (3.16)$$

It will satisfy the stationary condition

$$\left. \frac{\delta E_{tot}^{SCE}[\tilde{\rho}]}{\delta \tilde{\rho}(\mathbf{r})} \right|_{\tilde{\rho}=\rho} = 0 \quad (3.17)$$

i.e. we will have that

$$\left. \frac{\delta V_{ee}^{SCE}[\tilde{\rho}]}{\delta \tilde{\rho}(\mathbf{r})} \right|_{\tilde{\rho}=\rho} = -v_{SCE}[\rho](\mathbf{r}) \quad (3.18)$$

The functional $V_{ee}^{SCE}[\rho] - U[\rho]$ can be identified as the zeroth-order term in the $\lambda \rightarrow \infty$ expansion of the coupling-constant integrand $W_\lambda[\rho]$ (2.43). The next leading term in the series can be given by taking small vibrations of the electrons around their SCE positions into account and is twice the *zero-point energy* (ZPE) [102]

$$W'_\infty[\rho] = 2V_{ee}^{ZPE}[\rho] \quad (3.19)$$

For electrons in D dimensions it is given by

$$V_{ee}^{ZPE}[\rho] = \frac{1}{2} \int d\mathbf{r} \frac{\rho(\mathbf{r})}{N} \sum_i^{D N - D} \frac{\omega_i(\mathbf{r})}{2} \quad (3.20)$$

with $\omega_n(\mathbf{r})$ the zero-point vibrational frequencies around the SCE minimum. They are given by the square root of the eigenvalues of the Hessian matrix that enters the expansion of the SCE potential energy up to second order [102].

The physics of strong correlation encoded in the highly non-local density dependence of the SCE functional does not come for free: the SCE problem is sparse but non-linear, and an algorithm for its evaluation following the original formulation for general three-dimensional densities is still an open problem. Analytic expressions for the co-motion functions $f_i(\mathbf{r})$ for three-dimensional densities of spherical symmetry – and other systems with similar *quasi-one-dimensional* characteristics – will be given in the next section. An enticing route that avoids the co-motion functions involves the mass-transportation-theory reformulation of the SCE functional [120–122], in which $V_{ee}^{SCE}[\rho]$ is given by the maximum of the Kantorovich dual problem

$$V_{ee}^{SCE}[\rho] = \max_u \left\{ \int d\mathbf{r} \rho(\mathbf{r}) u(\mathbf{r}) : \sum_i^N u(\mathbf{r}_i) \leq \sum_{j>i}^N \frac{1}{|\mathbf{r}_i - \mathbf{r}_j|} \right\} \quad (3.21)$$

where $u(\mathbf{r}) = v_{SCE}[\rho](\mathbf{r}) + C$, and C is a constant. This is a maximization under linear constraints that yields at once the functional and its functional derivative. Although the number of linear constraints is infinite, this formulation may lead to approximate but accurate approaches for the construction of $V_{ee}^{SCE}[\rho]$ and v_{SCE} , as shown by Mendl and Lin [123]. However, the procedure is still cumbersome and needs further development. Recently a solution of the SCE problem was demonstrated for H₂ molecular densities [124] that bases on the Monge formulation of the optimal transport problem to determine the co-motion functions. Also here, the employed numerical discretization technique does not allow for a treatment of considerably larger systems. Currently the possibility of the construction of approximate co-motion functions for the diatomic molecules is also explored [125]. Models that derive from the SCE concept and provide approximate expressions for the strong-interaction limit will be introduced in section 3.3.

An alternative density functional framework, based on the study of the strong-interaction limit of the HK functional, was presented in ref. [126]. In this approach the SCE reference system was used instead of the non-interacting one of Kohn and Sham, and the universal functional was defined as

$$F[\rho] = V_{ee}^{SCE}[\rho] + E_{kd}[\rho] \quad (3.22)$$

where the *kinetic-decorrelation* energy $E_{kd}[\rho]$ accounts for the kinetic energy and corrects the correlation estimate of $V_{ee}^{SCE}[\rho]$

$$E_{kd}[\rho] = \langle \Phi_{\lambda=1} | \hat{T} | \Phi_{\lambda=1} \rangle + \langle \Phi_{\lambda=1} | \hat{V}_{ee} | \Phi_{\lambda=1} \rangle - V_{ee}^{SCE}[\rho] \quad (3.23)$$

A linear adiabatic connection for the kinetic energy can be used to obtain an exact expression for the kinetic-decorrelation energy $E_{kd}[\rho]$ [126]. Defining the scaled functional

$$K_\alpha[\rho] = \min_{\Phi \rightarrow \rho} \langle \Phi | \alpha \hat{T} + \hat{V}_{ee} | \Phi \rangle \quad \forall \alpha \in \mathbb{R} \quad (3.24)$$

$E_{kd}[\rho]$ results from the integration

$$E_{kd}[\rho] = \int_0^1 d\alpha \langle \Phi_\alpha[\rho] | \hat{T} | \Phi_\alpha[\rho] \rangle \quad (3.25)$$

where $\Phi_\alpha[\rho]$ is the minimizing wavefunction of the scaled functional $K_\alpha[\rho]$.

The first results obtained with such SCE-DFT neglecting $E_{kd}[\rho]$ showed its ability to describe systems in the extreme strongly correlated regime with a much better accuracy than standard KS-DFT [118, 126]. On the downside, SCE-DFT fails as soon as the fermionic nature of the electrons plays a significant role [118]. Functionals for the kinetic energy and correlation correction should therefore be developed. Furthermore, the formalism lacks some of the appealing properties of the Kohn-Sham approach, such as its capability to predict (at least in principle) exact ionization energies. Also crucial concepts widely employed in chemistry and solid state physics, like the Kohn-Sham orbitals and orbital energies, are totally absent in SCE-DFT. In chapter 5 of this thesis, a combination of the KS and SCE frameworks will be presented, with the aim to profit from the two complementary reference systems in a single ground state calculation.

3.2 Co-motion functions for quasi-one-dimensional densities

For the evaluation of the SCE energy $V_{ee}^{SCE}[\rho]$ (3.15) and its potential $v_{SCE}[\rho](\mathbf{r})$ (3.12) the co-motion functions are required. They are solutions to the differential equation (3.14). We will solve this differential equation in one dimension for densities of arbitrary shape, and in three dimensions for spherically symmetric densities.

One dimension To determine the SCE co-motion functions for the one-dimensional case we write the differential equation (3.14) in one dimension

$$\rho(x)dx = \rho(f_i(x)) \left| \frac{df_i(x)}{dx} \right| dx \quad (3.26)$$

Defining the cumulant

$$N_e(x) = \int_{-\infty}^x dy \rho(y) \quad (3.27)$$

we integrate (3.26) from $-\infty$ to x , and see that the one-dimensional solution to $f_i(x)$ satisfies

$$N_e(x) = \pm N_e(f_i(x)) \mp N_e(f_i(-\infty)) \quad (3.28)$$

where the signs depend on the signs of df_i/dx . As the inverse of the cumulant $N_e(x)$ is well defined in the domain $[0, N]$, $f_i(x)$ can be extracted from the above expression once the signs df_i/dx together with the initial conditions $N_e(f_i(-\infty))$ are known.

To this end the principle of “total suppression of charge fluctuations” [103] is useful. It expresses that the density in between two neighboring SCE positions always

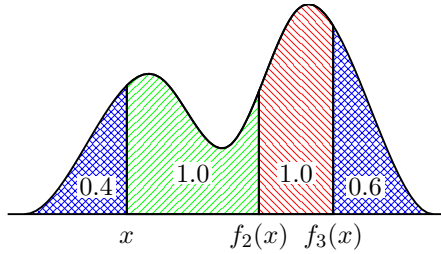


Figure 3.1: Schematic illustration of the principle of “total suppression of charge fluctuations” in one dimension. Two adjacent strictly correlated positions $f_i(x)$ are always separated by a distance such that the density between them integrates exactly to one.

integrates to one (cf. figure 3.1), and can be written as follows²

$$\begin{aligned} i - 1 &= N_e(f_i(x)) - N_e(x) && \text{for } x \leq f_i(x) \\ N - i + 1 &= N_e(x) - N_e(f_i(x)) && \text{for } x > f_i(x) \end{aligned} \quad (3.29)$$

An intuitive example is given by the one-dimensional analog of the Wigner crystal, where the electrons are at the SCE positions. For a rigorous proof of the “charge fluctuation suppression” principle see ref. [127].

Consequently, the signs df_i/dx are always positive and the initial conditions $N_e(f_i(\pm\infty)) = \{i - 1, -N + i - 1\}$ are set. The co-motion functions follow from (3.28)

$$f_i(x) = \begin{cases} N_e^{-1}[N_e(x) + i - 1] & \text{for } x \leq a_{N-i+1} \\ N_e^{-1}[N_e(x) - N + i - 1] & \text{for } x > a_{N-i+1} \end{cases} \quad (3.30)$$

where $a_k = N_e^{-1}(k)$.

One-dimensional, symmetric in origin Before considering the co-motion functions of spherical densities, it is illustrative to derive the co-motion functions for a one-dimensional symmetric density centered at the origin $\rho(x) = \rho(-x)$. A symmetry adapted coordinate system is chosen, which expresses the electronic positions by the distance to the origin and the orientation w.r.t. the origin $x \rightarrow \{|\mathbf{x}| = x, \theta\}$ with $\theta = +/ -$.

The orientations can be obtained from the minimization of the electrostatic energy of a single SCE configuration (3.7) for a given set of distances

$$E_{pot}[\rho](x_1 \dots x_N, \Theta) = \sum_{j>i}^N \frac{1}{|x_i \pm x_j|} + \sum_i^N v_{SCE}[\rho](x_i) \quad (3.31)$$

where Θ denotes collectively the orientations of the $N - 1$ electrons w.r.t. the reference electron at x_1 . As v_{SCE} is a variable of the distance alone, the minimizing orientations

²We label the co-motion functions from $f_1 = x$ to the right with increasing index i , and to the left with decreasing index whereby f_N the first co-motion function to the left of $f_1 = x$.

can be found by varying the signs only in the first term on the *r.h.s.* of the above equation.

For the distances we need to solve the differential equation (3.14)

$$\rho(x)dx = \rho(f_i(x)) \left| \frac{df_i(x)}{dx} \right| dx \quad (3.32)$$

The symmetry adapted cumulant is defined

$$N_e(x) = \int_0^x dy 2\rho(y) \quad (3.33)$$

and (3.32) is integrated from 0 to x

$$N_e(x) = \pm N_e(f_i(x)) \mp N_e(f_i(0)) \quad (3.34)$$

where the signs depend on the sign of $|df_i(x)/dx|$. From the “charge fluctuation suppression” principle the initial conditions $N_e(|f_i(0)|)$ can be found

$$2(i-1) = N_e(f_i(x)) - N_e(x) \quad \text{for } f_i(x) > x \quad (3.35)$$

where the factor of two arises due to the symmetry of the problem.

For the correlated position $f_i(x)$ being to the right of reference position x , $\text{sgn}(df_i/dx) = +$ follows, and we obtain the co-motion functions for the first branch

$$f_i(x) = N_e^{-1}[N_e(x) + 2i - 2] \quad \text{for } x < a_{N-2i+2} \quad (3.36)$$

For $f_i(x)$ to the left of x we have to distinguish the two cases: (i) $f_i(x)$ has the same orientation as the reference electron x , *i.e.* $\text{sgn}(\mathbf{f}_i(\mathbf{x})) = \text{sgn}(\mathbf{x})$, (ii) $f_i(x)$ is opposite to the reference electron x , *i.e.* $\text{sgn}(\mathbf{f}_i(\mathbf{x})) = -\text{sgn}(\mathbf{x})$.

In case (i) the “charge fluctuation suppression” principle reads

$$2(N-i+1) = N_e(x) - N_e(f_i(x)) \quad \text{for } f_i(x) > x, \text{sgn}(\mathbf{f}_i(\mathbf{x})) = \text{sgn}(\mathbf{x}) \quad (3.37)$$

and the co-motion functions in this branch read

$$f_i(x) = N_e^{-1}[N_e(x) - 2N + 2i - 2] \quad \text{for } x > a_{2N-2i+2} \quad (3.38)$$

For the second case (ii) we modify the “charge fluctuation suppression” expression

$$2(N-i+1) = N_e(x) + N_e(f_i(x)) \quad \text{for } f_i(x) > x, \text{sgn}(\mathbf{f}_i(\mathbf{x})) = -\text{sgn}(\mathbf{x}) \quad (3.39)$$

Taking into account the sign change in (3.34) due to the sign change in df_i/dx , the co-motion functions for the last branch read

$$f_i(x) = N_e^{-1}[-N_e(x) + 2N - 2i + 2] \quad \text{for } a_{N-2i+2} < x < a_{2N-2i+2} \quad (3.40)$$

Co-motion functions (3.38) and (3.40) conflate if the absolute value is taken in the square brackets, and the co-motion functions on the entire domain summarize to

$$f_i(x) = \begin{cases} N_e^{-1}[N_e(x) + 2i - 2] & \text{for } x \leq a_{N-2i+2} \\ N_e^{-1}[|N_e(x) - 2N + 2i - 2|] & \text{for } x > a_{N-2i+2} \end{cases} \quad (3.41)$$

Three dimensions, spherically symmetric We express the electronic positions in spherical coordinates and write the electrostatic energy of a single SCE configuration (3.7) in terms of these coordinates [117]

$$E_{pot}[\rho](r_1 \dots r_N, \Omega) = \sum_{j>i}^N \frac{1}{|\mathbf{r}_i - \mathbf{r}_j|} + \sum_i^N v_{SCE}[\rho](r_i) \quad (3.42)$$

where Ω denotes the $2N - 3$ relative angles with the reference electron on the z -axis and a second one in the xz -plane. Similar to the one-dimensional symmetric case, the minimizing angles are obtained by minimizing the first term on the *r.h.s.* of (3.42) independent of the second term. This corresponds to the equilibrium solution of N rotatable sticks of given lengths $r_1 \dots r_N$, with one end of a stick being fixed in the origin and the other end with a point charge pinned to it.

The radial distances are found again from the radial differential equation of (3.14)

$$4\pi x^2 \rho(x) dx = 4\pi f_i^2(x) \rho(f_i(x)) \left| \frac{df_i(x)}{dx} \right| dx \quad (3.43)$$

Defining the spherical cumulant

$$N_e(r) = \int_0^r ds 4\pi s^2 \rho(s) \quad (3.44)$$

the SCE co-motion functions derive as in the one-dimensional symmetric analog from above, and give the radial distances according to

$$f_i(r) = \begin{cases} N_e^{-1}[N_e(r) + 2i - 2] & \text{for } r \leq a_{N-2i+2} \\ N_e^{-1}[|N_e(r) - 2N + 2i - 2|] & \text{for } r > a_{N-2i+2} \end{cases} \quad (3.45)$$

In chapter 6 of this thesis we will generalize the co-motion functions given here to densities that integrate to non-integer electron numbers.

3.3 Models for the strong-interaction limit

An approximation to the indirect electrostatic energy $W_\lambda[\rho]$ of (2.28) in the strong-interaction limit, which can be evaluated for arbitrary three-dimensional densities, is given by the *point-charge-plus-continuum* (PC) model [104, 105, 128]. The idea is to rewrite $W_\lambda[\rho]$ as the electrostatic energy E_{es} of a system of N electrons in the state $\Phi_\lambda[\rho]$ embedded in a smeared background of positive charge $\rho_+(\mathbf{r}) = \rho(\mathbf{r})$

$$\begin{aligned} W_\lambda[\rho] &= E_{es}[\Phi_\lambda[\rho], \rho_+] = E_{ee} + E_{eb} + E_{bb} \\ &= \langle \Phi_\lambda[\rho] | \hat{V}_{ee} | \Phi_\lambda[\rho] \rangle - U[\rho] \end{aligned} \quad (3.46)$$

where the electronic repulsion energy is $E_{ee} = \langle \Phi_\lambda[\rho] | \hat{V}_{ee} | \Phi_\lambda[\rho] \rangle$, the electron-background interaction is $E_{eb} = -2U[\rho]$, and the background-background interaction is $E_{bb} = U[\rho]$, thus yielding exactly $W_\lambda[\rho]$.

Relation (3.46) is valid for every λ , but in the $\lambda \rightarrow \infty$ limit, when $\Phi_\lambda \rightarrow \Phi_{SCE}$, we expect that the electrons minimize $E_{es}[\Phi_\lambda, \rho]$ by occupying relative positions that divide the space into neutral cells with possibly zero (or weak) lowest-order electrostatic multipole moments [105]. The idea is then that for one of the SCE configurations $\{\mathbf{r}, \mathbf{f}_2(\mathbf{r}), \dots, \mathbf{f}_N(\mathbf{r})\}$ we may approximate the indirect electron-electron repulsion by the sum of the electrostatic energies of all the cells (i.e. we neglect the cell-cell interaction in view of their neutrality and low multipole moments)

$$E_{es}[\Phi_\lambda[\rho], \rho_+] \approx \sum_i^N E_{cell}([\rho]; \mathbf{f}_i(\mathbf{r})) \quad (3.47)$$

where $E_{cell}([\rho]; \mathbf{f}_i(\mathbf{r}))$ is the electrostatic energy of the cell around an electron at position $\mathbf{f}_i(\mathbf{r})$, equal to the sum of the attraction between the electron and the background contained in the cell and the background-background repulsion inside the cell.

To obtain the indirect electronic repulsion energy $W_\lambda[\rho]$ of a continuous density the probability weighted average is taken

$$W_\infty^{PC}[\rho] = \int d\mathbf{r} \frac{\rho(\mathbf{r})}{N} \sum_i^N E_{cell}([\rho]; \mathbf{f}_i(\mathbf{r})) \quad (3.48)$$

For the strictly correlated positions \mathbf{f}_i that obey the differential equation (3.14) it follows that (3.48) is equivalent to

$$W_\infty^{PC}[\rho] = \int d\mathbf{r} \rho(\mathbf{r}) E_{cell}([\rho]; \mathbf{r}) \quad (3.49)$$

that avoids eventually the dependence on the SCE co-motion functions. See chapter 4 for further discussion.

Finally, the cell energy is approximated. A simple model for the PC cell is a sphere of uniform background around the electron, set by the electronic position $\rho_+(\mathbf{r}') = \rho(\mathbf{r})$. From the condition of charge neutrality the cell radius is fixed to $r_s(\mathbf{r}) = (\frac{4\pi}{3} \rho(\mathbf{r}))^{-1/3}$, and the PC-LDA approximation for the electrostatic energy is obtained

$$E_{cell}^{LDA}(\mathbf{r}) = -\frac{9}{10} \left(\frac{4\pi}{3} \right)^{1/3} \rho(\mathbf{r})^{1/3} \quad (3.50)$$

For a more accurate model of $W_\infty[\rho]$ the density gradient $\nabla\rho$ can be used. A cell is constructed with homogeneously decaying background density fixed by $\rho(\mathbf{r})$ and $\nabla\rho(\mathbf{r})$. As the dipole moment of this cell will not be zero when the electron is put in the center of the cell, the origin of the cell is shifted away from the electron. The electrostatic energy of the PC-GGA cell is

$$E_{cell}^{GGA}(\mathbf{r}) = E_{cell}^{LDA}(\mathbf{r}) + \frac{3}{350} \left(\frac{3}{4\pi} \right)^{1/3} \frac{|\nabla\rho(\mathbf{r})|^2}{\rho(\mathbf{r})^{7/3}} \quad (3.51)$$

The coefficient $W'_\infty[\rho]$ in the $\lambda \rightarrow \infty$ expansion (2.43) of $W_\lambda[\rho]$ can also be given approximately within the PC-GGA model

$$W'^{PC}_\infty[\rho] = \int d\mathbf{r} \left[C\rho(\mathbf{r})^{3/2} + D \frac{|\nabla\rho(\mathbf{r})|^2}{\rho(\mathbf{r})^{7/6}} \right] \quad (3.52)$$

where $C = 1.535$ and $D = -0.02558$. For further explanation the reader is referred to [105].

Refs. [102] and [117] compare the PC solutions with the exact SCE values for small atoms: while $W'^{PC}_\infty[\rho]$ is a very reasonable approximation to its exact counterpart [117], the original $W'^{PC}_\infty[\rho]$ turned out to be much less accurate [102]. The exact SCE results could be used to propose a revised PC approximation $W'^{revPC}_\infty[\rho]$, having accuracy similar to the one of $W'^{PC}_\infty[\rho]$. Hence, the PC model can provide useful ingredients for an interaction-strength interpolation on the integrand $W_\lambda[\rho]$. On the downside, due to the approximate evaluation of the cell energy from (semi-)local quantities, the functional derivative of (3.48)-(3.49) will not embody the non-local features required to describe strong correlation.

Alternative models for the SCE electronic interaction can be constructed from the exchange-correlation hole and have just recently appeared [129].

Chapter 4

Energy Densities in the Strong-Interaction Limit of Density Functional Theory

A. Mirtschink, M. Seidl and P. Gori-Giorgi

“Energy densities in the strong-interaction limit of density functional theory”

J. Chem. Theory Comput. **8**, 3097 (2012)

4.1 An overview

The interaction-strength interpolation (ISI) idea to model the λ dependence of $W_\lambda[\rho]$ by an interpolation between the weak- and strong-interaction limits was first used for approximate functional development by Seidl and coworkers [103–105]. As at the time of construction of their ISI exact input quantities from the strong interaction limit were not available, the PC model was introduced. It provides approximate expressions for $W_\infty[\rho]$ and $W'_\infty[\rho]$ (2.43) in a DFA spirit by using (semi-)local quantities, *cf.* section 3.3, that can lead to erroneous behavior of $W_\lambda[\rho]$ (see below for more discussion). A full avoidance of DFA bias is possible with the SCE many-electron formalism, within which the functionals $W_\infty[\rho]$ and $W'_\infty[\rho]$ can be accurately computed.

Although free of any DFA bias (if we use exact input quantities), an unpleasant feature of the ISI is the violation of size consistency¹. This is due to the *non-linear* way the (on its own size consistent) ingredients $W_0[\rho]$, $W'_0[\rho]$, $W_\infty[\rho]$ and $W'_\infty[\rho]$ enter in the interpolation. *E.g.*, the revised ISI [102] (which behaves better in the $\lambda \rightarrow \infty$ limit

¹For a critical review on size consistency of approximate energy density functionals see, *e.g.*, ref. [130] and, especially, ref. [131].

than the original ISI) reads

$$W_\lambda^{revISI}[\rho] = \frac{\partial}{\partial \lambda} \left(a[\rho]\lambda + \frac{b[\rho]\lambda}{\sqrt{1 + c[\rho]\lambda + d[\rho]}} \right) \quad (4.1)$$

where a , b , c and d are non-linear functions of $W_0[\rho]$, $W'_0[\rho]$, $W_\infty[\rho]$ and $W'_\infty[\rho]$, determined by imposing the asymptotic expansions (2.42) and (2.43)

$$a[\rho] = W_\infty[\rho] \quad (4.2)$$

$$b[\rho] = -\frac{8 E_c^{GL2}[\rho] W'_\infty[\rho]^2}{(E_x[\rho] - W_\infty[\rho])^2} \quad (4.3)$$

$$c[\rho] = \frac{16 E_c^{GL2}[\rho]^2 W'_\infty[\rho]^2}{(E_x[\rho] - W_\infty[\rho])^4} \quad (4.4)$$

$$d[\rho] = -1 - \frac{8 E_c^{GL2}[\rho] W'_\infty[\rho]^2}{(E_x[\rho] - W_\infty[\rho])^3} \quad (4.5)$$

Notice that the lack of size consistency is shared by all functionals in which the exact exchange energy (or any global energy) enters in a non-linear way. Thus also, e.g., the MCY1 functional of section 2.2.7.

As a final remark on the revISI functional we add that, if one makes the approximation $E_c^{GL2} \approx E_c^{MP2}$, it can be viewed as a double hybrid functional. With respect to available double hybrids, the revISI lacks size consistency, but it has the advantage of being able to deal with the small-gap systems problematic for perturbation theory. The practical impact of the lack of size consistency of the revISI functional in this context still needs to be tested, but from theoretical grounds it can be expected that difficulties in the dissociation of chemical bonds arise (for further discussion in the context of fractional electron numbers see, e.g., ref. [132–135]).

A possible way to recover size consistency in the ISI framework is given by rewriting the integrand $W_\lambda[\rho]$ as integral of local quantities

$$E_{xc}[\rho] = \int_0^1 d\lambda \int d\mathbf{r} \rho(\mathbf{r}) w_\lambda[\rho](\mathbf{r}) \quad (4.6)$$

where $w_\lambda[\rho](\mathbf{r})$ is an interaction-strength dependent energy density. A local ISI model for $w_\lambda[\rho](\mathbf{r})$ can then be attempted by interpolating between the $\lambda \rightarrow 0$ and the $\lambda \rightarrow \infty$ limits in every point of space

$$w_\lambda[\rho](\mathbf{r}) \approx w_\lambda^{ISI}[\rho](\mathbf{r}) \quad (4.7)$$

As obvious from (4.6), the energy density $w_\lambda[\rho](\mathbf{r})$ is not uniquely defined², and an important requirement in the construction of interpolations is that the local input quantities in the weak- and in the strong-interaction limits are defined in a consistent manner (same gauge). For a further discussion on the gauge of the exchange-correlation energy density see, e.g., ref. [136], and for the kinetic energy density see, e.g., refs. [137–140]. Here we focus on the conventional, physically transparent, definition in terms of the electrostatic energy of the exchange-correlation hole.

²Adding any functional of the density that integrates to zero, will change the energy density locally, but not the integrated value.

4.2 Energy density: definitions

One of the most common definitions of the energy density of (4.6) is given by the interaction-strength dependent exchange-correlation hole $h_{xc}^\lambda(\mathbf{r}, \mathbf{r}')$ (see, e.g., refs. [141–143])

$$w_\lambda[\rho](\mathbf{r}) = \frac{1}{2} \int d\mathbf{r}' \frac{h_{xc}^\lambda(\mathbf{r}, \mathbf{r}')}{|\mathbf{r} - \mathbf{r}'|} \quad (4.8)$$

where $h_{xc}^\lambda(\mathbf{r}, \mathbf{r}')$ relates to the pair density $P_2^\lambda(\mathbf{r}, \mathbf{r}')$

$$h_{xc}^\lambda(\mathbf{r}, \mathbf{r}') = \frac{P_2^\lambda(\mathbf{r}, \mathbf{r}')}{\rho(\mathbf{r})} - \rho(\mathbf{r}') \quad (4.9)$$

and $P_2^\lambda(\mathbf{r}, \mathbf{r}')$ is obtained from the interaction-strength dependent wavefunction $\Phi_\lambda[\rho]$ of the adiabatic connection (2.26)-(2.28)

$$P_2^\lambda(\mathbf{r}, \mathbf{r}') = N(N-1) \sum_{\sigma_1 \dots \sigma_N} \int d\mathbf{r}_3 \dots d\mathbf{r}_N |\Phi_\lambda(\mathbf{r}\sigma_1, \mathbf{r}'\sigma_2, \mathbf{r}_3\sigma_3 \dots \mathbf{r}_N\sigma_N)|^2 \quad (4.10)$$

In the definition of (4.8) $w_\lambda[\rho](\mathbf{r})$ is the electrostatic potential of the exchange-correlation hole (a negative charge distribution normalized to -1) around a reference electron in \mathbf{r} . This quantity at the physical coupling strength $\lambda = 1$ (plus the Hartree potential) has been also called $v_{cond}(\mathbf{r})$ in the literature (see, e.g., ref. [144]).

Physical $\lambda = 1$ For the exact energy density at coupling-strength $\lambda = 1$ we enter the definition of the exchange-correlation hole (4.9) in (4.8)

$$w_1[\rho](\mathbf{r}) = \frac{1}{2\rho(\mathbf{r})} \int d\mathbf{r}' \frac{P_2^1(\mathbf{r}, \mathbf{r}')}{|\mathbf{r} - \mathbf{r}'|} - \frac{1}{2} \int d\mathbf{r}' \frac{\rho(\mathbf{r}')}{|\mathbf{r} - \mathbf{r}'|} \quad (4.11)$$

with the pair density given by the full many-body wavefunction Φ_1 according to (4.10). The density $\rho_1(\mathbf{r})$ corresponding to $P_2^1(\mathbf{r}, \mathbf{r}')$ defines the density that is to be held constant along the adiabatic connection $\rho(\mathbf{r}) \equiv \rho_1(\mathbf{r})$.

The exact $w_1[\rho](\mathbf{r})$ is computed in the following with accurate wavefunction approximations and can serve as benchmark for models on $w_\lambda[\rho](\mathbf{r})$. It gives also an impression on the relevance of the strong-interaction limit for accurate interpolations on $w_\lambda[\rho](\mathbf{r})$, and it is the aim of this work to explore this relevance. If the physical system is close to the KS one, correlation is less important and already Hartree-Fock should perform well. In this case, we expect the inclusion of the $\lambda \rightarrow \infty$ reference in the $w_\lambda[\rho](\mathbf{r})$ model to be less significant. In contrast, for more strongly correlated systems the physical energy density is expected to tend more towards the $\lambda \rightarrow \infty$ limit, and the SCE functional should provide useful input for an accurate $w_\lambda[\rho](\mathbf{r})$ model.

Kohn-Sham $\lambda = 0$ For non-interacting electrons the formal solution to the wavefunction is a Slater determinant $\Phi_0 \rightarrow \Psi$, and the energy density $w_0[\rho](\mathbf{r})$ is given by

the electrostatic potential of the KS exchange hole $h_x(\mathbf{r}, \mathbf{r}')$

$$w_0[\rho](\mathbf{r}) = \frac{1}{2} \int d\mathbf{r}' \frac{h_x(\mathbf{r}, \mathbf{r}')}{|\mathbf{r} - \mathbf{r}'|} \quad (4.12)$$

as the pair density writes

$$P_2^0(\mathbf{r}, \mathbf{r}') = \rho(\mathbf{r})\rho(\mathbf{r}') + \rho(\mathbf{r})h_x(\mathbf{r}, \mathbf{r}') \quad (4.13)$$

In models for $w_\lambda[\rho](\mathbf{r})$ with $w_0[\rho](\mathbf{r})$ input one can use the exact exchange hole built from a simple Hartee-Fock like expression in terms of the KS orbitals φ_i , or a density functional approximation for $h_x(\mathbf{r}, \mathbf{r}')$, e.g. the one of Becke and Roussel [145]. These two choices would correspond, respectively, to construct a hyper-GGA and a meta-GGA functional from a local interpolation along the adiabatic connection.

For our preliminary study of energy densities along the adiabatic connection, the exact KS orbitals φ_i – or equivalently the effective one-body potential $v_s(\mathbf{r})$ (2.25) – for the given physical density $\rho(\mathbf{r})$ have to be found. This can be done accurately. e.g., by inversion of the KS equations [146–151] or by the use of Lieb’s Legendre transform DFT formalism [46, 152, 153].

$w_0[\rho](\mathbf{r})$ will be a key ingredient for an ISI-like interpolation on the energy density. To obtain meaningful interpolations, knowledge of the next leading order in the asymptotic expansion of $w_\lambda[\rho](\mathbf{r})$ around $\lambda = 0$ is required additionally, but not available yet. An outlook will be given in the conclusions of this chapter.

Strictly correlated electrons $\lambda \rightarrow \infty$ The exchange-correlation energy density (4.8) in the strong-interaction limit $w_\infty[\rho](\mathbf{r})$ is the central quantity of this chapter. In this section we will derive an exact expression from the SCE formalism.

We start by inserting the strictly correlated state Φ_{SCE} (3.10) into the definition of the pair density (4.10) to obtain in the strong-interaction limit $P_2^\infty(\mathbf{r}, \mathbf{r}') = P_2^{SCE}(\mathbf{r}, \mathbf{r}')$

$$P_2^{SCE}(\mathbf{r}, \mathbf{r}') = \sum_{i \neq j}^N \int d\mathbf{s} \frac{\rho(\mathbf{s})}{N} \delta(\mathbf{r} - \mathbf{f}_i(\mathbf{s})) \delta(\mathbf{r}' - \mathbf{f}_j(\mathbf{s})) \quad (4.14)$$

which has a transparent physical meaning: two electrons can only be found at strictly correlated relative positions. We can then compute

$$\int d\mathbf{r}' \frac{P_2^{SCE}(\mathbf{r}, \mathbf{r}')}{|\mathbf{r} - \mathbf{r}'|} = \sum_{i \neq j}^N \int d\mathbf{s} \frac{\rho(\mathbf{s})}{N} \frac{\delta(\mathbf{r} - \mathbf{f}_i(\mathbf{s}))}{|\mathbf{r} - \mathbf{f}_j(\mathbf{s})|} \quad (4.15)$$

where on the r.h.s. we have already integrated over the variable \mathbf{r}' . By the properties of the Dirac delta distribution and of the co-motion functions, (4.15) becomes

$$\begin{aligned} \int d\mathbf{r}' \frac{P_2^{SCE}(\mathbf{r}, \mathbf{r}')}{|\mathbf{r} - \mathbf{r}'|} &= \frac{1}{N} \sum_{i \neq j}^N \frac{\rho(\mathbf{f}_i^{-1}(\mathbf{r})) |\det \partial_\alpha f_{i,\beta}^{-1}(\mathbf{r})|}{|\mathbf{r} - \mathbf{f}_j(\mathbf{f}_i^{-1}(\mathbf{r}))|} \\ &= \frac{\rho(\mathbf{r})}{N} \sum_{i \neq j}^N \frac{1}{|\mathbf{r} - \mathbf{f}_j(\mathbf{f}_i^{-1}(\mathbf{r}))|} \end{aligned} \quad (4.16)$$

with $|\det \partial_\alpha f_{i,\beta}^{-1}(\mathbf{r})|$ ($\alpha, \beta = x, y, z$) the determinant of the Jacobian of the transformation $\mathbf{r} \rightarrow \mathbf{f}_i^{-1}(\mathbf{r})$, and we have used the fact that all the $\mathbf{f}_i(\mathbf{r})$ satisfy the differential equation (3.14) (as do their inverses, which by virtue of the group properties of the co-motion functions (3.13) are also co-motion functions for the same configuration [102, 117]). Now we can use once more the group properties of the co-motion functions to recognize that for all $i \neq j$ the function $\mathbf{f}_j(\mathbf{f}_i^{-1}(\mathbf{r}))$ must be another co-motion function with the exclusion of $\mathbf{f}_1(\mathbf{r}) = \mathbf{r}$ (the identity can arise only if $i = j$). The double sum in the last term of (4.16) is then exactly equal to N times a single sum over all the co-motion functions $\mathbf{f}_k(\mathbf{r})$ with $k \geq 2$, so that

$$\int d\mathbf{r}' \frac{P_2^{SCE}(\mathbf{r}, \mathbf{r}')}{|\mathbf{r} - \mathbf{r}'|} = \rho(\mathbf{r}) \sum_{k=2}^N \frac{1}{|\mathbf{r} - \mathbf{f}_k(\mathbf{r})|} \quad (4.17)$$

Inserting (4.17) into (4.8)-(4.9), we finally obtain

$$w_\infty[\rho](\mathbf{r}) = \frac{1}{2} \sum_{k=2}^N \frac{1}{|\mathbf{r} - \mathbf{f}_k(\mathbf{r})|} - \frac{1}{2} v_H(\mathbf{r}) \quad (4.18)$$

representing the exchange-correlation energy density in the strong-interaction limit by means of the SCE co-motion functions.

Notice that in previous work the exact $W_\infty[\rho]$ was given as [102, 117, 118]

$$W_\infty[\rho] = \frac{1}{2} \int d\mathbf{r} \frac{\rho(\mathbf{r})}{N} \sum_{i \neq j}^N \frac{1}{|\mathbf{f}_i(\mathbf{r}) - \mathbf{f}_j(\mathbf{r})|} - U[\rho] \quad (4.19)$$

suggesting a corresponding energy density

$$\tilde{w}_\infty[\rho](\mathbf{r}) = \frac{1}{N} \sum_i^N \left(\frac{1}{2} \sum_{i \neq j}^N \frac{1}{|\mathbf{f}_i(\mathbf{r}) - \mathbf{f}_j(\mathbf{r})|} - \frac{1}{2} v_H(\mathbf{f}_i(\mathbf{r})) \right) \quad (4.20)$$

Expressions (4.18) and (4.20) yield the same $W_\infty[\rho]$ when integrated with the density $\rho(\mathbf{r})$, but are locally different. They show a general feature of the co-motion functions: Any given energy density $w_\infty^a(\mathbf{r})$ can always be transformed into a different energy density $w_\infty^b(\mathbf{r})$ defined as

$$w_\infty^b(\mathbf{r}) \equiv \frac{1}{N} \sum_i^N w_\infty^a(\mathbf{f}_i(\mathbf{r})) \quad (4.21)$$

such that $\rho(\mathbf{r})w_\infty^a(\mathbf{r})$ and $\rho(\mathbf{r})w_\infty^b(\mathbf{r})$ integrate to the same quantity. This gauge freedom arises because all the co-motion functions satisfy the differential equation (3.14). Though only expression (4.18) corresponds to the gauge of the exchange-correlation hole (4.8)-(4.10) as only this one derives from the pair density.

4.3 Energy densities for atoms

We have performed full-CI calculations in an aug-cc-pVTZ basis for some two and four electron atoms within the Gamess-US package [154] to obtain accurate ground state wavefunctions for the physical interaction strength. Starting from this, we are able to calculate the energy density in the gauge of the exchange-correlation hole for $\lambda = 0, 1, \infty$.

At $\lambda = 1$ we calculate the energy density from the full-CI pair density (4.11), by a program similar to the one used for the calculation of v_{cond} in ref. [144]. For the energy density at $\lambda = 0$ (4.12), we have to compute the single particle KS orbitals corresponding to the full-CI density first. In the case of two electron atoms they are readily accessible from the simple relationship

$$\varphi(\mathbf{r}) = \sqrt{\frac{\rho(\mathbf{r})}{2}} \quad (4.22)$$

For the four electron atoms we choose the scheme of van Leeuwen, Baerends and Gritsenko [147, 148] to invert the KS equations. In the strong-interaction limit $\lambda = \infty$, the co-motion functions $f_i(\mathbf{r})$ for the evaluation of the energy density are easily constructed within the Wolfram Mathematica computer algebra environment [155].

In figure 4.1 we show the energy densities at $\lambda = 0, 1$ and ∞ for two- and four-electron atoms. He and Be are relatively weakly correlated, and their $\lambda = 1$ energy densities are much closer to the KS ones than to the SCE ones. Hence, a description at the HF level is very reasonable and gives indeed at least 98.5% of the total energy. The anion H^- , instead being a system with a more diffuse density and thus more correlated, has a physical energy density that is much more in between the KS and the SCE curves. In this case the HF treatment gives only 94% of the total energy, that in addition is higher than the total energy of the neutral Hydrogen, *i.e.* in HF H^- is unbound. Here we expect the inclusion of the information from the strong-interaction limit in an ISI model to be important. The valence regions of Be and Li^- (see the insets in figure 4.1) can also be better described by a proper inclusion of the $\lambda = \infty$ information.

As a result we see that, an improved description of exchange and correlation can be expected by inclusion of the SCE reference. Within the accessible set of atomic systems here, the strongest correlation is given in the case of H^- . Though the correlation is not overly pronounced because of the prevailing influence of the nuclear potential, leading to non-vanishing amounts of kinetic energy. For the investigation of correlation dominated systems we turn to systems with tuneable correlation in which the impact of the external potential can be diminished.

4.4 Energy densities for Hooke's atom

Another useful class of systems for the study of the impact of the strong-interaction limit on the physical energy density is given by three-dimensional model quantum dots, also known as Hooke's atoms. Here two electrons (still interacting with the $1/r$ Coulomb repulsion) are confined in a harmonic external potential, and correlation

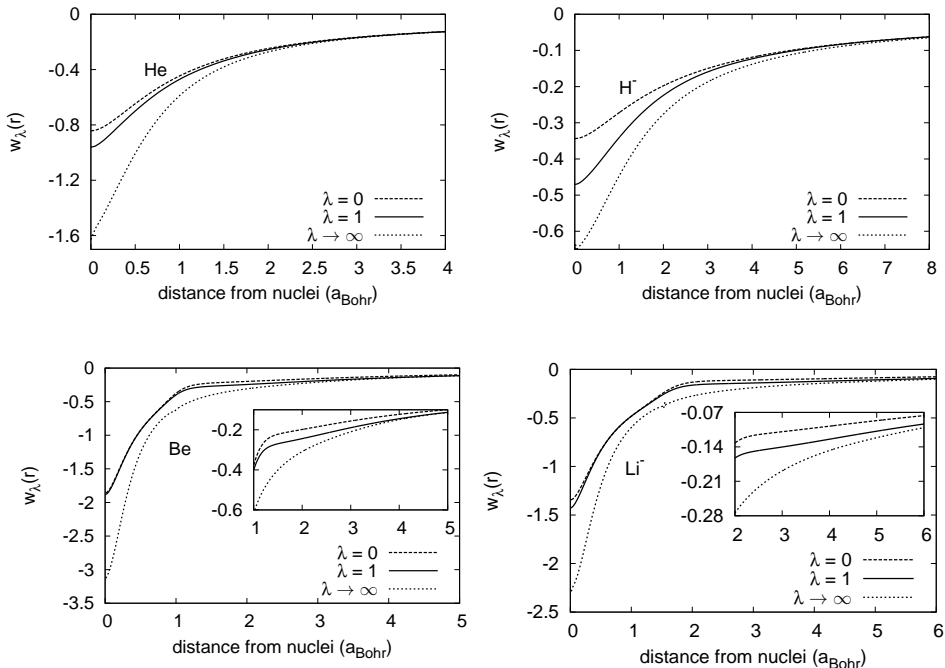


Figure 4.1: Energy densities $w_\lambda[\rho](r)$ in the definition of the electrostatic potential of the exchange-correlation hole for accurate full-CI densities (aug-cc-pVTZ) and coupling strength $\lambda = 0, 1, \infty$.

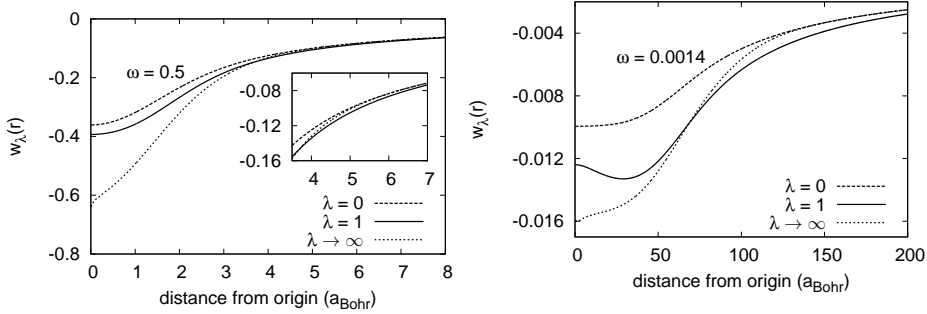


Figure 4.2: Energy densities $w_{\lambda}[\rho](\mathbf{r})$ in the definition of the electrostatic potential of the exchange-correlation hole for the exact density of Hooke's atoms [156] with subordinate correlation ($\omega = 0.5$) and pronounced correlation ($\omega = 0.0014$).

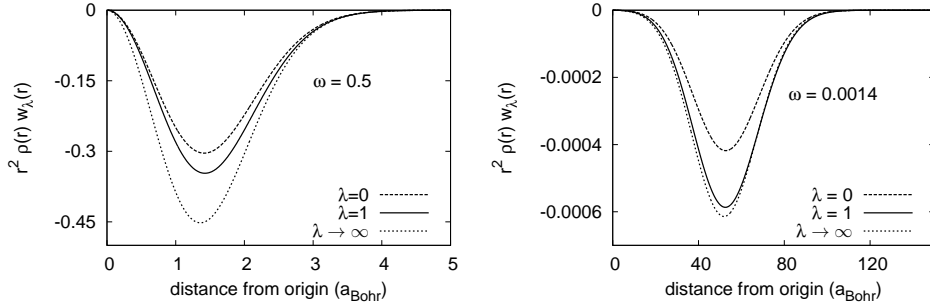


Figure 4.3: The same energy densities of figure 4.2 multiplied by the density $\rho(\mathbf{r})w_{\lambda}[\rho](\mathbf{r})$.

gains importance when the spring constant of the harmonic potential is lowered. We have computed the energy density for Hooke's atoms with spring constants for which the analytic solution to the physical wavefunction can be found [156].

Energy densities for the largest and smallest spring constant considered are displayed in figure 4.2 and figure 4.3. As expected, the physical energy density comes closer to the SCE energy density in the more strongly correlated case. An overall correspondence of the physical and SCE energy densities, however, is scarcely provided, *cf.* figure 4.2. The energetically meaningful product with the density $\rho(\mathbf{r})w_{\lambda}(\mathbf{r})$ is nevertheless remarkably well represented by the SCE curve, figure 4.3.

Additionally, we observe that the physical energy density crosses the SCE energy density. Intuitively one would expect the physical energy density to be always in between the KS and SCE energy densities, as the KS energy density represents the weakest possible correlation and the SCE energy density the strongest possible correlation for a given density. However, the wavefunctions are chosen according to

the global quantities

$$\begin{aligned} \min_{\Phi \rightarrow \rho} \langle \Phi | \hat{T} | \Phi \rangle &\Rightarrow \Psi_{KS} \\ \min_{\Phi \rightarrow \rho} \langle \Phi | \hat{V}_{ee} | \Phi \rangle &\Rightarrow \Phi_{SCE} \\ \min_{\Phi \rightarrow \rho} \langle \Phi | \hat{T} + \hat{V}_{ee} | \Phi \rangle &\Rightarrow \Phi_{\lambda=1} \end{aligned} \quad (4.23)$$

yielding the global inequalities

$$\langle \Phi_{SCE} | \hat{V}_{ee} | \Phi_{SCE} \rangle \leq \langle \Phi_{\lambda=1} | \hat{V}_{ee} | \Phi_{\lambda=1} \rangle \leq \langle \Psi_{KS} | \hat{V}_{ee} | \Psi_{KS} \rangle \quad (4.24)$$

Locally these inequalities can be violated without violating the global ones, and the physical energy density can go below the SCE energy density.

The crossing feature can be attributed to “polarization” effects between the two electrons, reflected in the pair density. By “polarization” we refer to two-body effects, *i.e.* how one electron is influenced by the other one [157]. For the two electrons considered here, when one of the electrons is at infinity, the other electron will be mainly found around the origin (where the minimum of the external potential is located). The physical ($\lambda = 1$) description of this electron is then a charge distribution around the origin due to the available kinetic energy. As the other electron approaches the origin from infinity, this charge distribution is deformed. For the KS ($\lambda = 0$) system, where we deal with an independent-electrons picture, this effect is not contained in the pair density as it would be expressed by a term of mutual dependence between the positions of the electrons, that can only arise in a beyond-orbital description of the wavefunction. For the SCE system ($\lambda = \infty$) there is a *perfect* mutual dependence between the two electronic positions, where the kinetic energy is neglected. In other words, the electrons are modeled as point charges and not as charge distributions. The proper description of this “polarization” effect is thus missed in the SCE wavefunction. It can probably be recovered, at least partially, by considering the next leading term in the $\lambda \rightarrow \infty$ expansion, corresponding to zero-point oscillations around the SCE solution [102].

To underline this argument we have computed the asymptotic behavior of the physical energy density for the Hooke's atom with $\omega = 0.5$, using the asymptotic expansion of the physical pair density [157]

$$\frac{P_2^1(\mathbf{r}, \mathbf{r}')}{\rho(\mathbf{r})\rho_{N-1}(\mathbf{r}')} \rightarrow 1 - 2\frac{r'}{r} \cos(\Delta\Omega) + \dots \quad (r \rightarrow \infty) \quad (4.25)$$

where $\rho_{N-1}(\mathbf{r}')$ is the density of the $N - 1$ -particle system and $\Delta\Omega$ the angle between \mathbf{r} and \mathbf{r}' . The second-order term in (4.25) represents the mentioned “polarization” correction [157]. As can be seen from figure 4.4, for large $|\mathbf{r} - \mathbf{r}'|$ the energy density in the KS and SCE case behaves like $-1/2r$, which corresponds to the first order in the expansion of the physical pair density. Inclusion of the second-order term in the energy density gives essentially the physical behavior and deviates from the KS and SCE energy densities.

Although the crossing happens in a region in which the density is very small, and thus with an almost negligible energetic contribution, *cf.* figure 4.3, the analysis presented here can be helpful in the construction of models for $w_\lambda[\rho](\mathbf{r})$.

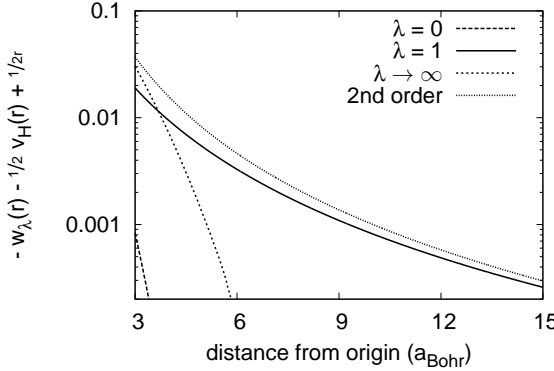


Figure 4.4: Difference between the energy density $w_\lambda[\rho](\mathbf{r})$ and the first-order correction $-1/2r$ of (4.25), including the Hartree contribution $1/2v_H(\mathbf{r})$, for Hooke's atom with $\omega = 0.5$. The energy densities are in the definition of the electrostatic potential of the exchange-correlation hole and are computed from the KS, physical and SCE pair density. Comparison is undertaken with the second-order correction from the asymptotic expansion of the physical pair density (4.25).

4.5 Local assessment of the point-charge-plus-continuum model in atoms

The availability of exact expressions for the strong-interaction limit within the SCE formalism allows for a validation of models for the same limit. In this section we extend further the analysis performed in refs. [102] and [117] for the global PC-model quantities $W_\infty^{PC}[\rho]$ and $W_\infty'^{PC}[\rho]$, by defining a local PC model for the energy density and comparing it to the SCE reference.

By comparison of the PC expressions for the global integrand $W_\infty[\rho]$ (3.48)-(3.49) with the local definition (4.6) a *local* PC model can be identified

$$W_\infty^{PC}[\rho] = \int d\mathbf{r} \rho(\mathbf{r}) w_\infty^{PC}[\rho](\mathbf{r}) \quad (4.26)$$

whereby the PC model tries to approximate the total electrostatic energy of an SCE configuration by means of the PC cells (3.47). The energy density that derives from this definition is

$$\tilde{w}_\infty^{PC}[\rho](\mathbf{r}) = \frac{1}{N} \sum_i^N E_{cell}([\rho]; \mathbf{f}_i(\mathbf{r})) \quad (4.27)$$

If the total energy of a configuration is approximated by the energy of a single cell

$$\sum_i^N E_{cell}([\rho]; \mathbf{f}_i(\mathbf{r})) \approx N E_{cell}([\rho]; \mathbf{r}) \quad (4.28)$$

the energy density writes

$$w_{\infty}^{PC}[\rho](\mathbf{r}) = E_{cell}([\rho]; \mathbf{r}) \quad (4.29)$$

From the exact SCE property (4.21) it shows that the integrated value $\int d\mathbf{r} \rho(\mathbf{r}) w(\mathbf{r})$ will not change upon the transformation (4.27)-(4.29). To determine the PC expression in the exchange-correlation hole gauge we compare to the SCE expressions (4.18)-(4.20). In (4.20) the total electrostatic energy is invoked, similar to the PC expression (4.27). Upon the gauge transform (4.21) of (4.20) to (4.18), the exchange-correlation hole gauge is obtained. Hence, the gauge transformed PC energy density (4.29) that is obtained from (4.27) should correspond to the exchange-correlation hole gauge.

It is important to stress that the PC cell is *not* an approximation to the exchange-correlation hole in the $\lambda \rightarrow \infty$ limit [105]. However, its electrostatic energy (electron-background attraction plus background-background repulsion) is an approximation to the electrostatic potential of the exchange correlation hole (4.8). This concept is further clarified in the appendix A, where the case of the uniform electron gas at extreme low density is treated explicitly.

From the cell energies (3.50) and (3.51), the approximate PC energy densities in the gauge of the exchange-correlation hole follow

$$w_{\infty}^{PC-LDA}(\mathbf{r}) = -\frac{9}{10} \left(\frac{4\pi}{3} \right)^{1/3} \rho(\mathbf{r})^{1/3} \quad (4.30)$$

$$w_{\infty}^{PC-GGA}(\mathbf{r}) = w_{\infty}^{PC-LDA}(\mathbf{r}) + \frac{3}{350} \left(\frac{3}{4\pi} \right)^{1/3} \frac{|\nabla \rho(\mathbf{r})|^2}{\rho(\mathbf{r})^{7/3}} \quad (4.31)$$

In figure 4.5 we compare the exact $\lambda \rightarrow \infty$ energy densities of (4.18) with the PC-LDA and PC-GGA approximations of (4.30)-(4.31) for the He atom, the sphericalized B and C atoms and for the Ne atom, using accurate Hylleras and quantum Monte Carlo densities [158–160]. We see that the PC model becomes a rather good approximation in the valence region of B, C and Ne, while being quite poor in the core region, and especially at the nucleus. The PC-LDA energy density is actually a better local approximation than the PC-GGA, except close to the nucleus. The PC-GGA performs better globally (see table 4.1), but we clearly see that this is due to error compensation between the core region and the inter-shell region. In the tail of the density the PC-GGA energy density diverges. Notice that the exact SCE energy densities have kinks (clearly visible in the insets of figure 4.5), which occur each time we have a configuration with one of the electrons at infinity.

The approximations made in the PC model are *i*) neglecting the cell-cell interaction, and *ii*) assuming the uniform- or slowly varying electron gas density for the background (4.30)-(4.31). At the nucleus, we can easily construct what would be the “exact” PC cell, so that we can at least remove approximation *ii*), and check the effect of approximation *i*) alone. The “exact” PC cell around the nucleus is the sphere Ω of radius a , with

$$\int_0^a dr 4\pi r^2 \rho(r) = 1 \quad (4.32)$$

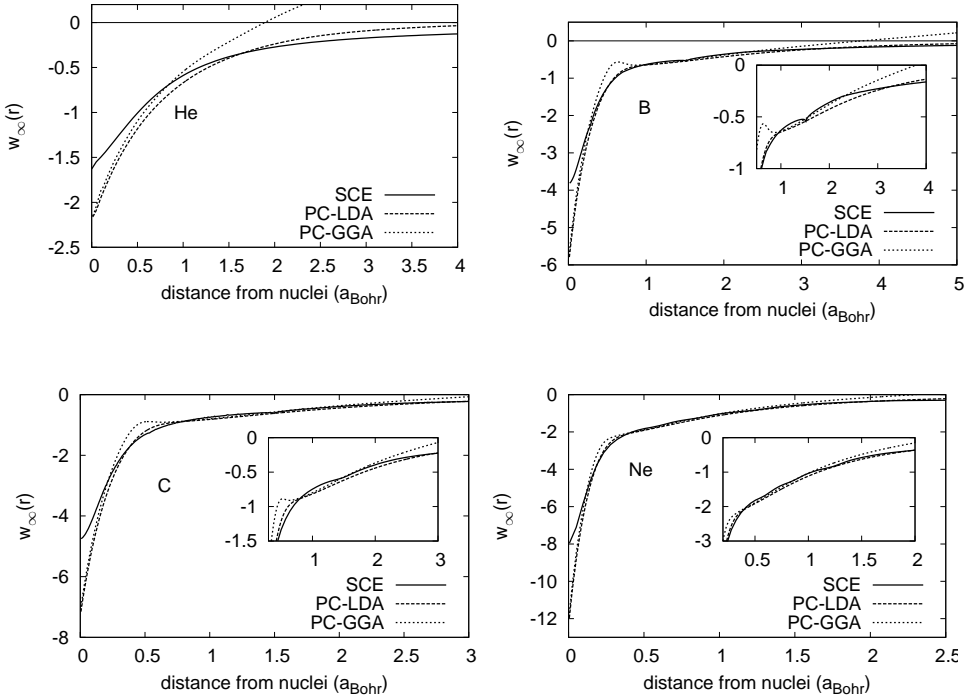


Figure 4.5: Energy density $w_\infty[\rho](r)$ in the definition of the electrostatic potential of the exchange-correlation hole. The exact SCE result of (4.18) is compared with the PC-LDA and PC-GGA approximations of (4.30)-(4.31).

	W_∞	W_∞^{PC-LDA}	W_∞^{PC-GGA}
H ⁻	-0.569	-0.664	-0.559
He	-1.498	-1.735	-1.468
Li	-2.596	-2.983	-2.556
Be	-4.021	-4.561	-3.961
B	-5.706	-6.412	-5.650
C	-7.781	-8.650	-7.719
Ne	-19.993	-21.647	-19.999

Table 4.1: Global value $W_\infty[\rho] = \int d\mathbf{r} \rho(\mathbf{r}) w_\infty[\rho](\mathbf{r})$ for small atoms at different levels of approximation. The exact value is given by the SCE expression (4.18), while the PC-LDA and PC-GGA values follow from (4.30) and (4.31), respectively.

	$w_\infty(0)$	$w_\infty^{PC-LDA/GGA}(0)$	$w_\infty^{PC}(0)$
H ⁻	-0.6825	-0.9671	-0.7157
He	-1.6883	-2.1729	-1.6672
Li	-2.2041	-3.4019	-2.6396
Be	-3.1568	-4.6578	-3.6354
B	-3.8230	-5.8995	-4.6190
C	-4.7727	-7.1446	-5.6050
Ne	-8.0276	-12.119	-9.5463

Table 4.2: Comparison of the energy density at the nucleus $w_\infty[\rho](r = 0)$ in the definition of the exchange-correlation hole for small atoms. The exact value w_∞ corresponds to the SCE expression of (4.18), the value $w_\infty^{PC-LDA/GGA}$ is the PC local density- or gradient expansion approximation of (4.30)-(4.31) equally, and w_∞^{PC} is the value from the “exact” PC cell of (4.33).

and the “exact” value of $w_\infty^{PC}(r = 0)$ is

$$w_\infty^{PC}(r = 0) = - \int_{\Omega} d\mathbf{r} \frac{\rho(\mathbf{r})}{r} + \frac{1}{2} \int_{\Omega} \int_{\Omega} d\mathbf{r} d\mathbf{r}' \frac{\rho(\mathbf{r})\rho(\mathbf{r}')}{|\mathbf{r} - \mathbf{r}'|} \quad (4.33)$$

In table 4.2 we compare the exact SCE values at the nucleus with the PC-LDA or PC-GGA (they become equal at the nucleus) and the result of (4.33) for several atoms. We see that the “exact” PC cell (4.33) is very accurate for $N = 2$: in fact, when the reference electron is at the nucleus, the other one is at infinity so that the cell-cell interaction becomes indeed zero. For $N > 2$ we see that the “smearing hypothesis,” *i.e.* the assumption of negligible cell-cell interaction, leads to some errors, although there is an improvement with respect to the PC-LDA and PC-GGA reducing the relative error by about a factor 2. Along these lines one might try to construct an improved PC model that performs locally better than the PC-GGA, which, as we have shown, achieves good global accuracy at the price of error cancellation between different regions of space.

4.6 Examination of the local Lieb-Oxford bound

Lieb and Oxford formulated a rigorous lower bound to the indirect part of the electron-electron repulsion energy $\tilde{W}[\Phi]$ associated with a given many-electron wavefunction Φ [161, 162]

$$\tilde{W}[\Phi] \equiv \langle \Phi | \hat{V}_{ee} | \Phi \rangle - U[\rho_\Phi] \geq -C \int d\mathbf{r} \rho_\Phi(\mathbf{r})^{4/3} \quad (4.34)$$

where $\rho_\Phi(\mathbf{r})$ is the density obtained from the wavefunction. The positive constant C is rigorously known to have a value $C \leq 1.679$ [162, 163]. It has been suggested

that a tighter bound can be obtained by taking the value of C that corresponds to the low-density limit of the uniform electron gas, $C \approx 1.44$ [164–166], since the bound is known to be more challenged when the number of electrons increases [162] and when the system has low density [167].

It is possible to translate the Lieb-Oxford (LO) bound into a lower bound for exchange and exchange-correlation functionals [164, 167]

$$E_x[\rho] \geq E_{xc}[\rho] \geq -C \int d\mathbf{r} \rho(\mathbf{r})^{4/3} \quad (4.35)$$

simply because $E_x[\rho] = W_{\lambda=0}[\rho]$ is the indirect Coulomb repulsion of the Slater determinant of KS orbitals, and $E_{xc}[\rho]$ is the sum of the indirect Coulomb repulsion of the physical wavefunction $W_{\lambda=1}[\rho]$, plus the correlation correction to the kinetic energy, which is always positive.

The way the LO bound is used in the construction of approximate functionals is, usually (with the exception of ref. [168]), by imposing it locally (see, e.g., refs. [63, 169]). That is, a given approximate exchange(-correlation) functional $E_{x(c)}^{DFA}[\rho] = \int d\mathbf{r} \rho(\mathbf{r}) \epsilon_{x(c)}^{DFA}(\mathbf{r})$ is required to satisfy

$$\epsilon_{x(c)}^{DFA}(\mathbf{r}) \geq -C \rho(\mathbf{r})^{1/3} \quad (4.36)$$

This is a sufficient condition to ensure the global bound (4.35), but it is by no means necessary (see, e.g., ref. [170]). In other words, there is no proof that a local version of the LO bound should hold. Actually, before even asking whether a local version of the LO bound does hold or not, we need to understand to which definition (gauge) of the energy density the local LO bound of (4.36) applies. In fact, since energy densities are not uniquely defined, the inequality (4.36) should be satisfied only for a well defined gauge: one can indeed always add a quantity to $\epsilon_{x(c)}^{DFA}(\mathbf{r})$ that integrates to zero and violates (4.36) in some region of space.

By our already presented considerations on the energy density we argue that: *i*) the gauge of the local LO bound is the conventional one of the electrostatic energy of the exchange-correlation hole, and *ii*) the local LO bound is then certainly violated, at least in the tail region of an atom or a molecule, and in the bonding region of a stretched molecule. The argument behind point *i*) is the following: For a given density ρ , the wavefunction $\Phi[\rho]$ that maximally challenges the LO bound is the one that minimizes the expectation $\langle \Phi[\rho] | \hat{V}_{ee} | \Phi[\rho] \rangle$ [119], *i.e.* by definition $\Phi_{SCE}[\rho]$. Hence, we also have

$$E_x[\rho] \geq E_{xc}[\rho] \geq W_\infty[\rho] \geq -C \int d\mathbf{r} \rho(\mathbf{r})^{4/3} \quad (4.37)$$

In section 4.2 we discussed the energy density associated with $W_\infty[\rho]$ in the gauge of the electrostatic potential of the exchange-correlation hole. We have also shown that this energy density can be approximated by the PC model that considers the electrostatic energy of a cell of positive charge $\rho_+(\mathbf{r}) = \rho(\mathbf{r})$ around the reference electron at \mathbf{r} . The LDA version (4.30) of this approximation has exactly the same form of the local LO bound (4.36). Moreover, the recently suggested value $C \approx 1.44$ [165] is remarkably close to the one of the PC-LDA model $C_{PC} \approx 1.45$. Notice the fact that

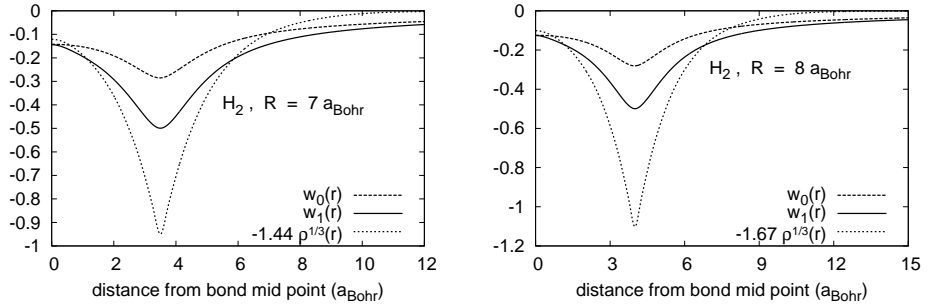


Figure 4.6: Violation of the local form of the Lieb-Oxford bound for the stretched H_2 molecule.

the PC model is in the gauge of the electrostatic energy of the exchange-correlation hole, as follows from the properties of the strong-interaction limit of DFT, in particular by (4.21). If the PC model is an approximation in this gauge, and if the LO bound is locally equal to it, then conclusion *i*) should follow. Although this is not a rigorous argument, but only a plausible one. Another way to arrive at the same conclusion comes from the fact that the local form of the tightened LO bound corresponds to approximate, in each point of space, the exchange-correlation hole with the one of the extremely correlated ($\lambda \rightarrow \infty$) electron gas, as illustrated in appendix A. This would imply, again, an energy density in the gauge of the exchange-correlation hole.

We then easily see that the local LO bound (4.36) is certainly violated in the tail region of an atom or a molecule, where the exact energy density in the conventional exchange-correlation hole gauge goes like $-1/(2r)$, while the r.h.s. of (4.36) decays exponentially. The local bound is also violated in the bond region of a stretched molecule. As an example we show in figure 4.6 the energy densities of the stretched H_2 molecule for $\lambda = 0$ and $\lambda = 1$: with $C = 1.44$ the local bound is violated in the bond region when the internuclear distance is $R \gtrsim 7$ a.u., and with $C = 1.67$ when $R \gtrsim 8$ a.u. The bonding region of a stretched molecule as shown in our figure 4.6 is energetically unimportant. However, the corresponding KS potential in the same region has important features for the proper description of bond breaking [144, 171], although this is expected to be a very non-local effect.

As concluding remark, we can say that it is very difficult, or maybe even impossible, to find a rigorous local lower bound for the energy density. In fact, we have just seen in section 4.4 that, at least for the harmonic external potential, it is not even true that $w_1(\mathbf{r}) \geq w_\infty(\mathbf{r})$ everywhere. This means that even if we maximize the correlation between the electrons, we do not construct a rigorous local lower bound, but only a global one.

4.7 Conclusions

We have derived an exact expression for the energy density in the strong-interaction limit of DFT in the gauge of the exchange-correlation-hole electrostatic potential, and we have computed it for small atoms and model quantum dots. A careful analysis of the PC model showed that this approximation is formulated in the same gauge, and a comparison with the exact results showed that it is locally reasonable in the atomic valence region.

Our formalism also strongly suggests that the local version of the Lieb-Oxford bound is formulated in the same conventional gauge of the exchange-correlation hole, and it is then certainly violated.

We have also discussed the idea of a local interpolation along the adiabatic connection. The values of the local energy density in the same gauge at $\lambda = 0$ and $\lambda = \infty$ are now available, either exactly or in an approximate way. Even if we have found that in the harmonic external potential, the physical energy density is not always in between the $\lambda = 0$ and the $\lambda = \infty$ curves, the regions of space in which the expected order is reversed are energetically not important. In the external Coulomb potential we have found, instead, the expected behavior $w_\infty(\mathbf{r}) \leq w_1(\mathbf{r}) \leq w_0(\mathbf{r})$ everywhere.

For accurate local interpolations at least the slope at $\lambda = 0$, and possibly the next leading term at $\lambda = \infty$, are also needed in a local form and in the same gauge. A first step towards the construction of a local slope at $\lambda = 0$ is to produce exact results for this quantity, crucial to assess approximations. This can be achieved with the Legendre transform techniques developed in refs. [45, 46]. A possible way to construct an approximate local slope is by the use of the “extended Overhauser model” [172–174] locally in a perturbative way. A local next leading term at $\lambda = \infty$ could also be constructed by deriving the exact exchange-correlation hole corresponding to the wavefunction of the zero-point oscillations, discussed in ref. [102].

Chapter 5

Kohn-Sham Density Functional Theory With Exchange-Correlation Functionals From the Strong-Interaction Limit

F. Malet, A. Mirtschink, J. C. Cremon, S. M. Reimann and P. Gori-Giorgi

“Kohn-Sham density functional theory for quantum wires in arbitrary correlation regimes”
editor’s suggestion, Phys. Rev. B **87**, 115146 (2013)

F. Malet, A. Mirtschink, K. J. H. Giesbertz, L. O. Wagner and P. Gori-Giorgi

“Exchange-correlation functionals from the strongly-interacting limit of DFT: Applications to model chemical systems”

Phys. Chem. Chem. Phys. **16**, 14551 (2014)

5.1 Kohn-Sham density functional theory with the strictly correlated electrons functional

The SCE expressions (3.12) and (3.18) show how the effects of strong correlation, captured by the $\lambda \rightarrow \infty$ limit of $F_\lambda[\rho]$ and rigorously represented by the highly non-local functional $V_{ee}^{SCE}[\rho]$ (3.15), are *exactly* transferred into the one-body SCE potential $v_{SCE}[\rho](\mathbf{r})$. This potential is exactly the one that *compensates* for the net electronic repulsion of a classical point-charge distribution. The KS-SCE approach to zeroth order consists in using this compensating potential to model the electronic

interaction in the Kohn-Sham reference system, *i.e.*

$$v_{Hxc}[\rho](\mathbf{r}) \approx \tilde{v}_{SCE}[\rho](\mathbf{r}), \quad \tilde{v}_{SCE}[\rho](\mathbf{r}) \equiv -v_{SCE}[\rho](\mathbf{r}) \quad (5.1)$$

Notice that we have defined $\tilde{v}_{SCE}[\rho](\mathbf{r}) = -v_{SCE}[\rho](\mathbf{r})$, as here we seek for an effective KS potential corresponding to the net electronic repulsion *acting* on an electron at position \mathbf{r} and not compensating for it. This idea was first presented by Malet and Gori-Giorgi [5].

More rigorously, by considering the $\lambda \rightarrow \infty$ asymptotic expansion of the integrand of (2.43) one obtains [102–104, 117, 128]

$$V_{ee}^\infty[\rho] = V_{ee}^{SCE}[\rho] + \frac{V_{ee}^{ZPE}[\rho]}{\sqrt{\lambda}} + O(\lambda^{-p}) \quad (5.2)$$

where $V_{ee}^{ZPE}[\rho]$ is the zero-point energy (ZPE) (3.20), which takes small oscillations of the electrons around their SCE equilibrium positions into account, and $p \geq 5/4$ [102]. Setting V_{ee}^λ equal to this expansion for all λ results by virtue of (2.27) in the general KS-SCE approximation to $E_{Hxc}[\rho]$

$$E_{Hxc}[\rho] \approx V_{ee}^{SCE}[\rho] + 2V_{ee}^{ZPE}[\rho] + \dots \quad (5.3)$$

When considering only the zeroth-order term of the $\lambda \rightarrow \infty$ expansion, *i.e.* $E_{Hxc}[\rho] \approx V_{ee}^{SCE}[\rho]$, the zeroth-order KS-SCE method results with the corresponding functional derivative

$$\frac{\delta E_{Hxc}[\rho]}{\delta \rho(\mathbf{r})} = \tilde{v}_{SCE}[\rho](\mathbf{r}) \quad (5.4)$$

which also sets the arbitrary constant in the potential (3.7)-(3.12) by requiring

$$\tilde{v}_{SCE}(|\mathbf{r}| \rightarrow \infty) = 0 \quad (5.5)$$

for the finite systems considered here. This to align the highest occupied KS (HOMO) eigenvalue with the exact chemical potential from the electron-deficient side $\varepsilon_{HOMO} = \mu^- = E_N - E_{N-1}$ [175, 176].

Taking the definition of the SCE functional $V_{ee}^{SCE}[\rho]$ (3.3) into account, the zeroth-order KS-SCE is equivalent to an approximation of the HK functional (2.15) of the form

$$\begin{aligned} \min_{\Phi \rightarrow \rho} \langle \Phi | \hat{T} + \hat{V}_{ee} | \Phi \rangle &\approx \min_{\Phi \rightarrow \rho} \langle \Phi | \hat{T} | \Phi \rangle + \min_{\Phi \rightarrow \rho} \langle \Phi | \hat{V}_{ee} | \Phi \rangle \\ &= T_s[\rho] + V_{ee}^{SCE}[\rho] \end{aligned} \quad (5.6)$$

Obviously, the minimizing wavefunctions for \hat{T} and \hat{V}_{ee} will be different: for the non-interacting functional $T_s[\rho]$ the minimizing wavefunction is usually a single Slater determinant $\Phi \rightarrow \Psi$, whereby for the second minimization the minimizing wavefunction is given by the SCE reference state $\Phi \rightarrow \Phi_{SCE}$ (3.10).

From the scaling properties of the functionals $F[\rho]$, $T_s[\rho]$ and $V_{ee}^{SCE}[\rho]$ [118, 177] it follows that the approximation (5.6) becomes accurate in the weak- and in the

strong-interaction limits, while probably less precise in between. To use the scaling relations one defines, for electrons in D dimensions, a scaled density

$$\rho_\gamma(\mathbf{r}) \equiv \gamma^D \rho(\gamma \mathbf{r}), \quad \gamma > 0 \quad (5.7)$$

We then have [118, 177]

$$\begin{aligned} F[\rho_\gamma] &= \gamma^2 F_{1/\gamma}[\rho] \\ T_s[\rho_\gamma] &= \gamma^2 T_s[\rho] \\ V_{ee}^{SCE}[\rho_\gamma] &= \gamma V_{ee}^{SCE}[\rho] \end{aligned} \quad (5.8)$$

where $F_{1/\gamma}[\rho]$ means that the coupling constant λ in $F_\lambda[\rho]$ (2.26) has been set to $1/\gamma$. We see that, both sides of (5.6) tend to $T_s[\rho_\gamma]$ when $\gamma \rightarrow \infty$ (high-density or weak-interaction limit) and to $V_{ee}^{SCE}[\rho_\gamma]$ when $\gamma \rightarrow 0$ (low-density or strong-interaction limit).

The KS-SCE approach treats thus both the kinetic energy and the electron-electron repulsion energy on the same footing, combining the advantages of KS-DFT with SCE-DFT. It allows one to address systems in the weak- and strong-interacting regime, as well as in the crossover regime. Standard KS-DFT emphasizes the non-interacting shell structure, properly described through the functional $T_s[\rho]$, but it misses the features of strong correlation. SCE-DFT, on the contrary, is biased towards localized “Wigner-like” structures in the density, described by $V_{ee}^{SCE}[\rho]$, and missing the fermionic shell structure. Many interesting systems lie in between the weak- and the strong-interaction limit, and their complex behavior arises precisely from the competition between the fermionic structure embodied in the kinetic energy and the correlation effects due to the electron-electron repulsion. By implementing the SCE potential in the KS scheme, we let these two factors compete in a self-consistent solution of the restricted KS equations with the SCE potential

$$\left[-\frac{1}{2} \nabla^2 + v_{ext}(\mathbf{r}) + \tilde{v}_{SCE}[\rho](\mathbf{r}) \right] \varphi_i(\mathbf{r}) = \varepsilon_i \varphi_i(\mathbf{r}) \quad (5.9)$$

which also follow from varying the KS-SCE functional (5.6) w.r.t. the single-particle orbitals appearing in $T_s[\rho]$.

Another neat property of the zeroth-order KS-SCE approach is that it yields always a lower bound to the exact ground-state energy. In fact, for any given ρ the r.h.s. of (5.6) is always less or equal than the l.h.s., as the minimum of a sum is always larger than the sum of the minima. As a consequence, for the ground state density $\rho = \rho_0$ we have the inequality

$$E[\rho_0] = F[\rho_0] + \int \rho_0 v_{ext} \geq T_s[\rho_0] + V_{ee}^{SCE}[\rho_0] + \int \rho_0 v_{ext} \quad (5.10)$$

which becomes even stronger when one minimizes the functional on the r.h.s. within the self-consistent KS-SCE procedure. This constitutes an important difference to the variational wavefunction methods section 2.1.2, which, instead, provide an upper bound to the exact ground state energy.

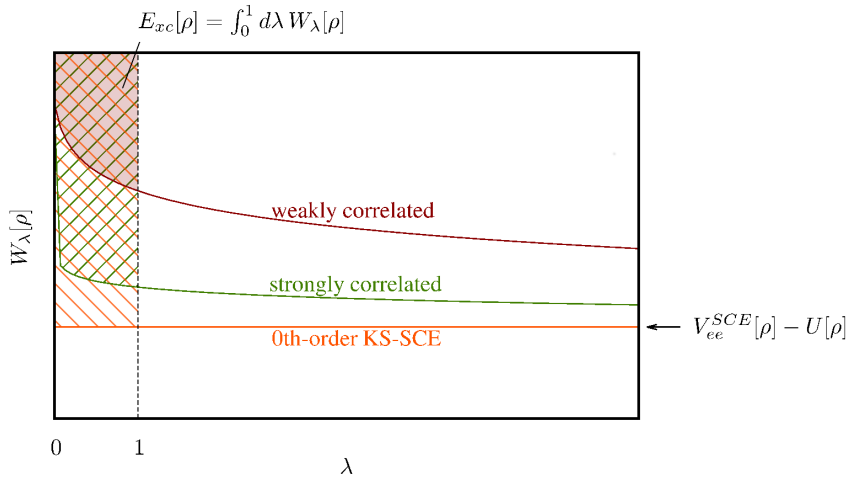


Figure 5.1: The KS-SCE approximation from the point of view of the adiabatic connection, section 2.2.3. We show typical $W_\lambda[\rho]$ curves for a weakly correlated and a strongly correlated system. The shaded areas represent the exchange-correlation energy $E_{xc}[\rho] = \int_0^1 d\lambda W_\lambda[\rho]$. The zeroth-order KS-SCE approximates $W_\lambda[\rho]$ with its value at $\lambda \rightarrow \infty$ for all λ , and is a good approximation for strongly correlated systems.

It is illustrative to represent the approximation made in KS-SCE graphically in terms of the standard adiabatic connection of DFT. In figure 5.1 we show $W_\lambda[\rho]$ as a function of λ for a weakly and a strongly correlated system. The area drawn by $W_\lambda[\rho]$, the λ -axis and the verticals $\lambda = 0$ and $\lambda = 1$, gives the exchange-correlation energy $E_{xc}[\rho]$. Zeroth-order KS-SCE approximates $W_\lambda[\rho]$ with its value at $\lambda \rightarrow \infty$ for all λ . This is evidently a good approximation only when the system is very correlated. In the weak-correlation regime the approximation becomes of minor importance, since here the essential accuracy of the KS-SCE method is provided by the non-interacting kinetic energy as derived from the scaling relations (5.8).

The accuracy in the intermediate-correlation regime can not be assessed from theoretical grounds and the impact of the approximation has to be studied by actual self-consistent solutions of the KS equations (5.9). Similar systems to Hooke's atom of chapter 4 with tuneable correlation can be used for a systematic analysis. Here, however, we restrict ourselves to one dimension. This sets a prototyping laboratory in which the implementational effort remains limited, and that allows for an emphasis on further functional development. One-dimensional systems of N electrons confined in a harmonic external potential also serve as useful models for quantum wires, where experimentally observable charge localizations occur as signatures of strong correlation, and the KS-SCE method will be used in section 5.3.4 to describe this localizations within DFT. A one-dimensional test laboratory for elementary chemistry will be employed in section 5.4, where quantitative corrections to the zeroth-order KS-SCE will be investigated as well.

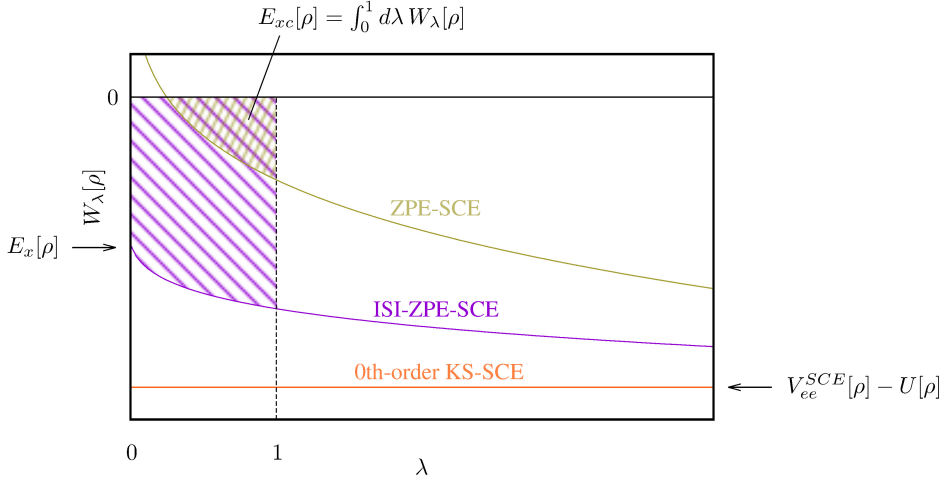


Figure 5.2: Schematic representation of the functional $W_\lambda[\rho]$ as a function of λ for the SCE approaches. Adding the zero-point term to the zeroth-order KS-SCE yields an overcorrected KS-ZPE-SCE energy, including also the positive area. The simple ISI approximation of (5.13)-(5.14) removes the excess energy by shifting the value of $W_\lambda[\rho]$ at $\lambda = 0$ to the exact exchange energy.

5.2 Higher-order corrections to zeroth-order KS-SCE

We have shown that the zeroth-order KS-SCE approximation of (5.6) corresponds to setting the coupling-constant integrand of (2.28) to $W_\lambda[\rho] = W_\infty[\rho]$, cf. figure 5.1. The exact correction to the zeroth-order approach would be the sum of the kinetic correlation energy $T_c[\rho]$ plus the electron-electron decorrelation energy $V_{ee}^d[\rho]$ [126, 178]

$$\begin{aligned} F[\rho] &\equiv T_s[\rho] + V_{ee}^{SCE}[\rho] + T_c[\rho] + V_{ee}^d[\rho] \\ T_c[\rho] &= \langle \Phi_{\lambda=1}[\rho] | \hat{T} | \Phi_{\lambda=1}[\rho] \rangle - T_s[\rho] \\ V_{ee}^d[\rho] &= \langle \Phi_{\lambda=1}[\rho] | \hat{V}_{ee} | \Phi_{\lambda=1}[\rho] \rangle - V_{ee}^{SCE}[\rho] \end{aligned} \quad (5.11)$$

From the expansion (5.3) we identify to the order $\lambda^{-1/2}$

$$T_c[\rho] + V_{ee}^d[\rho] \approx 2 V_{ee}^{ZPE}[\rho] \quad (5.12)$$

and the KS-ZPE-SCE method results. It turns out that this correction is in general way too large, as it includes the positive contribution to the integrand, coming from the integrable divergence $\propto \lambda^{-1/2}$. See also figure 5.2.

In order to get a more realistic correction, we consider here a simplified interaction-strength interpolation (ISI) on $W_\lambda[\rho]$ (2.28) [104, 128], which sets the value of $W_\lambda[\rho]$ at $\lambda = 0$ equal to its exact value, i.e. the exact exchange energy $E_x[\rho]$ with the KS

orbitals

$$\begin{aligned} W_{\lambda}^{ISI-ZPE}[\rho] &= W_{\infty}[\rho] + \frac{W'_{\infty}[\rho]}{\sqrt{\lambda + a[\rho]}} \\ a[\rho] &= \left(\frac{W'_{\infty}[\rho]}{E_x[\rho] - W_{\infty}[\rho]} \right)^2 \end{aligned} \quad (5.13)$$

In this way, we remove the excess positive contribution, as shown in fig 5.2. We then obtain the renormalized correction

$$T_c[\rho] + V_{ee}^d[\rho] \approx 2V_{ee}^{ZPE}[\rho] \left(\sqrt{1 + a[\rho]} - \sqrt{a[\rho]} \right) \quad (5.14)$$

This correction is size consistent only when a system dissociates into equal fragments. A full size-consistent approximation requires a local interpolation along the adiabatic connection, as already discussed in chapter 4 of this thesis.

A self-consistent solution of the KS equations with the ZPE-SCE functionals can not be obtained, as the functional derivative of the ZPE energy is yet not accessible (though it can be derived for $N = 2$ [179]). In section 5.4 this functionals will be applied at the post-functional level on the converged zeroth-order KS-SCE solution.

5.3 Strong correlation in one-dimensional model quantum wires

5.3.1 An overview

Carbon nanotubes, metallic-, semiconductor- and molecular nanowires can be identified as quantum wires. Among their common characteristics is a quantization effect in conductance that shows off with wire diameters at or below nanometer scale. Due to the low diameter compared to the electronic wavelength, electronic momentum is only transferred along the longitudinal and a one-dimensional model description is appropriate. The quantization in conductance can then be readily explained by assuming a harmonic confinement of the electrons, with the shape of the parabola related to the length of the wire. Another quantum mechanical effect manifests in the so-called $2k_F \rightarrow 4k_F$ crossover with increasing wire lengths, giving rise to charge localizations in the electronic density. This crossover can be seen as strong-correlation effect, as in long wires the electronic density is low and the Coulomb repulsion dominates over the kinetic energy of the electrons.

Charge localizations – reminiscent of the low-density Wigner crystallization [180] of the bulk electron gas and therefore commonly also referred to as Wigner localizations – have been observed experimentally in one-dimensional cleaved-edge overgrowth structures [181] or in the transport properties of InSb nanowire quantum-dots [182]. More recent experimental work clearly identified the formation of Wigner molecules in a one-dimensional quantum dot that was capacitively coupled to an atomic force microscope probe [183]. Wigner localization has also been investigated in other one-dimensional systems such as carbon nanotubes [184–186] (For a review see, e.g., ref. [187]). Finally, regarding practical applications, Wigner-localized

systems have been shown to be potentially useful, *e.g.*, for quantum-computing purposes [184, 188].

A lot of previous theoretical work on Wigner localization in nanostructures has focused on finite-sized quantum dots (see, *e.g.*, refs. [189–194]), and the crossover from liquid to localized states in the transport properties of the nanostructure has been addressed [195, 196].

When trying to model strongly correlated systems, the commonly employed methods encounter serious difficulties of different nature. *E.g.*, the configuration interaction (CI) approach, despite being in principle capable of describing any correlation regime, is in practice limited to the study of small systems with only very few particles due to its high computational cost. Such numerical challenges overwhelm even more in the strong-correlation limit due to the degeneracy of the different quantum states and the consequent need of larger Hilbert spaces in the calculations. The CI method will be described in more detail and used below for benchmarking purposes. Other wave-function methods, like quantum Monte Carlo [194, 197–199] and density matrix renormalization group [200], which rely to some extent on various approximations, can treat systems larger than the CI approach, but are still computationally expensive and limited to $N \lesssim 10^2$.

KS-DFT in contrast, highlights a computationally efficient approach for the treatment of larger quantum systems. The currently available approximations for the exchange-correlation functional, however, fail to describe the strongly correlated regime even at the qualitative level [133, 194, 201–204]. Allowing spin- and spatial-symmetry breaking may yield reasonable total energies, without, however, capturing the physics of charge localization in non-magnetic systems. Moreover, broken-symmetry solutions often yield a wrong characterization of various properties and the rigorous KS-DFT framework is partially lost (see, *e.g.*, refs. [200, 201, 203]).

Because it is in principle an exact theory, KS-DFT should be able to yield the exact energy and density even in the case of strong electronic correlation, without artificially breaking any symmetry. However, when dealing with practical KS-DFT, the KS non-interacting reference system might not be the best choice to address systems with dominant electron-electron interaction. For many years, huge efforts have been made in order to get a better characterization and understanding of the properties of the exact Kohn-Sham reference system (see, *e.g.*, refs. [45, 46, 133, 144, 148, 153, 171, 200, 205–215]). All these works reflected the large difficulties encountered when trying to obtain adequate approximations to describe strong correlation in the exact KS theory [88].

A new approach for the treatment of strong correlation in DFT was proposed in ref. [5] with the KS-SCE method as also described in section 5.1. Pilot tests of the KS-SCE framework showed that it is able to capture the features of both, the weakly and the strongly correlated regimes in model quantum wires, as well as in the $2k_F \rightarrow 4k_F$ crossover occurring in between them. A computational cost comparable to the one of standard KS-LDA was given. It has shown that the SCE functional yields a highly non-local approximation for the exchange-correlation energy functional, which is able to capture key features of strong correlation within the KS scheme without any artificial symmetry breaking. In this chapter we extend the studies presented in ref. [5] on one-dimensional model quantum wires, demonstrating once more the ability of

the KS-SCE framework to describe strong-correlation phenomena. Conclusions on the quantitative performance of the KS-SCE method can be drawn by comparison to CI calculations, when quantum wires in different correlation regimes are considered. Further comparison is made with the KS-LDA method.

5.3.2 A quantum wire model in one dimension

We consider N electrons in the one-dimensional model of a quantum wire, as suggested in refs. [204, 216]

$$\hat{H} = -\frac{1}{2} \sum_i^N \frac{\partial^2}{\partial x_i^2} + \sum_{i,j>i}^N w_b(|x_i - x_j|) + \sum_i^N v_{ext}(x_i) \quad (5.15)$$

in which the effective electron-electron interaction is obtained by integrating the Coulomb repulsion on the lateral degrees of freedom of the physical wire [216, 217], and is given by

$$w_b(x) = \frac{\sqrt{\pi}}{2b} \exp\left(\frac{x^2}{4b^2}\right) \operatorname{erfc}\left(\frac{x}{2b}\right) \quad (5.16)$$

The parameter b fixes the thickness of the wire, set to $b = 0.1$ throughout this work, and $\operatorname{erfc}(x)$ is the complementary error function. The interaction $w_b(x)$ has a long-range coulombic tail, $w_b(x \rightarrow \infty) = 1/x$, and is finite at the origin, where it has a cusp. As in ref. [204], we consider an external harmonic confinement in the direction of motion of the electrons

$$v_{ext}(x) = \frac{1}{2} \omega^2 x^2 \quad (5.17)$$

The wire can be characterized by an effective confinement-length parameter L defined by

$$\omega \equiv \frac{4}{L^2} \quad (5.18)$$

5.3.3 Supplemental computational approaches

CI method In the configuration-interaction calculations, the full many-body wavefunction is expanded as a linear combination of Slater determinants, constructed with the non-interacting harmonic oscillator orbitals. A matrix representation of the Hamiltonian in this basis is then numerically diagonalized to find the eigenstates of the system. The number of possible ways to place N particles in a given set of orbitals increases rapidly as a function of N , such that only small particle numbers are tractable. For our studies we could perform calculations for $N \leq 5$. Also, the stronger the interaction, the more basis orbitals are generally required to obtain a good approximation. For the present physical systems with the largest length L , about 20–40 orbitals were needed to get converged solutions, which resulted in Hilbert space dimensions in the range 10^5 – 10^6 . For a more detailed description of the method, see refs. [218, 219].

KS-LDA method KS-DFT calculations were carried out with the local density approximation (LDA) using the exchange-correlation energy per particle $\epsilon_{xc} = \epsilon_x + \epsilon_c$ for a one-dimensional homogeneous electron gas, with the renormalized Coulomb interaction $w_b(x)$, as detailed in ref. [204]. The exchange term ϵ_x is given by

$$\epsilon_x(r_s) = \frac{1}{2} \int_{-\infty}^{+\infty} \frac{dq}{2\pi} v_b(q) [S_0(q) - 1] \quad (5.19)$$

where $v_b(q)$ is the Fourier transform of the interaction potential, $S_0(q)$ is the non-interacting static structure factor, and $r_s \equiv \frac{1}{2\rho}$ [220]. To increase the numerical stability, we have interpolated between the Taylor expansions of $\epsilon_x(r_s)$ at small and large r_s up to order 14. For the correlation term we have used the results of Casula *et al.* [221], who have parametrized their QMC data as

$$\epsilon_c(r_s) = -\frac{r_s}{A + Br_s^{\gamma_1} + Cr_s^2} \ln(1 + Dr_s + Er_s^{\gamma_2}) \quad (5.20)$$

where the different parameters are given in table IV of ref. [221] for several values of b .

5.3.4 KS-SCE treatment of one-dimensional model quantum wires

We have implemented the zeroth-order KS-SCE method in one-dimension by self-consistently solving the KS equations with the SCE potential $\tilde{v}_{SCE}[\rho](\mathbf{r})$ (5.9) in a spin-restricted framework. With the co-motion functions for one dimension, *cf.* section 3.2, the SCE potential is evaluated by integrating its derivative

$$\tilde{v}'_{SCE}(x) = \sum_{i=2}^N w'_b(|x - f_i(x)|) \text{sgn}(x - f_i(x)) \quad (5.21)$$

with the boundary condition $\tilde{v}_{SCE}(|x| \rightarrow \infty) = 0$, and the interaction $w_b(x)$ from (5.16). The corresponding SCE energy writes

$$V_{ee}^{SCE}[\rho] = \frac{1}{2} \int_0^\infty dx \rho(x) \sum_{i=2}^N w_b(|x - f_i(x)|) \quad (5.22)$$

Figure 5.3 shows the electron densities for $N = 4$ and different effective confinement lengths $L = 2\omega^{-1/2}$, obtained with the KS-SCE, the CI and the KS-LDA approaches. One can see that the three methods show qualitative agreement in the weakly-correlated regime with $L = 1$. The densities have $N/2$ peaks, given by Friedel-like oscillations with wave number $2k_F^{eff}$, where $k_F^{eff} = \pi\tilde{\rho}/2$ is the effective Fermi wavenumber, determined by the average density in the bulk of the trap $\tilde{\rho}$.

As the confinement length of the wire increases, $L = 15, 70$, the interactions start to dominate. Whereas the KS-SCE and the CI results are still in qualitative agreement for this correlation regimes, the KS-LDA clearly provides a physical wrong description

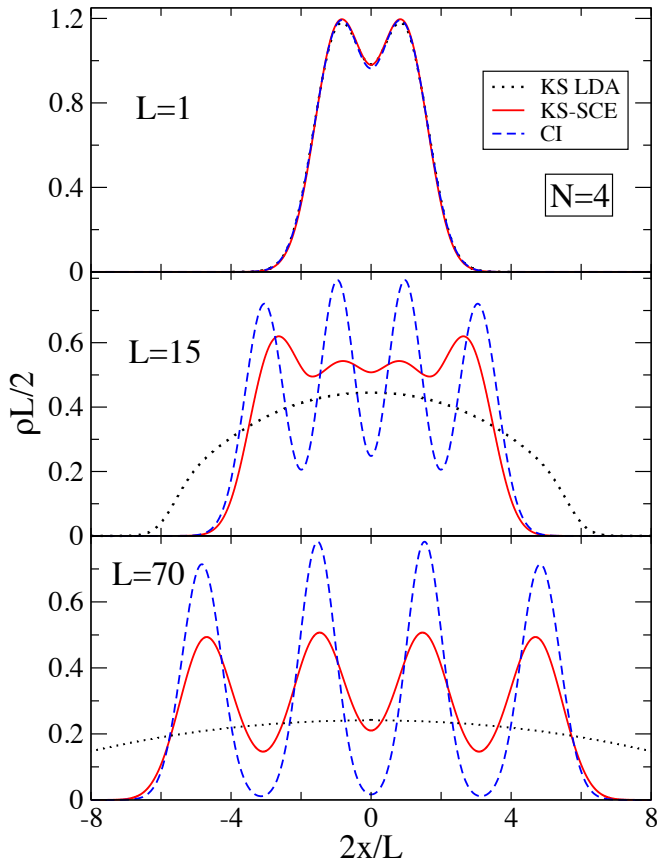


Figure 5.3: Electron densities $\rho(\mathbf{r})$ for $N = 4$ and $L = 1, 15$ and 70 obtained with the KS-SCE, CI and KS-LDA approaches. The results are given in units of the effective confinement length $L = 2\omega^{-1/2}$.

of the systems. Indeed one can see that the densities obtained from the KS-SCE and the CI methods develop a four-peak structure, corresponding to charge localization and indicating that the system enters the crossover between the weakly and the strongly correlated regimes (the $2k_F \rightarrow 4k_F$ crossover), and the KS-LDA yields a flat density. This is a typical error of local and semi-local density functionals that leads to difficulties in the description of, e.g., systems close to the Mott insulating regime and in bond breaking (yielding wrong molecular dissociation curves, see also section 5.4). In such cases, better total energies are obtained by spin-symmetry breaking. This, as already discussed, does not yield a satisfactory physical description of such systems, missing many key features and giving a wrong characterization of several properties (see, e.g., refs. [200, 201, 203]).

In order to obtain charge localization within the restricted KS scheme, the self-consistent KS potential must build “bumps” (or barriers) between the electrons. These barriers are a very non-local effect and are known to be a key property of the exact Kohn-Sham potential [144, 171]. From figure 5.4 we see that also the KS-SCE method shows the above-mentioned barriers in the self-consistent KS potentials, which we plot together with the corresponding densities for $N = 4$ and $N = 5$ for $L = 70$. One can see that each of the N peaks in the density corresponds to a minimum in the KS potential, which is separated from the neighboring ones by barriers. At the maxima the KS potential has a discontinuous, but finite, first derivative [120]. It arises due to the classical nature of the SCE potential, and it is not expected to appear in the exact KS potential (indeed, it does not appear in any of the available calculations of the “exact” KS potential obtained by inversion).

One can also parallel our results with the recent work on the KS exchange-correlation potential for the one-dimensional Hubbard chains [215, 222, 223]. Vieira [215] has shown that the exact exchange-correlation potential for a one-dimensional Hubbard chain with hopping parameter t and on-site interaction U , obtained by inversion from the exact many-body solution, always oscillates with frequency $4k_F$, while the density oscillations undergo a $2k_F \rightarrow 4k_F$ crossover with increasing U/t . The crossover in the density is thus due to the increase in the amplitude of the exchange-correlation potential oscillations. In figure 5.5 we show the KS-SCE exchange-correlation potentials for $N = 4$ electrons in the weakly ($L = 2$) and strongly ($L = 70$) correlated regimes together with the densities and the occupied KS eigenvalues. We see that the KS-SCE self-consistent results are in qualitative agreement with the findings of ref. [215]: the oscillations in the exchange-correlation potential have essentially a frequency $4k_F$ also in the weakly correlated case, with amplitude that increases with increasing L (due to the scaling (5.8), the parameter L plays here a role similar to U/t for the Hubbard chain). In the two lower panels of the same figure we also further clarify the $2k_F \rightarrow 4k_F$ crossover in the KS framework: the $4k_F$ regime in the density oscillations occurs when the barriers in the total KS potential (due to the large oscillations of the xc potential) are high enough to accommodate the KS eigenvalues. Classically forbidden regions inside the trap are therefore created moderating the density crossover.

In table 5.1 we report the total energies obtained with the three approaches, KS-SCE, CI and KS-LDA, for different values of the parameters L and N . It can be seen that in the weakly correlated regime, represented here by $L = 1$ and 2 , the error

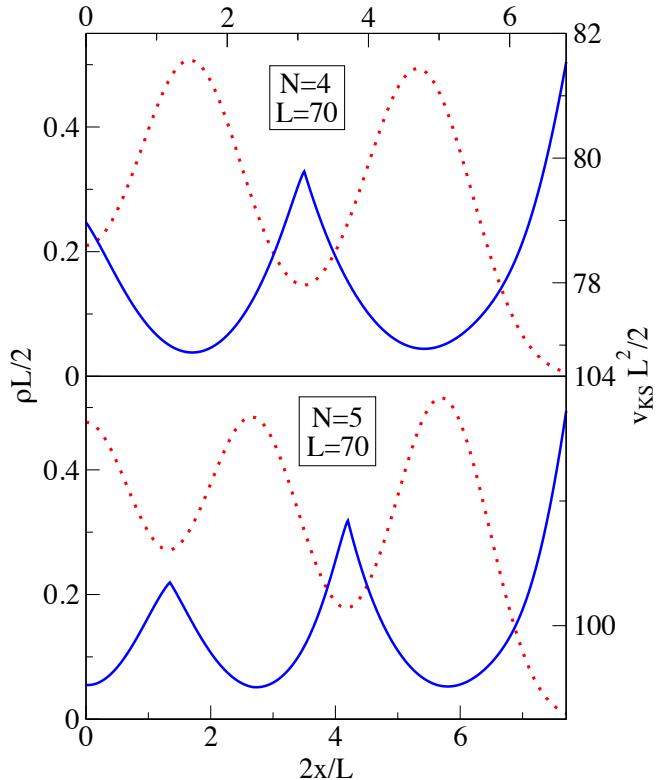


Figure 5.4: Self-consistent KS potentials $v_{KS}(\mathbf{r})$ obtained with the KS-SCE method for $N = 4$ and $N = 5$, with effective confinement length $L = 70$ (blue solid lines). The corresponding densities $\rho(\mathbf{r})$ are also shown (red dotted lines). Notice that for the sake of clarity only the results for $x > 0$ are shown. The results are given in units of the effective confinement length $L = 2\omega^{-1/2}$.

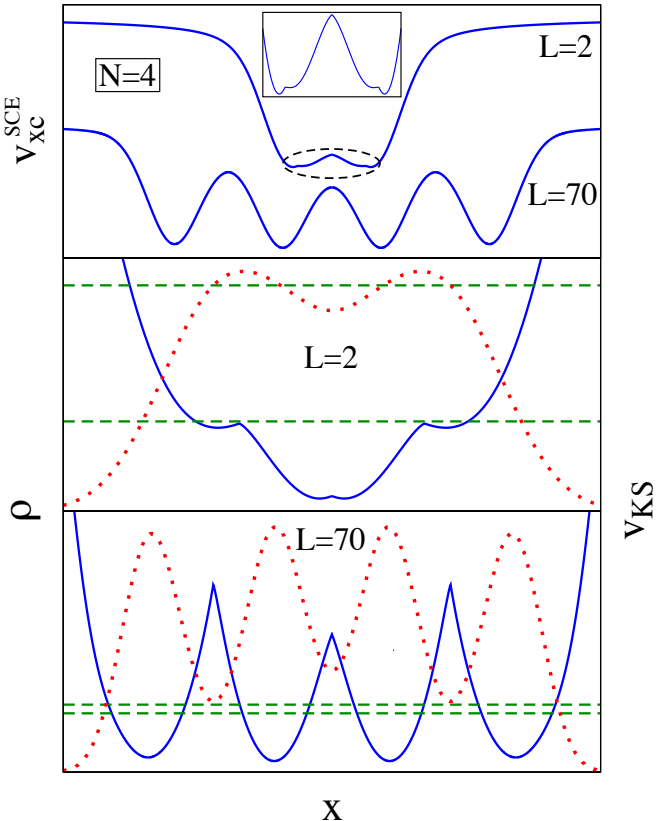


Figure 5.5: Top panel: the self-consistent KS-SCE exchange-correlation potential $v_{xc}(\mathbf{r})$ for $N = 4$ at weak correlation $L = 2$ and strong correlation $L = 70$. In the inset the oscillating part of the exchange-correlation potential at $L = 2$ is enlarged. Both potentials are shifted w.r.t. each other, the usual asymptotic limit for each one is 0. Middle panel: the total self-consistent KS-SCE potential $v_{KS}(\mathbf{r})$ (blue, solid line), the corresponding density $\rho(\mathbf{r})$ (red dotted line), and the two occupied KS eigenvalues (green dashed horizontal lines) for the weakly correlated $L = 2$ wire. In this case we see that in the KS system there are no classically forbidden regions inside the trap. Bottom panel: the same as in the middle panel for the strongly correlated $L = 70$ wire. In this case we clearly see the classically forbidden regions inside the trap created by the barriers in the SCE potential. The results are given in arbitrary units.

N	L	E^{KS-SCE}	E^{CI}	E^{KS-LDA}
2	2	1.81	2.49	2.59
2	15	0.0942	0.106	0.130
2	70	0.0112	0.0115	0.0182
4	1	25.08	28.42	28.57
4	2	8.46	10.60	10.68
4	15	0.491	0.541	0.580
4	70	0.0602	0.0629	0.0771
5	15	0.787	0.871	0.915
5	70	0.099	0.102	0.121

Table 5.1: Total ground-state energies obtained with the KS-SCE, full-CI and KS-LDA approaches for different values of the particle number N and effective-confinement length $L = 2\omega^{-1/2}$.

made by the KS-SCE approach is larger than the one corresponding to the KS-LDA. The results also clearly show that, as previously discussed, KS-SCE is always a lower bound to the total energy. As the systems become more correlated with increasing L , the KS-SCE and the CI results approach each other, whereas the values given by the KS-LDA are less accurate, similar to the corresponding densities of figure 5.3.

The KS-SCE method is, in all respects, a standard KS formalism with a highly non-local exchange-correlation functional, whose functional derivative yields a local multiplicative KS potential. We can thus compare the highest occupied KS eigenvalue with the exact ionization potential. This is done in table 5.2 where we compare the KS-SCE and the KS-LDA eigenvalues with the accurate ionization potentials $E_{N-1} - E_N$, calculated from the total energies of the CI method. Notice that $\tilde{v}_{SCE}(\mathbf{r})$ as an approximate $v_{Hxc}(\mathbf{r})$ has the right asymptotics in the limit $|\mathbf{r}| \rightarrow \infty$ as can be implied from (5.21). Hence, the KS-SCE gives good results also in the weaker correlated regimes. KS-LDA, as commonly known, yields too high eigenvalues due to the too fast exponential decay of the exchange-correlation potential for $|x| \rightarrow \infty$.

The numerical cost of the CI method increases exponentially with the number of particles, and this limitation becomes stronger as correlation starts to dominate. In the calculations reported above, for the $N = 5, L = 70$ case we diagonalized a matrix where the eigenvectors had a dimension of about 3.5×10^5 . While it is technically possible to treat larger matrices, the rapid growth of the basis size still efficiently limits the number of particles one can handle. (For $N = 6$ electrons, using the same basis orbitals, the corresponding dimension is roughly 2.6×10^6 .) The KS-SCE method in one-dimension, on the contrary, has a numerical cost comparable to the one of KS-LDA, therefore allowing to study strongly correlated systems with much larger particle numbers. In figure 5.6 we show the electron densities and corresponding KS potentials obtained with the KS-SCE method for $N = 8, 16$ and 32 , for different values of L : in the upper two panels we see how, at fixed number of particles $N = 8$,

N	L	$-\varepsilon_{HOMO}^{KS-SCE}$	ΔE^{CI}	$-\varepsilon_{HOMO}^{KS-LDA}$
2	2	1.65	1.99	2.56
2	15	0.104	0.097	0.263
2	70	0.0126	0.0111	0.04087
4	1	11.26	11.86	12.56
4	2	4.08	4.65	5.02
4	15	0.248	0.256	0.453
4	70	0.0318	0.0304	0.06909
5	15	0.325	0.330	0.539
5	70	0.0408	0.0391	0.08172

Table 5.2: Same as table 5.1 for the highest occupied KS eigenvalues ε_{HOMO} obtained from KS-SCE and KS-LDA with the full-CI values for $\Delta E = E_{N-1} - E_N$.

the bumps in the KS potential and the amplitude of the density oscillations become larger with increasing L . For fixed effective confinement length $L = 150$, we see from the lower three panels how an increasing particle number N leads to less pronounced features of strong correlation, according to the scaling (5.8).

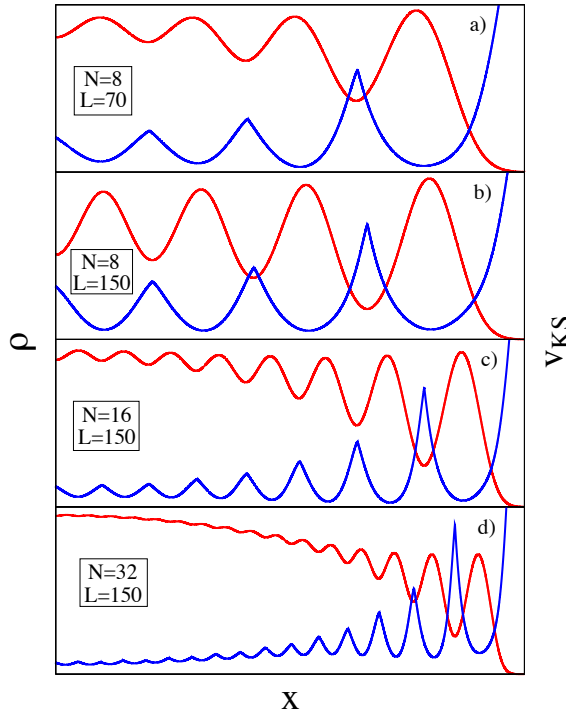


Figure 5.6: Ks-SCE electron density $\rho(\mathbf{r})$ (red) and corresponding potential $v_{KS}(\mathbf{r})$ (blue) for different particle numbers N and effective confinement lengths L . As in figure 5.4, only the results for $x > 0$ are shown. The results are given in arbitrary units.

5.3.5 Conclusions

We have used the exact strong-interaction limit of the Hohenberg-Kohn functional to approximate the exchange-correlation energy and potential of KS-DFT. The obtained zeroth-order KS-SCE approach was used subsequently to address quasi-one-dimensional quantum wires in the weak-, intermediate- and strong-correlation regime, comparing the results with those obtained from CI and KS-LDA runs.

In the weakly correlated regime, the three approaches give qualitatively similar results, with electronic densities showing $N/2$ peaks, associated with the double occupancy of the single-particle levels that dominate the system. In this regime, KS-LDA performs overall better than KS-SCE. As correlations become dominant, the KS-SCE and the CI densities start to develop additional maxima, corresponding to charge-density localization, whereas the KS-LDA provides a qualitatively wrong description of the system, yielding a very flat and delocalized density.

For an accurate method in the intermediate-correlation regime corrections to the KS-SCE method are required. This corrections can follow the same hierarchy as conventional DFAs, meaning local, semi-local and fully non-local corrections to KS-SCE can be explored. An example of a local correction will be introduced in chapter 7 of this thesis. To improve the energy estimate at least at a post-functional level the ZPE-SCE functionals can be used, as done in the next section.

The well-known “bumps” show up in the SCE potential of the KS-SCE approach and are responsible for the proper description of charge localization in strongly correlated wires. Moreover, the associated KS-SCE exchange-correlation potential shows the right asymptotic behavior, yielding accurate chemical potentials across the entire correlation range.

5.4 Strong correlation in one-dimensional models for elementary chemistry

5.4.1 An overview

The applications of the KS-SCE method to one-dimensional model quantum wires have shown that the SCE exchange-correlation potential is able to describe the physics of strong correlation within the restricted KS non-interacting system. One can thus ask, if this formalism also accurately describes chemical systems, especially in situations where standard DFAs fail. Examples are provided by negative ions, that fall in the intermediate-correlation regime, and stretched bonds, where strong correlation is significant.

Before venturing into the challenging task of an implementation of the SCE functional (or approximations thereof) for general three-dimensional systems, we can explore the relevance of this functional already in one dimension. Models for simple chemical systems are employed, which have recently been shown to be a useful testing ground for functionals in a chemistry context [224, 225], offering a reasonably close one-dimensional description of their three-dimensional counterparts. For comparison the KS-SCE method is solved self-consistently along with the DMRG, full-CI, KS-LDA and KS-LSDA methods. The ZPE corrections to the SCE functional are evaluated at a post-functional level on the KS-SCE solution.

5.4.2 Chemistry models in one dimension

One-dimensional models for different atoms, ions and for the H₂ molecule are given in refs. [204, 216]. For N electrons the Hamiltonian reads

$$\hat{H} = -\frac{1}{2} \sum_i^N \frac{\partial^2}{\partial x_i^2} + \sum_{i,j>i}^N v_{soft}(|x_i - x_j|) + \sum_i^N v_{ext}(x_i) \quad (5.23)$$

where $v_{soft}(x)$ is the soft-Coulomb interaction¹

$$v_{soft}(x) = \frac{q_1 q_2}{\sqrt{1 + x^2}} \quad (5.24)$$

that is also used for the electron-nuclei interaction in $v_{ext}(x)$, and the charges q_1 and q_2 are given *w.r.t.* the electrons/nuclei. For the calculations presented here we have considered nuclear charges $q = 1, 2, 3$ and 4 , corresponding to the elements H, He, Li and Be. In each case we have also studied different ionic species. Finally, for the H_2 molecule, we have considered interatomic separations R_{H-H} in the range between 0 and 20 atomic units.

5.4.3 Supplemental computational approaches

We validate the KS-SCE method by comparing it with the density matrix renormalization group (DMRG) method as described in *ref.* [224]. For the H_2 potential energy curve, we have also carried out full-CI calculations on a numerical grid. For further comparison, calculations with KS-LDA in both the spin-restricted (LDA) and spin-unrestricted (LSDA) formulations were performed. The parametrization of the L(S)DA exchange-correlation functional with soft-coulomb interaction is taken from *ref.* [225].

5.4.4 KS-SCE treatment of one-dimensional atoms and ions

Total energies and ionization potentials for the elements H, He, Li and Be in their neutral and ionic configurations can be obtained with the same numerical implementation of the KS-SCE method as in the section above. One therefore only has to replace the external potential and the electronic interaction in (5.21)-(5.22) by their corresponding soft-coulomb counterparts from (5.24). The post-functional calculations with the ZPE-SCE functionals on the converged KS-SCE solution were undertaken within the Wolfram Mathematica environment [155].

Table 5.3 shows the total energies for different atomic elements, comparing the results obtained with the KS-SCE, DMRG and KS-L(S)DA approaches. We see that KS-SCE in almost all cases largely underestimates the total energies, except for the $N = 1$ systems, for which it is exact. It provides a lower bound to the total energy that is not very tight, and resulting in an accuracy worse than the one of L(S)DA. This is not surprising, as the considered systems fall in the intermediate-correlation regime, where it has already been shown that quantitative accuracy can not be expected from the KS-SCE method. Adding the bare ZPE correction of (5.12) yields energies way too high, as discussed in section 5.2: *e.g.*, for Li we obtain -3.66 H and for Be -5.92 H. The ISI-ZPE correction of (5.13), instead, improves the results consistently, getting much closer to the DMRG calculations than L(S)DA.

Particularly interesting are the negative ions, which are a notorious problem in approximate KS-DFT. Similarly to the three-dimensional case, the anions are all unbound in L(S)DA, while KS-SCE overbinds, yielding bound systems also for He^- and Li^- , which are unbound in DMRG. Notice that within a Hartree-Fock description and

¹The regular Coulomb interaction has to be avoided, as due to the divergence in the Coulomb interaction the Hartree energy $U[\rho]$ would diverge too, not allowing for an KS-LDA treatment of this systems.

	E^{KS-LDA}	$E^{KS-LSDA}$	E^{DMRG}	E^{KS-SCE}	$E^{ISI-ZPE-SCE}$
H	-0.60	-0.65	-0.67	-0.67	-0.67
H^-	-	-	-0.73	-0.89	-0.75
He	-2.20	-2.20	-2.24	-2.38	-2.24
He^-	-	-	-	-2.42	-2.21
He^+	-1.41	-1.45	-1.48	-1.48	-1.48
Li	-4.16	-4.18	-4.21	-4.43	-4.21
Li^-	-	-	-	-4.51	-4.17
Li^+	-3.85	-3.85	-3.90	-4.02	-3.90
Li^{2+}	-2.26	-2.30	-2.34	-2.34	-2.34
Be	-6.76	-6.76	-6.79	-7.12	-6.77
Be^+	-6.39	-6.41	-6.45	-6.65	-6.45
Be^{2+}	-5.56	-5.56	-5.62	-5.72	-5.61
Be^{3+}	-3.13	-3.18	-3.21	-3.21	-3.21

Table 5.3: Total ground state energies obtained with the different approaches. The DMRG data is taken from ref. [224].

the one-dimensional model settings employed here, H^- is predicted to be found bound ($E_{H^-}^{HF} = -0.69$ and $\varepsilon_{HOMO,H^-}^{HF} = -0.05$). This is in contrast to the HF treatment of three-dimensional H^- , and care has to be taken when inferring from one to three dimensions. An extended study of the anion binding in the He isoelectronic series in three dimensions with the KS-SCE method will be presented in chapter 7 of this thesis. The inclusion of the ISI-ZPE term correctly predicts H^- to be bound (with a rather good energy) and He^- and Li^- to be unbound (as their energy becomes higher than the one of the corresponding neutral system). Notice also that in contrast to the findings in ref. [225], where the one-dimensional He^- and Li^- were reported to be bound although the value for the energy of Li^- was higher than the one of Li, with DMRG we found these two one-dimensional anions to be unbound.

Table 5.4 compares the HOMO eigenvalues with the ionization energies obtained from DMRG. We see that the KS-SCE HOMO yields again quite accurate estimates of the ionization energies, thanks to the right asymptotic behavior of the SCE potential. Since we applied the ISI-ZPE correction only at the postfunctional level, there are no corrected HOMO eigenvalues.

5.4.5 KS-SCE treatment of the one-dimensional H_2 molecule

We now turn to a paradigmatic case example for strong correlation in molecular compounds, given by the stretched H_2 molecule. From theoretical grounds it can be already said that the KS-SCE method will yield the correct dissociation limit (it

	$-\varepsilon_{HOMO}^{KS-LDA}$	$-\varepsilon_{HOMO}^{KS-LSDA}$	$\Delta E_{N=1,2}^{DMRG}$	$-\varepsilon_{HOMO}^{KS-SCE}$
H	0.35	0.41	0.67	0.67
H^-	-	-	0.06	0.089
He	0.48	0.48	0.75	0.72
He^+	1.12	1.18	1.48	1.48
Li	0.14	0.17	0.31	0.32
Li^+	1.24	1.24	1.56	1.50
Li^{2+}	1.95	2.00	2.34	2.34
Be	0.16	0.16	0.34	0.34
Be^+	0.60	0.63	0.83	0.81
Be^{2+}	2.06	2.06	2.41	2.34
Be^{3+}	2.81	2.86	3.21	3.21

Table 5.4: Same as table 5.3 for the ionization energies (using the HOMO eigenvalue ε_{HOMO} for the DFT approaches). The DMRG values are given by $\Delta E = E_{N-1} - E_N$ [224].

is size-consistent and self-interaction free). When the dissociation limit is left by positioning the nuclei closer together, the intermediate-correlation regime is entered again, and corrections to the zeroth-order KS-SCE approach become relevant.

Figure 5.7 shows the dissociation energy curves for the considered methods. One can see that, whereas the KS-LDA, KS-LSDA and HF energies are relatively close to the CI values near equilibrium, the KS-SCE approach yields a large error due to its overestimation of the electronic correlation. As the interatomic distance increases, one can see that the spin-restricted LDA and HF energies as usual become too positive. The KS-SCE result becomes now increasingly more accurate, tending to the exact dissociation limit where the KS-SCE approach adequately captures the effects of strong correlation. In total is the binding energy error of the KS-LDA approach comparable to the one of the KS-SCE.

In the same figure we also show the energy curve when the full ZPE correction and the renormalized ISI-ZPE corrections are added, at a post-functional level, to the zeroth-order KS-SCE energies. One can see that the addition of the bare ZPE yields again too high energies. The correction by the ISI-ZPE, instead, gives very good results for $R_{H-H} \lesssim 4$ a.u, but displays a “bump” in the potential energy curve, which now tends from above to the exact dissociation limit, reached only at $R_{H-H} \gtrsim 20$.

Figure 5.8 shows the electronic densities obtained with the KS-SCE, KS-LDA and full-CI approaches for different interatomic separations R_{H-H} . One can see that for the near-equilibrium configuration $R_{H-H} = 1.5$ at the bond midpoint, the KS-SCE density is slightly less peaked due to the above-mentioned overestimation of the correlation, leading to a too diffuse density in the self-consistent competition of kinetic- and electronic energy in the KS-SCE functional (5.6). The KS-LDA approach

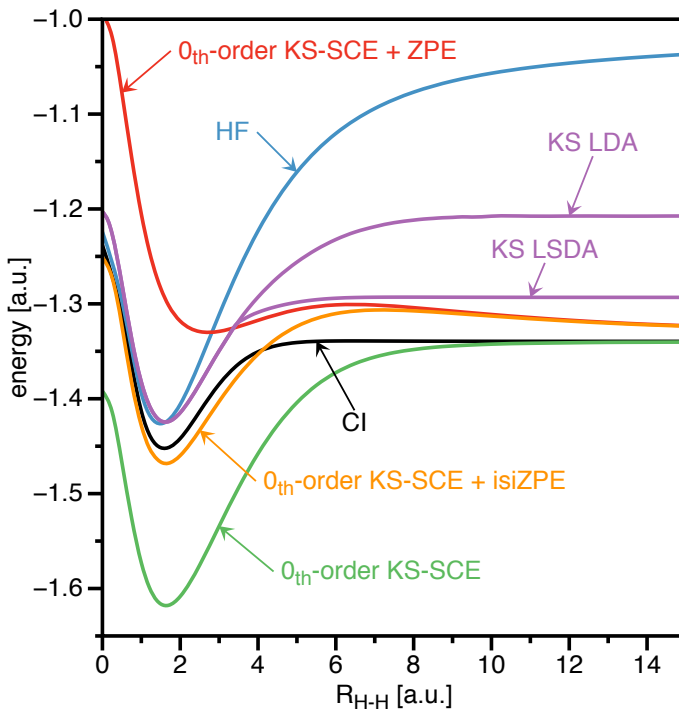


Figure 5.7: Dissociation energy curves for H_2 with several approaches.

shows very good agreement with the exact result at small bond distances. As the interatomic separation increases to $R_{\text{H}-\text{H}} = 5$, the KS-LDA largely overestimates the density at the bond midpoint, clearly reflecting its inability to properly describe the molecular dissociation process. This is due to self-interaction errors and the entailed delocalization error in the LDA. The KS-SCE approach, instead, shows an improving tendency in the direction of the exact result, in accordance with the energy curve of figure 5.7. Finally, in the dissociation limit $R_{\text{H}-\text{H}} = 15$, the agreement between the KS-SCE and CI densities is excellent, whereas the spin-restricted KS-LDA density is still too delocalized.

The rapid decrease of the exact density at the bond midpoint with increasing atomic separations $R_{\text{H}-\text{H}}$ is related to the presence of a barrier in the KS potential, the same barrier as observed in section 5.3.4 [144, 171]. In figure 5.9 the KS potential for the H_2 molecule and is shown for various approaches. The exact barrier has a component that is known to saturate for large internuclear distances $R_{\text{H}-\text{H}}$, with a height determined by the ionization potential [171]. This component is due to the kinetic correlation energy [144, 171], and is consequently not captured by the SCE functional, as it lacks the kinetic energy contribution. The KS-SCE barrier therefore decreases when $R_{\text{H}-\text{H}}$ increases, and becomes small at large $R_{\text{H}-\text{H}}$. However, at large internuclear distances, the energetic contribution of the barrier is negligible, and even a very small barrier (as the one obtained in KS-SCE) is enough to get an accurate

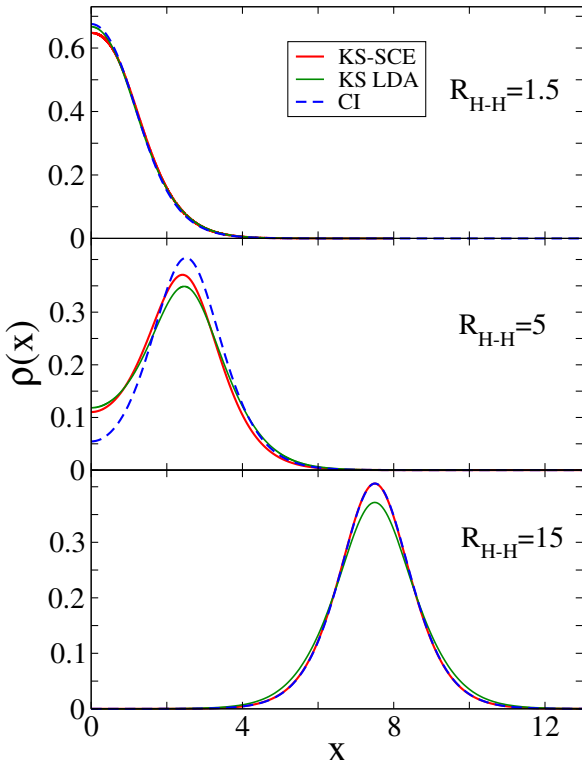


Figure 5.8: Densities for the H_2 molecule corresponding to different interatomic separations obtained with the KS-SCE, KS-LDA and full-CI approaches.

localized density with the correct energy at dissociation. In KS-LDA we see at large $R_{\text{H}-\text{H}}$ a barrier localized on the atoms rather than in the bond midpoint. Due to the locality of the LDA potential a barrier in the bond midpoint can not arise, as the LDA potential always follows the density profile.

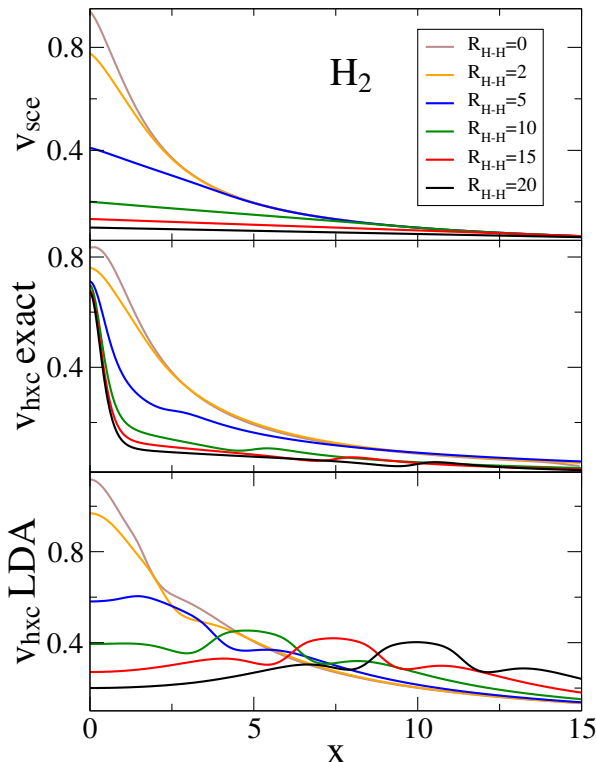


Figure 5.9: Exact Kohn-Sham potential (by inversion), Hartree-exchange-correlation potential from KS-LDA, and SCE potential for different interatomic separations $R_{\text{H-H}}$ for the one-dimensional H_2 molecule.

5.4.6 Conclusions

While for low-dimensional nanodevices the KS-SCE approach is very accurate in the strong-correlation regime [226, 227], and therefore offering an original DFT tool for the realistic modeling of such systems, chemical systems are usually not close enough to the strong-interaction regime and total energies are underestimated within KS-SCE. We see, however, that the SCE functional is able to bind anions, and to capture the strong correlation of a stretched bond, both situations in which traditional DFAs fail. Due to the right asymptotic properties of the SCE potential, the KS-SCE HOMO always yields an accurate estimate for ionization energies. With a correction that is renormalized by exact exchange, the post-functional ISI-ZPE is finally able to yield accurate results for total energies, predicting the delicate physics of negative ions.

Overall, it seems promising to use the SCE physics as an ingredient for functional approximations. An exact evaluation of the co-motion functions in the general three-dimensional case might turn out to be too demanding, but it should be possible to build approximate co-motion functions, or, more generally, non-local functionals inspired by the SCE mathematical formalism.

It seems also clear that the accuracy of KS-SCE is somewhat complementary to the ones of standard functionals, so that corrections to SCE either including exact exchange, or based on standard approximations can be pursued in the future. An LDA correction to the SCE functional will be considered in chapter 7 of this thesis.

Chapter 6

The Derivative Discontinuity in the Strong-Interaction Limit of Density Functional Theory

A. Mirtschink, M. Seidl and P. Gori-Giorgi

“The derivative discontinuity in the strong-interaction limit of density functional theory”

Phys. Rev. Lett. **111**, 126402 (2013)

6.1 An overview

Exact KS-DFT has many weird and counterintuitive features often missed by the available approximations. One of the weirdest and most elusive of these features is the derivative discontinuity of the exact exchange-correlation energy functional at integer particle numbers N [228], which has been an incredibly long-debated issue [116, 214, 229–237] because its formal derivation relies on some (very reasonable) assumptions. This discontinuity is a shift of the exact KS potential by a constant Δ_{xc} when to an N -electron system even a only very tiny fraction η of an electron is added, aligning the chemical potential of the non-interacting KS system to the exact, interacting, one. An illustration can be found in figure 6.1. The derivative discontinuity is crucial for the KS-DFT description of some physical properties. E.g., it gives the difference between the KS gap and the fundamental conductance gap [238–240], it allows for a correct dissociation of molecular bond [133, 228], and it is required for the proper modeling of long-range charge-transfer excitations in time-dependent DFT [241–243]. It also plays a significant role in quantum transport, especially to capture the physics of the Coulomb blockade and the Kondo effect [208, 209, 244–246]. These are all cases in which the standard approximations, which miss the discontinuity jump in the potential, work poorly. Corrections based on the

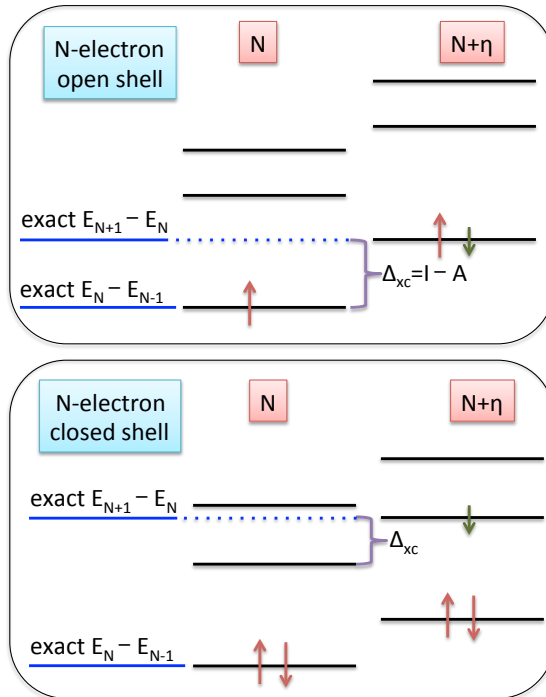


Figure 6.1: Schematic illustration of the spin-restricted (same potential for spin- \uparrow and spin- \downarrow electrons) KS spectrum when adding a tiny fraction η of an electron to an N -electron system. Top panel: when the KS N -electron system is open shell, the whole KS spectrum “jumps” by a positive constant $\Delta_{xc} = I_N + A_N$, which aligns the KS highest occupied eigenvalue (HOMO) to the electron affinity $A_N = E_{N+1} - E_N$. Bottom panel: when the KS system is closed shell, the positive constant Δ_{xc} aligns the KS N -electron lowest unoccupied orbital (LUMO) to the exact affinity A_N . In both cases, in the exact KS system the HOMO is equal to the many-body chemical potential.

explicit enforcement of the discontinuity have been often proposed as a practical solution (see, e.g., refs. [247–250]).

For the study the exchange-correlation derivative discontinuity an extension of the KS reference to fractional electron numbers is performed. After briefly reviewing the essential background material of this extension, we present the rigorous generalization of the SCE functional to fractional electron numbers. We investigate further on the derivative discontinuity in the self-consistent solution of the KS equations with the SCE functional, for the case of strong correlation in one-dimensional and three-dimensional harmonic confinements, by analyzing the HOMO eigenvalue for an extended range of particle numbers. As our results follow without imposing any *ad hoc* constraint, they also support the assumptions that were made to derive the existence of the derivative discontinuity [228]. The SCE formalism provides therefore insight, that can be used for the construction of approximate functionals with an inherent derivative discontinuity.

6.2 Fractional particle numbers in KS-DFT

At zero temperature, open systems with fluctuating particle numbers have been first introduced in the KS framework by considering statistical mixtures [228]. When dealing with DFT for quantum mechanical systems, we can work with pure states in which a degenerate system is composed by well separated fragments, and one focuses on the energy and density of one of the fragments alone [132, 135, 251]. A very simple example is the stretched H₂⁺ molecule [133, 214], in which on each nucleus we find, on average, 1/2 electrons. A key point to prove the existence of the derivative discontinuity is the (empirical) observation that the energy E_N of an integer electron number system in a given external potential is a monotonic and convex function, *i.e.* $E_N \leq \frac{1}{2}(E_{N+1} + E_{N-1})$. This implies that for fractional electron numbers $Q = N + \eta$ (with $0 \leq \eta \leq 1$), the minimizing many-electron ground state energy E_Q and density $\rho_Q(\mathbf{r})$ lie on the connecting line between the values at the two adjacent integers

$$\begin{aligned} E_{N+\eta} &= (1 - \eta)E_N + \eta E_{N+1} \\ \rho_{N+\eta}(\mathbf{r}) &= (1 - \eta)\rho_N(\mathbf{r}) + \eta \rho_{N+1}(\mathbf{r}) \end{aligned} \quad (6.1)$$

In exact KS theory the eigenvalue of the highest occupied orbital (HOMO) ε_{HOMO} is the derivative of the total energy of (6.1) *w.r.t.* the particle number Q [228, 252]

$$\frac{\partial E_Q}{\partial Q} = \varepsilon_{HOMO} \quad (6.2)$$

Thus, the exact ε_{HOMO} is constant between any two adjacent integers (say, N and $N + 1$) and equal to the interacting chemical potential $E_{N+1} - E_N$, jumping to a different value when crossing an integer. This step-like behavior of the KS ε_{HOMO} is not captured by the standard approximate functionals (see, *e.g.*, refs. [251, 253, 254]), unless imposed *a priori* via additional constraints in a spin-unrestricted framework, as, *e.g.*, in refs. [247, 248, 250]. The alignment of the exact KS HOMO eigenvalue with the interacting chemical potential to a shift of the exact KS one-body potential by a constant Δ_{xc} (the derivative discontinuity) when crossing an integer particle number, $v_s[\rho_{N+}](\mathbf{r}) - v_s[\rho_{N-}](\mathbf{r}) = \Delta_{xc}$ (*cf.* figure 6.1).

6.3 Extension of the SCE formalism to fractional electron numbers

A generalization of the SCE formalism to non-integer electron numbers is not obvious, because in the SCE energy expressions

$$V_{ee}^{SCE}[\rho] = \frac{1}{2} \int d\mathbf{r} \rho(\mathbf{r}) \sum_{i=2}^N w(\mathbf{r} - \mathbf{f}_i(\mathbf{r})) \quad (6.3)$$

$$= \int d\mathbf{r} \frac{\rho(\mathbf{r})}{N} \sum_{j>i}^N w(\mathbf{f}_i(\mathbf{r}) - \mathbf{f}_j(\mathbf{r})) \quad (6.4)$$

the sums run over the integer electron number N , requiring always an integer number of co-motion functions $f_i(\mathbf{r})$ ($w(\mathbf{x})$ depicts the interaction of choice, which, e.g., in the three-dimensional case is the usual Coulombic one $w(\mathbf{x}) = 1/|\mathbf{x}|$). To proceed in a rigorous way [88, 132, 133, 135, 214], we employ the fact that the exact SCE solution in one-dimensional systems can be found analytically to arbitrary integer particle number and symmetry, and analyze in the following a well separated Q -electron fragment inside a degenerate system with total integer electron number M . An example of such a degenerate system is provided by figure 6.2. Though the analysis is undertaken in one dimension, the main findings and conclusions should also hold for two- and three-dimensional systems [224]. Indeed, we have also performed a three-dimensional self-consistent calculation for a spherically symmetric density, for which we can deduce the fractional SCE solution from our one-dimensional construction, finding similar results.

Before elaborating on our analysis, we already note that it is crucial to evaluate $V_{ee}^{SCE}[\rho]$ from (6.3), as the sum in the alternative expression (6.4) for the integer- M electron system does not decompose into equal sums of isolated fragments (the interaction $w(f_i(\mathbf{r}) - f_j(\mathbf{r}))$ between two electrons on a given fragment may contribute significantly to the integral when x in the region of another fragment). The first expression demonstrates the size consistency of $V_{ee}^{SCE}[\rho]$.

One dimension In the illustrated example of figure 6.2, we have solved the SCE problem for $M = 5$ electrons, for a density made of two well-separated identical fragments, each integrating to $Q = 2.5 = N + 0.5$ particles. We have then studied the isolated SCE solution on one fragment, indicated in figure 6.2 by black circles. Here the positions $f_i(x)$ of the other 4 electrons are shown as a function of the position x of the first electron. We see that two adjacent strictly correlated positions $f_i(x)$ and $f_{i+1}(x)$ on the fragment still satisfy the condition of “total suppression of charge fluctuations” [103], as already encountered in the integer- N solution of section 3.2

$$\int_{f_i(x)}^{f_{i+1}(x)} dy \rho(y) = 1 \quad (6.5)$$

so that there are values of x for which we have three electrons in the fragment, and values of x for which we find only two particles (the third electron is in the other fragment). In this way the co-motion functions incorporate the fractional electron character on the fragment. See also figure 6.3 for further illustration.

A straightforward generalization of the co-motion functions to fractional electron numbers can be attempted along the lines of section 3.2. We rewrite the condition (6.5) for the position $f_i(x)$ to be determined to the right of the reference electron

$$\int_x^{f_i(x)} dy \rho(y) = i - 1 \quad (6.6)$$

By the use of the cumulant

$$N_e(x) = \int_0^x dy \rho(y) \quad (6.7)$$

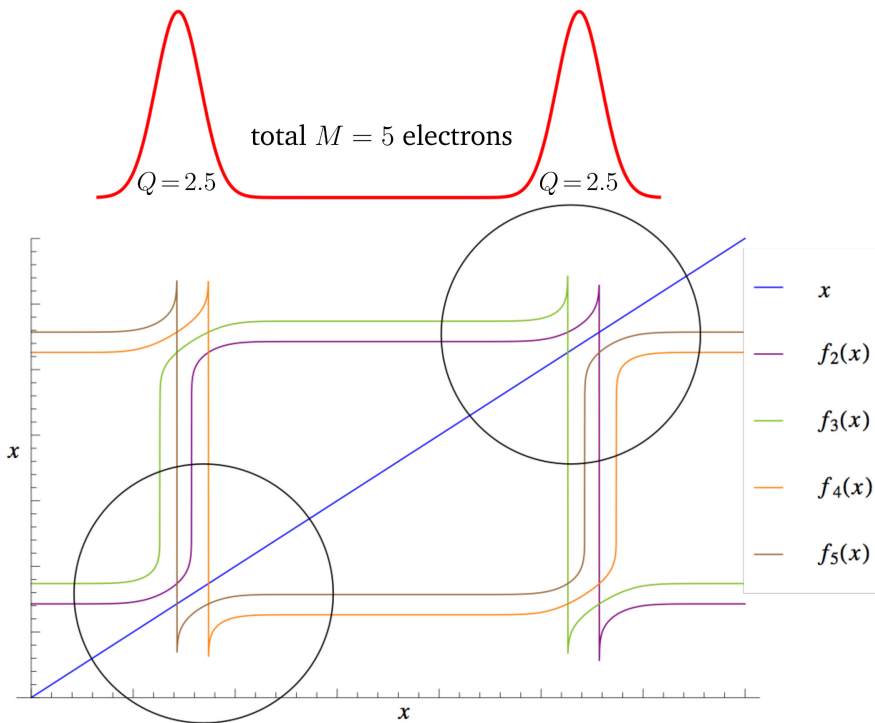


Figure 6.2: Simple example of the analysis used to deduce the SCE solution for fractional electron numbers: we considered a density with $M = 5$ electrons, made of two separated identical fragments (here given by two Gaussians), and we have studied the exact SCE solution on each fragment. The graphic shows the positions $f_i(x)$ of the other 4 electrons as a function of the position x of the first electron. The two black circles represent the “local” SCE solution on each fragment.

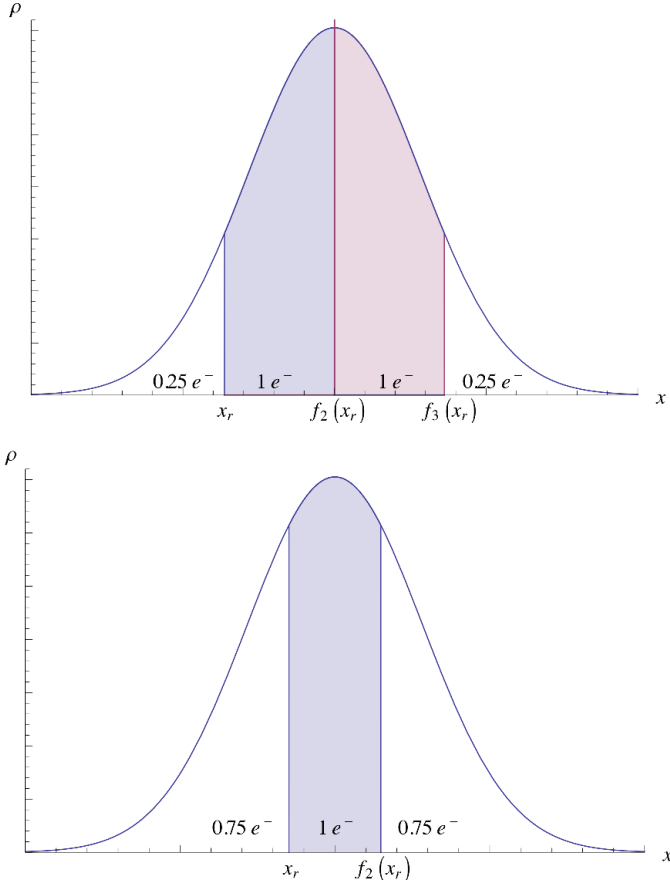


Figure 6.3: The SCE solution for a density integrating to $Q = 2.5$ electrons, taking the condition into account that the density in between two adjacent electrons always has to integrate to one. For some reference values of x_r we find two other strictly correlated positions and the density contains three electrons in total (upper panel). For other reference values of $x = x_r$, we can only find one other co-motion function in the density and the third electron is pushed to infinity (lower panel).

and its inverse $N_e^{-1}(x)$, this equation can be resolved for $f_i(x)$ to yield the co-motion function in the first branch

$$f_i(x) = N_e^{-1}[N_e(x) + i - 1] \quad \text{for } x < a_{N+\eta-(i-1)} \quad (6.8)$$

where the boundary value $a_k = N_e^{-1}(k)$ takes into account that the position $f_i(x)$ is to the right of the reference position x .

The second branch follows from considering $f_i(x)$ to the left of x

$$\int_{f_i(x)}^x dy \rho(y) = N + 1 - (i - 1) \quad (6.9)$$

and we obtain

$$f_i(x) = N_e^{-1}[N_e(x) - N + i - 2] \quad \text{for } x > a_{N+2-i} \quad (6.10)$$

For the third branch $a_{N-i+2} < x < a_{N+\eta-i+1}$ we find from our analysis above, that the respective electron is at infinity, and the co-motion functions for the entire domain write

$$f_i(x) = \begin{cases} N_e^{-1}[N_e(x) + i - 1] & \text{for } x < a_{N+\eta-i+1} \\ N_e^{-1}[N_e(x) - N + i - 2] & \text{for } x > a_{N-i+2} \\ \infty & \text{otherwise} \end{cases} \quad (6.11)$$

with $i = 2 \dots N + 1$. To no surprise, the expressions from above coincide with the ones for integer electron numbers (3.26) for $\eta = 0$ and $\eta = 1$.

$V_{ee}^{SCE}[\rho]$ can be evaluated as in the integer system (6.3), with the sum now running up to $N + 1$. This is also true for the SCE potential, that is obtained in the one-dimensional case by integrating

$$\nabla \tilde{v}_{SCE}(\mathbf{r}) = \sum_{i=2}^{N+1} w' [|x - f_i(x)|] \operatorname{sgn}[x - f_i(\mathbf{r})] \quad (6.12)$$

The constant C , up to which the SCE potential is defined, is always fixed by requiring $\tilde{v}_{SCE}(|\mathbf{r}| \rightarrow \infty) + C = 0$.

Three dimensions, spherically symmetric We have seen in section 3.2 that the co-motion functions for the three-dimensional spherically symmetric case can be deduced from the one-dimensional ones with a density symmetric *w.r.t.* the origin. This yields along the lines of the preceding paragraph

$$f_i(r) = \begin{cases} N_e^{-1}[N_e(r) + 2i - 2] & \text{for } r < \tilde{a}_{N+\eta-2i+2} \\ N_e^{-1}[|N_e(r) - 2N + 2i - 4|] & \text{for } r > \tilde{a}_{N-\eta-2i+4} \\ \infty & \text{otherwise} \end{cases} \quad (6.13)$$

where the cumulant is adapted to the symmetry of the problem

$$N_e(r) = \int_0^r ds 4\pi s^2 \rho(s) \quad (6.14)$$

Again, in the case of $\eta = 0, 1$ these co-motion functions agree with the ones of the integer electron numbers (3.43).

6.4 The derivative discontinuity in harmonic external potentials

With the generalized co-motion functions to fractional electron numbers, we are able to solve self-consistently KS-SCE equations for open systems. Fractional occupation for the KS HOMO orbital is taken in the construction of the density from the orbitals [252, 253, 255]. As usually, the spin- \uparrow and spin- \downarrow electrons exhibit the same potential, and we remain in a *spin-restricted* framework.

We then consider Q electrons in an external harmonic confinement $v_{ext}(\mathbf{r}) = \frac{1}{2}\omega^2|\mathbf{r}|^2$ in one and three dimensions. For the one-dimensional case, the same model parameters as in section 5.3.2 are employed. As we seek for the strong-correlation regime of this systems, where we expect our SCE functional to become the exact one, the density has to be kept low through the system. This is achieved by shallow confinements, *i.e.* setting the spring constant ω in the external harmonic potential sufficiently small.

In figure 6.4 we show our self-consistent KS-SCE results for the HOMO eigenvalue as a function of the particle number in the one-dimensional confinement. Comparison is undertaken with the KS-LDA HOMO eigenvalue and the full-CI chemical potential $E_{N+1} - E_N$. A moderately correlated case $L = 1$ is shown, and two strongly correlated cases $L = 70$ and $L = 150$, where L is the effective confinement-length with $\omega = 4/L^2$. For moderate correlation, $L = 1$, we see that KS-LDA, having $\Delta_{xc} = 0$, shows a discontinuity in the HOMO value only when filling a new shell (even N ; second panel of figure 6.1), while KS-SCE shows a small vertical change also when the N system is open shell (at odd N). When correlation becomes stronger ($L = 70, 150$), the KS-SCE self-consistent HOMO approaches more and more the exact step structure, with very good quantitative agreement with the full-CI chemical potentials. For such cases KS-LDA yields essentially a continuous curve, since the single particle energies are all very close.

In figure 6.5 we show the results for a three-dimensional system (Hooke's atom) with small ω . We find again that the self-consistent KS-SCE HOMO eigenvalue resembles the exact step structure¹, similar to the one-dimensional results of figure 6.4. This is remarkable in a spin-restricted formalism. KS-LDA results are not shown as the self-consistent solution with LDA functional does not converge.

As promising feature of the SCE derivative discontinuity we note that the HOMO eigenvalue shows non-analytic behavior at integer electron numbers in all correlation regimes. The SCE kernel $\delta^2 E_{xc}/\delta\rho^2$ can then probably produce the quasi-singular behavior as required [243], and the SCE functional is potentially suitable to model long-range charge transfer and Coulomb blockade in time-dependent DFT calculations. Investigations along this lines are currently undertaken [258, 259].

¹In appendix B we also show that the KS-SCE total energy becomes exact in the limit of small ω . For the failure of standard functionals at this correlation regime see, *e.g.*, ref. [256].

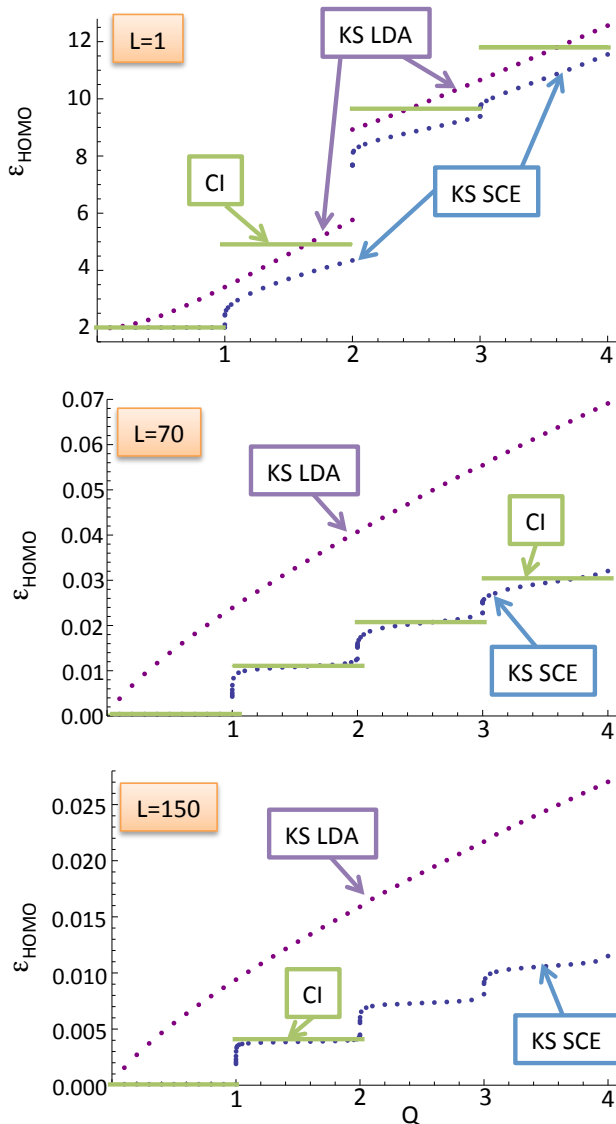


Figure 6.4: Self-consistent results for the spin-restricted KS HOMO eigenvalue as a function of the particle number Q for a quasi-one-dimensional quantum wire with harmonic confinement in the direction of motion of the electrons, $v_{\text{ext}}(x) = \frac{1}{2}\omega^2x^2$, and $\omega = \frac{4}{L^2}$. The KS-SCE results are compared to the KS-LDA method and the exact chemical potential $E_{N+1} - E_N$ from full-CI calculations [226].

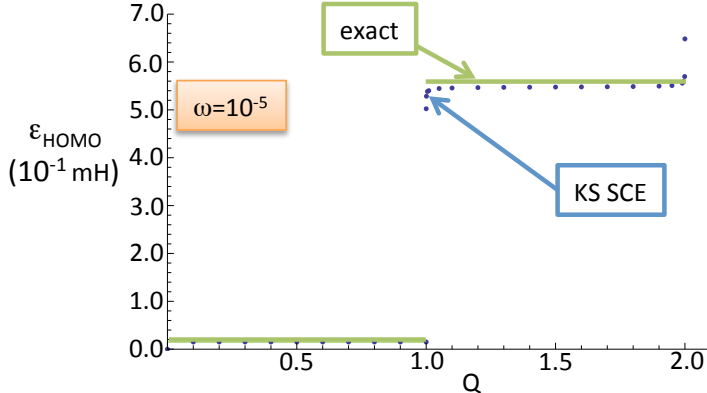


Figure 6.5: Self-consistent results for the spin-restricted KS HOMO eigenvalue as a function of the particle number Q for a three-dimensional electronic system with an external harmonic potential $v_{ext}(\mathbf{r}) = \frac{1}{2}\omega^2 r^2$, in the strong-correlation regime $\omega = 10^{-5}$. The KS-SCE results are compared with the exact chemical potential $E_{N+1} - E_N$ [156, 257].

6.5 Conclusions

The discontinuity in the HOMO eigenvalue for open shell systems from the self-consistent KS-SCE is not just a unique result, but also an independent proof that the exact spin-restricted KS formalism should have this feature. In fact, we have only used the exact $V_{ee}^{SCE}[\rho_Q]$ in the KS self-consistent procedure, without imposing any other condition on our functional. Until now this feature has only been captured in the context of lattice hamiltonians [260], or by imposing it in a spin-unrestricted framework² as, e.g., in refs. [247, 248, 250].

From a practical point of view our results could already be used to model transport through a correlated quantum wire or quantum dot, going beyond the lattice calculations of refs. [208, 246, 258]. Our findings also provide novel insight for the construction of approximate exchange-correlation functionals. The challenge is to transfer this exact behavior into approximations for less extreme correlation regimes, relevant for solid-state physics and chemistry. First attempts are presented in the next chapter of this thesis with an LDA correction to the SCE functional.

²An exception to the spin-unrestricted construction is ref. [214], which attempts at constructing, in a spin-restricted framework, a functional showing the linear behavior of (6.1).

Chapter 7

Energy Density Functionals From the Strong-Coupling Limit Applied to the Anions of the Helium Isoelectronic Series

A. Mirtschink, C. J. Umrigar, J. D. Morgan III and P. Gori-Giorgi

“Energy Density Functionals From the Strong-Coupling Limit Applied to the Anions of the He Isoelectronic Series”

invited article, J. Chem. Phys. **140**, 18A532 (2014)

7.1 An overview

Both, low-density nanostructures and stretched bonds involve charge localization due to strong spatial correlations. This is by definition the case in which SCE tends asymptotically to the exact exchange-correlation functional. To gain insight into the performance of the SCE functional for a wider class of chemical systems, we consider here a conceptually different problem in which electronic correlation still plays a crucial, but less pronounced, role. This is the anions of the He isoelectronic series, described by the Hamiltonian

$$\hat{H} = -\frac{1}{2}\nabla_1^2 - \frac{1}{2}\nabla_2^2 - \frac{Z}{r_1} - \frac{Z}{r_2} + \frac{1}{r_{12}} \quad (7.1)$$

with $Z < 2$. Despite its simplicity, the problem nonetheless is very challenging for DFAs, because a balanced description of kinetic and electronic-interaction contributions is needed. Accurate wavefunction calculations [261] have shown that, when the

nuclear charge Z is lowered and crosses a critical value $Z_{crit} \approx 0.91103$, a quantum phase transition occurs from a bound to an unbound two-electron system. Thus, with this simple Hamiltonian we can explore a whole class of very loosely bound anions, including the quantum phase transition at Z_{crit} .

As is well known, anions are problematic for state-of-the-art KS-DFT. Standard approximations often yield a positive eigenvalue for the HOMO, corresponding to a quasi-bound state (or resonance) instead of a properly bound state. Estimates of electron affinities are then obtained by the energy difference $E_{N=2} - E_{N=1}$ [262], ignoring the inconsistency with the HOMO eigenvalue. In the complete basis set limit, here by inclusion of plane waves, a positive orbital eigenvalue would lead to an unbound electron extending over the entire space. Consequently within the finite basis set, orbitals with positive orbital energies should not be occupied. In practice, however, convergence of these calculations can only be achieved if the orbital with positive eigenvalue is occupied, corresponding to an electron artificially bound by the finite basis, and this procedure has been criticized [263].

The failure of standard DFAs in binding anions is often attributed to the self-interaction error. However, despite being self-interaction free the Hartree-Fock method fails for H^- , yielding a negative binding energy for the second electron in contradiction to experiment [264]. It shows that, a proper accounting of correlation is required to stabilize the system, and the SIE is not the only problem.

For the SCE functional we know that it overestimates electronic correlation, leading to a severe underestimation of the total energy in the intermediate-correlation regime. An accurate treatment requires corrections to the SCE energy, and in this chapter we explore a correction based on the local density approximation (LDA) to improve on the SCE energy densities for exchange and correlation. The major physics in these corrected functionals, however, is still captured by the SCE functional. Due to the formal simplicity of the corrections self-consistent solutions with the corrected functionals are feasible. We focus on the anions close to the quantum phase transition, and results (including energies, densities and KS potentials) are compared to a very accurate wavefunction treatment and to standard approximate exchange-correlation functionals. To allow for a better comparison of DFT and wavefunction methods, we also perform an extended analysis of some exact properties of the density and of the KS potential at Z_{crit} .

7.2 The SCE functional for two electrons

In section 3.2 the co-motion functions for the case of spherically symmetric densities were derived that give the radial distances from the nucleus of $N - 1$ electrons w.r.t. an electron at some reference position. For the evaluation of the SCE energy and potential (3.12)-(3.15) additionally the minimizing angles for the angular part of electrostatic energy (3.42) are required. In a $N = 2$ system the two electrons in the SCE solution will be always opposite to each other around the origin at a relative angle π (maximum angular correlation), and the angular minimization can be omitted.

Therefore the SCE functional (3.15) writes

$$V_{ee}^{SCE}[\rho] = \frac{1}{2} \int dr 4\pi r^2 \rho(r) \frac{1}{r + f(r)} \quad (7.2)$$

with the single co-motion function for the $N = 2$ case

$$f(r) = N_e^{-1}[2 - N_e(r)] \quad (7.3)$$

The SCE potential $\tilde{v}_{SCE}(r)$ is then simply obtained by integrating the spherically symmetric equivalent of (3.12) taking the orientation of the electrons into account

$$\tilde{v}'_{SCE}(r) = \frac{1}{[r + f(r)]^2} \quad (7.4)$$

with boundary condition $\tilde{v}_{SCE}(r \rightarrow \infty) = 0$. As can be seen from this equation, the correct asymptotic behavior of the Hartree plus exchange-correlation potential is obtained $\tilde{v}_{SCE}(r \rightarrow \infty) \sim 1/r$, since $f(r \rightarrow \infty) \rightarrow 0$. This is also true for the general N -electron case, since the correct $(N - 1)/r$ asymptotic leading term can be similarly derived from (3.12) [117].

7.3 Quantitative corrections to the SCE functional

In general, given an approximate exchange-correlation functional $E_{xc}^{approx}[\rho]$, it is possible to extract from it an approximation to $T_c[\rho]$ and $V_{ee}^d[\rho]$ (5.11) in KS-SCE by using the scaling properties [177, 265] of DFT. Considering in D dimensions the with $\gamma > 0$ scaled density $\rho_\gamma(\mathbf{r}) \equiv \gamma^D \rho(\gamma \mathbf{r})$, we have [265]

$$T_c[\rho] + V_{ee}^d[\rho] \approx E_{xc}^{approx}[\rho] - \lim_{\gamma \rightarrow 0} \frac{1}{\gamma} E_{xc}^{approx}[\rho_\gamma] \quad (7.5)$$

that efficiently replaces the SCE exchange-correlation energy estimate by the one from the DFA (first term), as SCE estimate can be written as the low-density limit of the approximate functional (second term). This as long as the DFA by construction also yields the exact low-density limit.

A simple, yet accurate, way to construct the correction term $T_c[\rho] + V_{ee}^d[\rho]$ is to progress in an LDA spirit

$$T_c^{LDA}[\rho] + V_{ee}^{d,LDA}[\rho] = \int d\mathbf{r} \rho(\mathbf{r}) \{(t_c(\rho(\mathbf{r})) + v_{ee}^d(\rho(\mathbf{r}))\} \quad (7.6)$$

where $t_c(\rho)$ and $v_{ee}^d(\rho)$ are the kinetic correlation energy per particle and the electron-electron decorrelation energy per particle of the homogeneous electron gas (HEG) of density ρ . They can be easily obtained from (7.5)

$$t_c(\rho(\mathbf{r})) + v_{ee}^d(\rho(\mathbf{r})) = \epsilon_{xc}(\rho(\mathbf{r})) - \epsilon_{SCE}(\rho(\mathbf{r})) \quad (7.7)$$

where $\epsilon_{xc}(\rho)$ and $\epsilon_{SCE}(\rho)$ are, respectively, the exchange-correlation energy per particle and the indirect part of the SCE interaction energy per particle for the HEG.

The latter can be obtained by considering that in the external potential due to an infinite uniform background with positive charge density $\rho_+ = (\frac{4}{3}\pi r_s^3)^{-1}$ the minimum possible electron-electron repulsion is attained with the electrons localized at the sites of the bcc crystal with lattice parameter $a = 2(\pi/3)^{1/3}r_s$. A uniform electronic density $\rho = \rho_+$ is constructed by taking a linear superposition of all the possible origins and orientations of the crystal. In other words, in the simple uniform-density case the co-motion functions are just the lattice vectors of the bcc crystal with origin in the reference electron, whose position is distributed uniformly. This means that *for all values of the density parameter r_s* the SCE energy of the uniform electron gas is equal to the low-density leading term of the HEG energy

$$\epsilon_{SCE}(\rho) = -\frac{d_0}{r_s(\rho)} \quad (7.8)$$

Here we have set $d_0 \approx 0.891687$, which is the value from the Perdew-Wang-92 LDA parametrization [50]. We denote this method KS-SCE+LDA.

It is also possible to consider the local correction only for the electron-electron repulsion part, assuming that the error made by the KS kinetic energy is, for these systems, less serious than the one made by the SCE functional, so that the correction needs to rebalance the two terms. This corresponds to taking as correction only

$$V_{ee}^{d,LDA}[\rho] = \int d\mathbf{r} \rho(\mathbf{r}) v_{ee}^d(\rho(\mathbf{r})) \quad (7.9)$$

where $v_{ee}^d(r_s)$ is obtained by subtracting from (7.7) the kinetic correlation contribution $t_c = -\frac{d}{dr_s}(r_s \epsilon_{xc})$. We call this approximation KS-SCE+LV_{ee,d}.

Because of the linear ansatz for the corrections (7.5) size consistency is preserved in the SCE+LDA functionals. As undesired feature we note an occurring self-interaction error, as the integral (7.6) does not vanish for one-electron densities. However, the self-interaction error present in the KS-SCE+LDA approach is substantially different from the self-interaction error in standard KS-LDA or KS-GGA. In KS-LDA and GGA the self-interaction error manifests in the wrong asymptotic decay of the KS potential ($-\frac{Z-N}{r}$ instead of $-\frac{Z-N+1}{r}$). KS-SCE has the correct $-\frac{Z-N+1}{r}$ decay and this is not altered by the exponentially vanishing LDA contribution upon going from KS-SCE to the local corrections.

In the realm of the adiabatic connection, *cf.* section 2.2.3, the correction corresponds to approximating the global integrand W_λ by its LDA value, that itself stems from the physical HEG reference. By this a quantitatively meaningful total energy is expected. The corresponding potential, however, still carries over the SCE contributions when the derivative of the functional is taken, which evaluate in a non-local fashion from the actual, usually non-uniform, density, and the resulting self-consistent solution will differ substantially from the self-consistent LDA solution.

Z	k	c
0.9110289	0.60672	0.448
0.92	0.67	0.41
0.93	0.68	0.40
0.94	0.69	0.39
0.95	0.70	0.38

Table 7.1: Approximately optimal values of k and c used for several values of Z in the accurate wavefunctions. The first row is from ref. [261].

7.4 Accurate results for the anions of the He isoelectronic series

For a transparent analysis of the KS-SCE results at the quantum phase transition we extend the work of Umrigar and Gonze [266] by studying the accurate densities and KS potentials for $Z < 1$. We use Hylleraas-type wavefunctions, where very accurate results for the He isoelectronic series with nuclear charge Z between one and ten [158], and for weakly bound anions close to and at the quantum phase transition [261], are obtained by using basis functions that depend explicitly on the interelectronic coordinates. For the latter the wavefunction is a linear combination of 476 basis functions consisting of 244 modified [158] Frankowski-Pekeris [267] basis functions $\phi_{n,l,m,j}^{FP}(2Zks, 2Zkt, 2Zku)$, where

$$\phi_{n,l,m,j}^{FP}(s, t, u) = s^n t^l u^m (\ln s)^j e^{-s/2} \quad (7.10)$$

and 232 Frankowski [268] basis functions $\phi_{n,l,m,j}^F(2Zks, 2Zkt, 2Zku)$, where

$$\phi_{n,l,m,j}^F(s, t, u) = s^n t^l u^m (\ln s)^j (e^{ct} \pm e^{-ct}) e^{-s/2} \quad (7.11)$$

Here k and c are flexible scaling parameters and s , t , and u are the Hylleraas coordinates

$$s = r_1 + r_2, \quad t = r_2 - r_1, \quad u = r_{12} \quad (7.12)$$

The \pm sign depends on whether l is even or odd, to assure the proper symmetry of the basis functions under exchange of two electrons ($t \rightarrow -t$). The powers n , l , m , and j are chosen to duplicate the first several leading terms in the behavior of the exact wavefunction of a Helium-like ion near the three-particle coalescence, which is given by the Fock expansion [269–271]. This composite basis was used in ref. [261] to obtain compact and highly accurate representations of the wavefunction of the sole bound state of the Helium isoelectronic sequence for values of Z between $Z_{crit} \simeq 0.9110289$ and 1. Table 7.1 shows the approximately optimal values of k and c used for several values of Z in the present work.

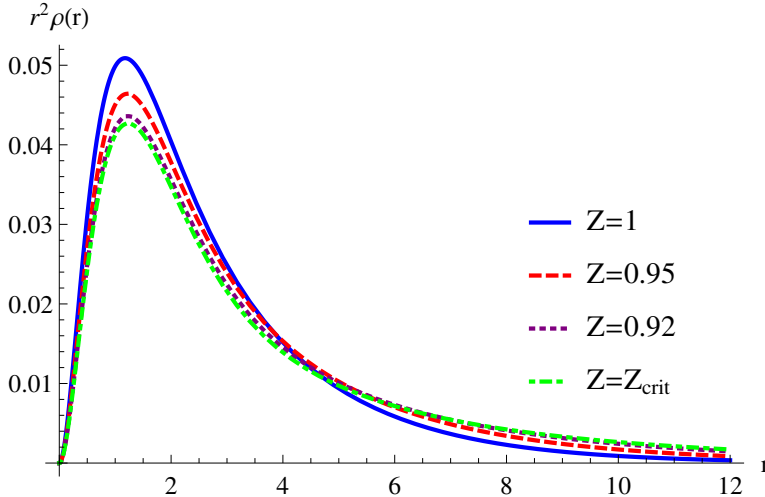


Figure 7.1: Accurate density $r^2 \rho(r)$ for various anions with nuclear charge Z of the He isoelectronic series.

The exact density of an atomic or molecular system is commonly known to decay (with exceptions when the ground-state of the ion is not asymptotically accessible by symmetry) as [175, 176, 272]

$$\rho(r \rightarrow \infty) \sim \exp(-2\sqrt{2 I_p} r) \quad (7.13)$$

This would suggest an increasingly spread out density when the critical value Z_{crit} with the ionization potential $I_p \rightarrow 0$ is approached ($I_p = E_{N-1} - E_N$). The expansion, however, is valid only for $1/r \ll I_p$, and from rigorous analysis [273] it can be proven that the density remains compact and satisfies the boundary conditions

$$C_-(\delta)r^{-3/2-\delta}e^{-2[8(1-Z_{crit})r]^{1/2}} \leq \rho(r) \leq C_+(\delta)r^{-3/2+\delta}e^{-2[8(1-Z_{crit})r]^{1/2}} \quad (7.14)$$

where δ is an arbitrary small positive number and $C_{\pm}(\delta)$ is a constant depending on δ . Accurate densities for selected values of $Z \leq 1$ are shown in figure 7.1 and confirm the argument.

Further refinement of the asymptotic decay of the density at Z_{crit} can be achieved by studying the corresponding differential equation for $\sqrt{\rho}$ [176] (which for a $N = 2$ singlet coincides with the KS equation). At the quantum phase transition, with the asymptotic potential to fourth order [175, 266], this equation is

$$\left[-\frac{1}{2} \nabla_r^2 - \frac{Z - N + 1}{r} + O\left(\frac{1}{r^4}\right) \right] \sqrt{\rho(r)} = 0 \quad (7.15)$$

By solving this equation asymptotically ($r \rightarrow \infty$), we obtain, order by order, a solution for the leading terms of the asymptotic density to order $O(r^{-4})$

$$\rho(r \rightarrow \infty) \sim \frac{e^{-4a\sqrt{r}}}{r^{3/2}} \left(1 + \frac{3}{8a r^{1/2}} - \frac{3}{128a^2 r} + \frac{15}{1024a^3 r^{3/2}} - \frac{405}{32768a^4 r^2} \right) \quad (7.16)$$

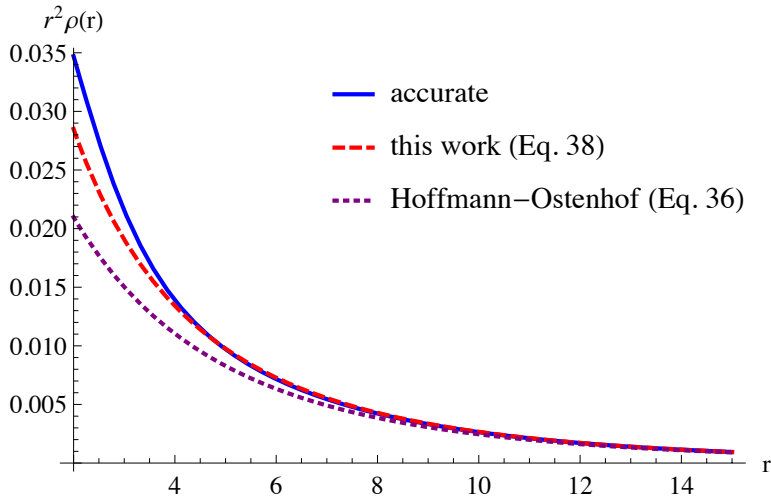


Figure 7.2: Comparison of the long-range behaviour of $r^2 \rho(r)$ at Z_{crit} obtained from the asymptotic decay in expressions (7.14) and (7.16) with the very accurate result from the Hylleras-type wavefunction of this section.

with $a = \sqrt{2(-Z + N - 1)}$. This decay agrees to leading order with the independent result of (7.14). The accurate density at the quantum phase transition together with the decays from (7.14) and (7.16) are displayed in figure 7.2, where in both cases the proportionality constant has been adjusted to match the accurate density at the end of the radial grid ($r \approx 100$). Notice that (7.15) implies that for the exact KS system (which yields the exact ground-state density) the equality $\varepsilon_{HOMO} = -I_p$ also holds at $Z = Z_{crit}$ when $I_p = 0$.

KS potentials, accessible by the inversion of the KS equations [266], for selected values of $Z \leq 1$ are shown in figure 7.3. We see that the KS potentials have a bump at intermediate length scale. This bump increases for smaller Z , as can be expected from the asymptotic first order contribution at large r , $v_{KS}(r \rightarrow \infty) = (1 - Z)/r$, which will be positive for $Z < 1$. The bump is present also for the Hydrogen anion, where this first order contribution vanishes.

In figure 7.4 we show the correlation potentials for selected values of Z . As was found in ref. [266], the accurate correlation potential close to the nucleus has a nearly quadratic behavior. In refs. [274, 275] it has been shown that the linear term in the correlation potential is due to the kinetic contribution, which, thus, turns out to be very small.

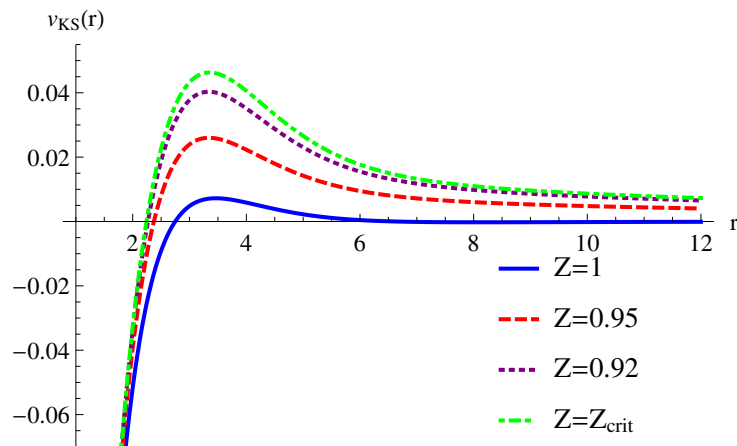


Figure 7.3: Accurate KS potential $v_{KS}(r)$ for the same anions as in figure 7.1.

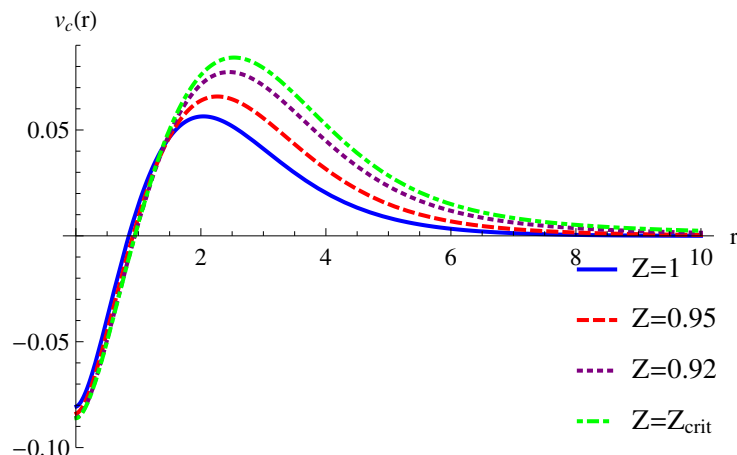


Figure 7.4: Accurate correlation potential $v_c(r)$ for the same anions as in figure 7.1.

7.5 SCE functionals for the anions of the He isoelectronic series

For the He isoelectronic series with $Z \leq 2$ we have solved self-consistently the restricted KS equations with various approximate functionals. Calculations for the HF method¹, KS-LDA, KS-SCE and KS-SCE with the two local corrections of section 7.3 were performed with a numerical code developed in our group. We chose the Perdew-Wang-92 (PW92) LDA parametrization [50]. For comparison of our calculations with the available standard approximations we have further performed restricted KS-DFT calculations with the Amsterdam Density Functional package (ADF) [276–278] for an extended range of functionals. From the GGA class of functionals we chose the PBE functional [63], from the metaGGA class the revTPSS functional [279], and from the hybrid functionals B3LYP [49, 61, 82, 95]. If not mentioned otherwise, all ADF calculations were carried out in the even-tempered(ET)-QZ3P basis supported by 3 diffuse s-functions with the parametrization of Hydrogen [280]. To assess the quality of the basis set we have also performed KS-LDA (PW92 functional) calculations with the ADF package, and compare them to our numerical grid implementation.

As definition of the critical nuclear charge Z_{crit} for the various DFT approximations we consider the value of Z at which either the ionization energy $I_p = E_{N=1} - E_{N=2}$ becomes smaller than 0, or the HOMO eigenvalue ε_{HOMO} becomes positive. Although the equality $\varepsilon_{HOMO} = -I_p$ is not strict for approximate functionals, we invoke the HOMO eigenvalue criterion to avoid the already mentioned conceptual and numerical issue of occupying orbitals with a positive eigenvalue.

Table 7.2 shows the predicted Z_{crit} for the quantum phase transition together with the corresponding ionization energy I_p and the HOMO energies for the various approximations. Of the DFT approximations considered, only the SCE functionals (SCE and SCE with local corrections) and the hybrid functional are able to bind the Hydrogen anion. The hybrid functional, however, yields an unphysical description of the bound anion, as will be further outlined below. Remarkably, all the standard functionals at different levels of approximation yield a similar value of $Z_{crit} \approx 1.2$. This shows that the nonlocality encoded in the SCE functional is able to capture different many-body effects than the standard approximations.

As already discussed in chapter 5, KS-SCE yields a lower bound to the total energy. From the underestimation of $Z_{crit} \approx 0.7307$ versus the actual value $Z_{crit} \approx 0.9110289$ we see again that, in the present intermediate-correlated regime, this bound is not very tight. The inherent strong-correlation nature of the electrons in the SCE formulation underestimates the realistic electronic repulsion energy drastically, because it minimizes the repulsion energy of point-charges. Another consequence of the underestimated repulsion energy is that the electron density can be more contracted closer in a self-consistent KS-SCE procedure to lower the attraction energy

¹For $N = 2$ the HF method becomes equivalent to the exact-exchange optimized effective potential method, as the HF exchange potential in this case is a local potential

$$v_x(\mathbf{r}) = -\frac{1}{2} \int d\mathbf{r}' \frac{\rho(\mathbf{r}')}{|\mathbf{r} - \mathbf{r}'|} \quad (7.17)$$

	Z_{crit}	ε_{HOMO}	$-I_p$
Accurate	0.9110289	0.0	0.0
<i>numerical</i>			
HF	1.0312	-0.05809	0.0
KS-LDA, PW92	1.2244	0.0	-0.18509
KS-SCE	0.7307	0.0	-0.05639
KS-SCE+LDA, PW92	0.9474	0.0	-0.05253
KS-SCE+LV _{ee,d} , PW92	0.9012	0.0	-0.04964
<i>ET-QZ3P+3diffuse</i>			
KS-LDA, PW92	1.2240	0.0	-0.18477
KS-GGA, PBE	1.2303	0.0	-0.19179
KS-metaGGA, revTPSS	1.2120	0.0	^a
KS-Hybrid, B3LYP	0.6932	-0.0041	0.0
(KS-Hybrid, B3LYP) ^b	1.1403	0.0	-0.15909

^aNot supported by ADF [276–278]

^bET-QZ3P basis

Table 7.2: Z_{crit} estimate with corresponding negative ionization energy $-I_p = E_{N=2} - E_{N=1}$ and HOMO energies ε_{HOMO} for various approaches.

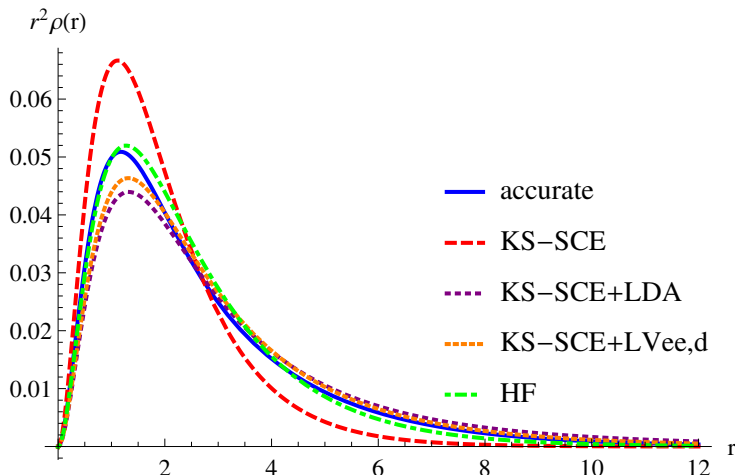


Figure 7.5: $r^2\rho(r)$ for H^- and various approaches.

	KS-SCE	KS-SCE+LDA	KS-SCE+LV _{ee,d}	accurate	HF
E_H	-0.5	-0.3562	-0.3755	-0.5	-0.5
E_{H^-}	-0.6972	-0.4275	-0.4614	-0.5278	-0.4879
A_H	-0.1972	-0.0713	-0.0859	-0.0278	

Table 7.3: Self-consistent ground state energies for H and H^- and electron affinities $A_H = E_{\text{H}^-} - E_H$. Only the methods are considered that yield a negative HOMO eigenvalue.

with the nucleus up to the point where the kinetic energy starts to dominate. This is shown in figure 7.5, where a more compact KS-SCE density is observed when compared to the accurate solution.

The local corrections to the SCE functional improve considerably the predicted Z_{crit} , see table 7.2, mainly due to the preserved correct long-range behavior of the locally corrected SCE potentials, which yield accurate HOMO eigenvalues. Ground-state energies, reported in table 7.3, are improved in the case of H^- , which corrects the electron affinities. On the downside, the self-interaction error of the LDA corrections significantly worsens the result for the one-electron atom. The same self repulsion will in general lead to a too spread out density, as also observed in figure 7.5, where the KS-SCE+LDA densities are too spread out compared to the other approaches.

In figure 7.5 and table 7.3 we report also the Hartree-Fock results. This is possible because of the negative HOMO eigenvalue even though $E_{N=1} < E_{N=2}$ (If the electron number were treated as variational parameter the minimum energy would be attained for $N < 2$.) We see from figure 7.5 that the accurate density is resembled more closely by the HF density than by the densities of the other approaches. This supports the

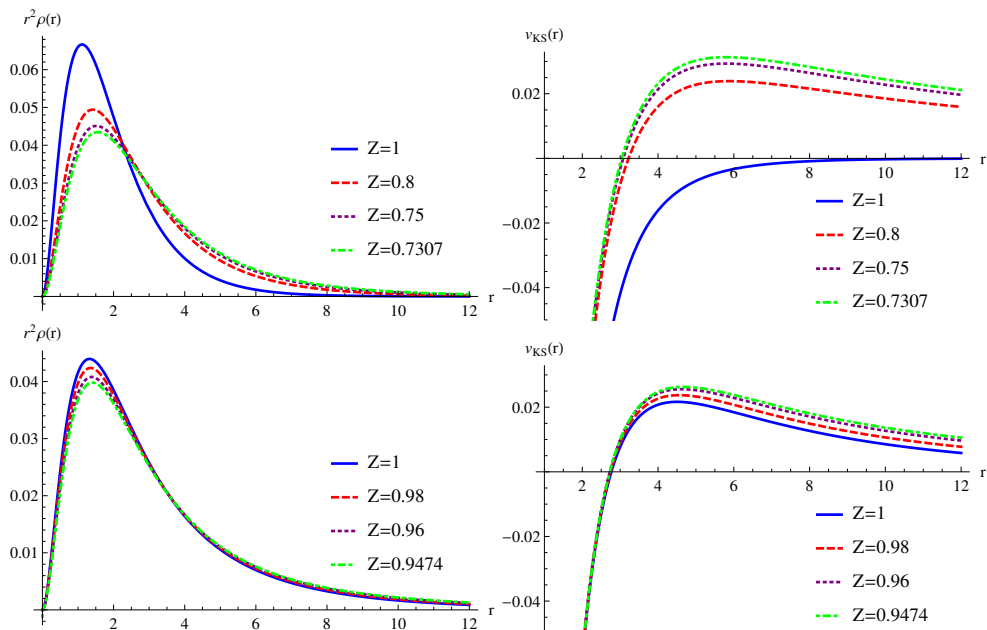


Figure 7.6: $r^2 \rho(r)$ and $v_{KS}(r)$ for various $Z \leq 1$ for the KS-SCE (above) and KS-SCE+LDA (below) method.

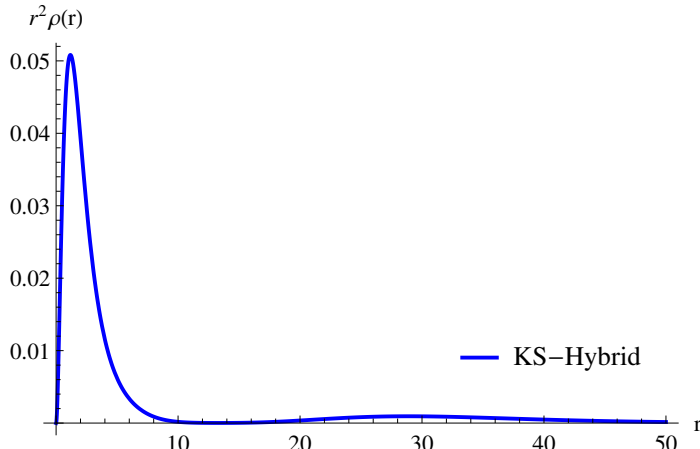


Figure 7.7: $r^2 \rho(r)$ for H^- with the B3LYP functional and a ET-QZ3P plus 3 diffuse function basis. It displays a second unphysical maximum in the density.

point of view of ref. [281] and the general idea of using HF densities as input for DFA energies in the case of negative ions [282, 283], even when HF energetically does not bind the last electron. A properly self-interaction free functional, however, is required for accurate total energies.

For the hybrid functional in the ET-QZ3P+3diffuse basis we obtain a negative $\varepsilon_{\text{HOMO}}$ and $E_{N=1} > E_{N=2}$ for H^- . Formally the hybrid thus binds the additional electron. When inspecting the density, however, one observes that the electron partially escapes from the nucleus, as shown in figure 7.7. By removing the 3 diffuse basis functions from the basis set to prevent the density accumulation in the outside region, we obtain a value of Z_{crit} in between that from HF and conventional DFT, as one would expect.

We turn to the discussion of the Kohn-Sham and exchange-correlation potentials for the self-consistent densities, displayed in figure 7.6 and 7.8. We see that the SCE total Kohn-Sham potential does not develop the bump for $Z = 1$, but only for smaller nuclear charges when the interelectronic repulsion dominates over the weaker nuclear attraction, see figure 7.6. As already observed in figure 7.5 this corresponds to a very compact density. For larger distances, the SCE potential is in good agreement with the accurate one. This also manifests the absence of the self-interaction error in the SCE potential. From figure 7.8 we also see that the SCE potential is quadratic close to the nucleus, as can be easily proven analytically from (7.4), since when $r \rightarrow 0$ we have $f(r \rightarrow 0) \rightarrow \infty$, so that $\tilde{v}'_{\text{SCE}}(r \rightarrow 0) = 0$. This is in agreement with the findings of refs. [274, 275], as there is no kinetic contribution in the SCE potential.

Although the SCE functional approximates exchange and correlation together, in figure 7.9 we show the SCE correlation potential alone, obtained by subtracting from the SCE exchange-correlation potential the exchange potential (7.17) computed from the self-consistent KS-SCE densities. We see that the SCE correlation potential is always negative, in contrast to the exact one in figure 7.4. The positive part of the

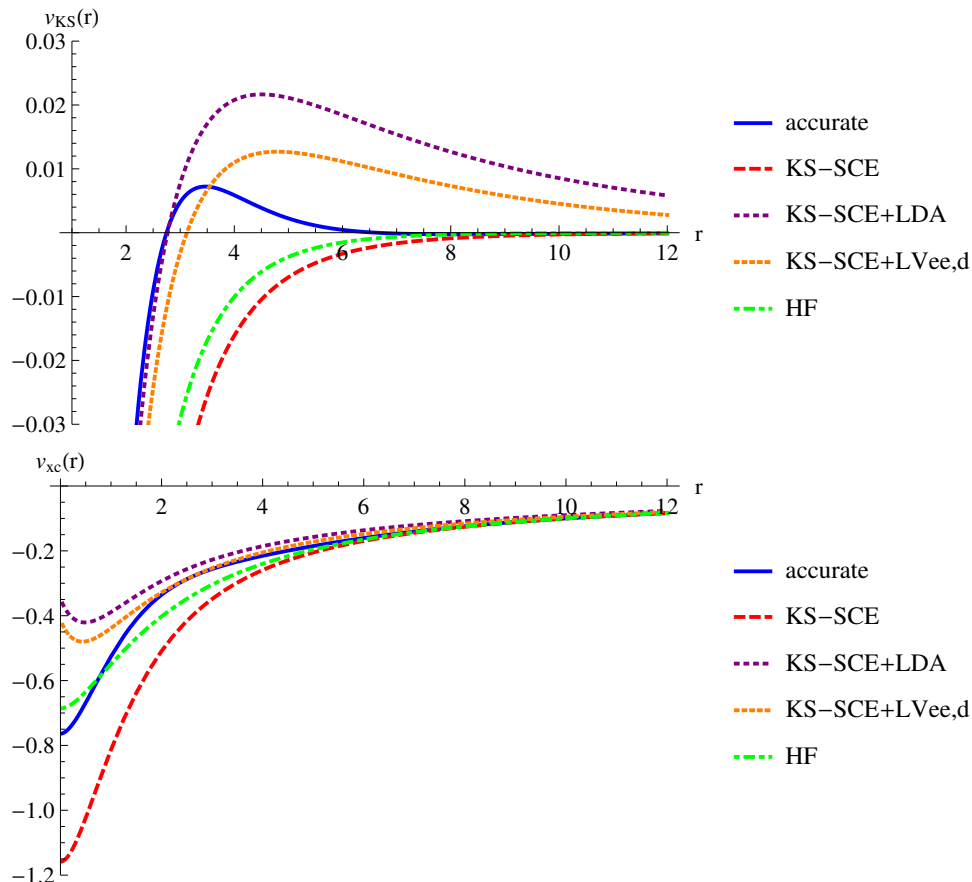


Figure 7.8: $v_{KS}(r)$ and $v_{xc}(r)$ for H^- and various approaches.

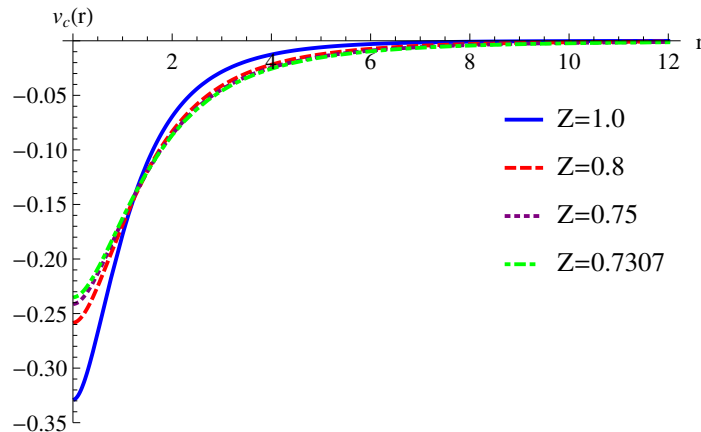


Figure 7.9: The self-consistent correlation potentials $v_c(r)$ from the bare KS-SCE method.

exact correlation potential is mainly due to kinetic correlation effects [144, 284] that are, as said, missed in the bare SCE.

A bump for H^- in the total KS potential is introduced by the locally corrected SCE functionals, though the bump is too pronounced, particularly in KS-SCE+LDA. This is also responsible for the overestimation of Z_{crit} , and can to some extend be attributed to the self-interaction error present in this functionals. The KS-SCE+LV_{ee,d} is more attractive at short distance than the exact KS potential, achieving error compensation with the overestimation of the bump (less severe than in the KS-SCE+LDA method), which results in a good estimate for $Z_{crit} \approx 0.9012$. Of the methods studied the KS-SCE approaches with the local corrections are the ones in which the HOMO energy deviates the least from the corresponding $E_N - E_{N-1}$, see table 7.2.

The HF (or exact exchange) potential is also shown in figure 7.8, although, once more, we have to keep in mind that in this case $E_{N=2} > E_{N=1}$.

7.6 The derivative discontinuity in the Hydrogen nuclear field

We complete our analysis by also allowing for fractional electron numbers Q , with $0 \leq Q \leq 2$, in the Hydrogen nuclear potential, which is often considered a paradigmatic model for a Mott insulator [214]. As already discussed in chapter 6, in exact KS-DFT the HOMO eigenvalue should be constant between any two adjacent integer electron numbers (say, N and $N + 1$), equal to the negative of the exact, interacting, ionization energy $-I_p = E_{N+1} - E_N$, and should jump whenever an integer electron number is crossed [228, 236].

In KS-DFT with the standard functionals, an extension to fractional electron numbers is easily achieved by giving fractional occupation to the HOMO [253, 255].

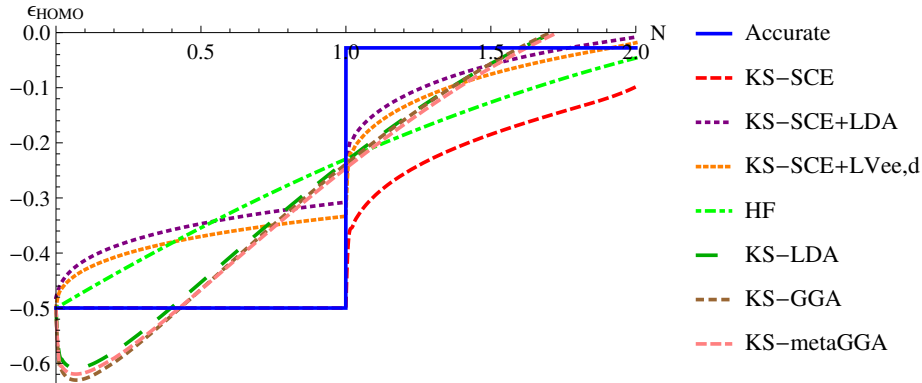


Figure 7.10: HOMO eigenvalue ϵ_{HOMO} versus particle number N in the Hydrogen nuclear potential for various approaches.

For the KS-SCE method we additionally need to consider co-motion functions for fractional electron numbers, see ref. [285] and chapter chapter 6 of this thesis. In the case of $1 < Q \leq 2$ the radial co-motion function $f(r)$ of section 6.2 write

$$f(r) = \begin{cases} N_e^{-1}[2 - N_e(r)] & \text{for } r > N_e^{-1}[2 - Q] \\ \infty & \text{otherwise} \end{cases} \quad (7.18)$$

The illustration of (7.18) is very simple: if the two electronic positions are always separated by a radial distance such that the density integrates to 1 (“total suppression of charge fluctuations”)

$$\int_r^{f(r)} ds 4\pi s^2 \rho(s) = 1 \quad (7.19)$$

for densities integrating to less than 2, there are values of r for which the second electron “cannot enter” in the density.

We mention again that here we consider the challenging case of the *restricted* KS method. Also in this framework for singlet $N = 2$ systems, as we increase the occupancy Q of the HOMO orbital, we should observe a jump in its energy at $Q = 1$. Notice that in the restricted KS method the conditions of ref. [214] regarding the spin degree of freedom are automatically fulfilled, so that the gap at $Q = 1$ is the same as the “Mott gap” for 1/2 spin-up and 1/2 spin-down electrons.

Figure 7.10 displays the HOMO eigenvalues for $0 < Q \leq 2$ for various approaches in the restricted KS scheme. The SCE functional shows a vertical change at $Q = 1$ in the HOMO energy even in the restricted approach. As seen in chapter 6, a sharp KS-SCE step is only obtained in the extremely strong-correlation (or low-density) limit [285], from which H^- is still far. The two SCE functionals with the local corrections exhibit the same smoothed step, but the self-interaction error leads to a non-constant HOMO energy between $0 < Q < 1$. The HF curve we report here has been obtained by keeping the occupancies of the two lowest spin orbitals equal at all

<i>numerical</i>	<i>ET-QZ3P+3diffuse</i>			
KS-LDA (PW92)	KS-LDA (PW92)	KS-GGA (PBE)	KS-metaGGA (revTPSS)	KS-Hybrid (B3LYP)
Q_{max}	1.71	1.71	1.70	1.73

^aBy integrating over the inside region ($0 < r < 13$) in figure 7.7.

Table 7.4: Maximum number of electrons Q_{max} bound in the Hydrogen nuclear potential for methods unable to bind H^- .

Q , thus restricted HF. This is the situation encountered in HF on an isolated fragment when stretching a bond or expanding a lattice [214].

Finally, figure 7.10 allows for a determination of the maximum number of electrons Q_{max} bound by the conventional DFT approaches. The results are compiled in table 7.4. We observe, similarly to Z_{crit} , that the predicted value of Q_{max} is insensitive to the level of approximation of the standard functionals, further supporting the idea behind the model potential of ref. [255].

7.7 Conclusions

We have applied functionals based on the exact strong-coupling limit of DFT to the loosely bound negative ions of the He isoelectronic series, which are a prototypical case for the delicate physics of anions and radicals. Whereas standard DFT functionals either do not bind anions, or bind them with unphysical long-range features in the charge density, the functionals based on SCE have a rigorous tendency to overbind that can be mitigated by local corrections. This shows that the SCE functional and its corrections are able to capture many-body effects radically different from the ones described by the standard functionals, although improvements are still needed. In particular one should aim at corrections based on correlation kinetic energy effects and/or on self-interaction free approaches like exact exchange [286].

Besides improving the accuracy of the functionals based on SCE, the challenge for the future is also to implement SCE physics into routinely applicable approximations. This can be done by either developing algorithms that evaluate the exact SCE functional exploiting its formal similarity to an optimal transport problem [120, 121], as in the pilot implementation of ref. [123], or by constructing new approximations based on the idea of co-motion functions, *i.e.* by trying to build approximate and simplified co-motion functions. These, in turn, could be used in local interpolations along the adiabatic connection that preserve size consistency [287].

Finally, our study also provides reference data for the anions of the He isoelectronic series close to and at the quantum phase transition, which can be valuable to test the accuracy of new DFT approximations (see, *e.g.*, ref. [288] that presents correlation potentials from RPA approaches, and are good approximations to the true correlation potential).

Chapter 8

Summary and Outlook

The significance of the strong-interaction limit of DFT for the development of approximate density functional was demonstrated, and approximate density functionals were designed by the inclusion of this limit in their formulation. Applications of the KS-SCE method to model quantum wires, models for chemistry, Hooke's atom and the negative ions of the Helium isoelectronic series show that good quantitative accuracy can be already obtained for systems with weak or strong electronic correlations. Additionally, strong-correlation phenomena are correctly captured in all correlation regimes within a restricted KS-DFT scheme. Improvements in accuracy in the intermediate-correlated regime can be achieved by corrections to the SCE functional, either by taking into account higher order terms in the expansion of the interelectronic energy in the strong-interaction limit (KS-ZPE-SCE methods), or by resorting to the homogeneous electron gas for quantitative reference (KS-SCE-LDA methods).

For the KS-ZPE-SCE methods a self-consistent implementation was not achieved due to the formal difficulties in the functional derivative of these energy functionals. The KS-SCE-LDA methods show improvements in some respects, but are yet not overall satisfactory. This can be attributed to the self-interaction error that is introduced by the LDA correction, and future developments should focus on self-interaction free variants. Such a method is given, *e.g.*, by modifying the definition of the Wigner-Seitz radius r_s , which serves as input variable for the LDA. Instead of estimating it from the homogeneous electron gas by

$$r_s^{HEG} = \left(\frac{3}{4\pi\rho_0} \right)^{1/3} \Big|_{\rho_0=\rho(\mathbf{r})} \quad (8.1)$$

r_s can be evaluated from the actual density by requiring that the sphere Ω of radius r_s around the reference position \mathbf{r} exactly integrates to one

$$1 = \int_{\Omega_{r_s}(\mathbf{r})} d\mathbf{s} \rho(\mathbf{s}) \quad (8.2)$$

This complicates the functional derivative, but a self-consistent implementation is still feasible as demonstrated in *ref.* [129].

Attempts towards a generalization of the SCE formalism towards arbitrary three-dimensional densities are also pursued. An approximate computation of the co-motion functions could be achieved by geometrical arguments. This possibility is currently investigated for the H₂ molecule [125].

An interesting area of application for the SCE functional is the modeling of charge transport in nanodevices. Due to the presence of the derivative discontinuity in the SCE functional, the possibility of describing the Coulomb blockade or the Kondo effect can be explored [258]. Other improvements can be expected in the simulation of long-range charge transfer (CT) processes. Pilot applications of the SCE functional to a one-dimensional model for a stretched H₂ molecule show that the electron hopping excitation HH → H⁺H⁻ is correctly captured in the absorption spectra, which can be computed from the real-time propagation of the time-dependent Kohn-Sham equations within an adiabatic TDDFT framework [259]. Absorption spectra of the H atom and stretched H₂ molecule, obtained with the SCE functional, are shown in figure 8.1, where the CT peak can be identified in the H₂ molecule at $\omega \approx 0.516\text{Ha}$, which agrees well with the estimate from the orbital eigenvalues

$$\begin{aligned}\omega_{CT}^{SCE} &\approx -\varepsilon_{HOMO}^H + \varepsilon_{HOMO}^{H^-, SCE} - 1/R \\ &= 0.541\text{Ha}\end{aligned}\tag{8.3}$$

whereby the exact CT peak is estimated at

$$\begin{aligned}\omega_{CT} &\approx I_H - A_H - 1/R \\ &= 0.569\text{Ha}\end{aligned}\tag{8.4}$$

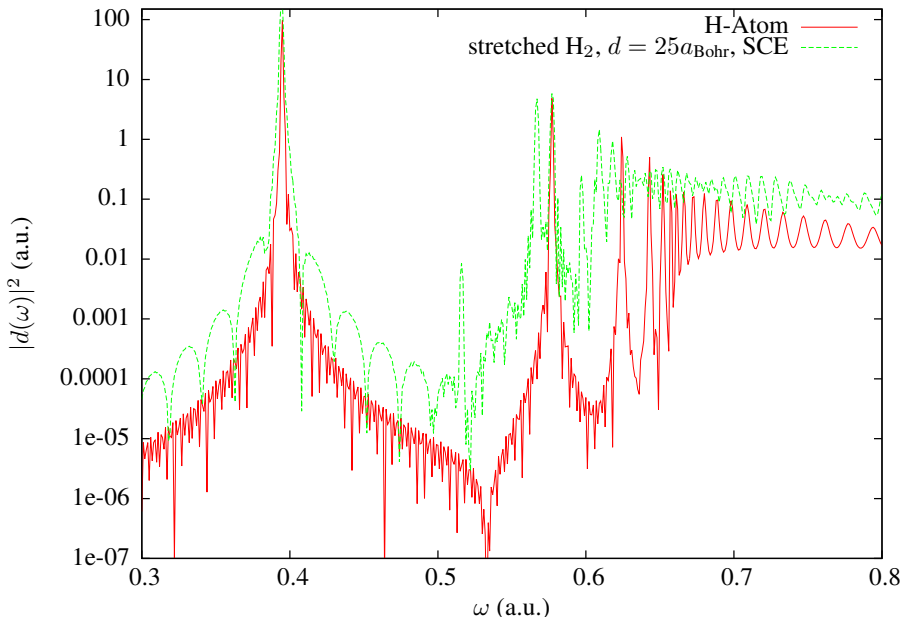


Figure 8.1: Linear-response photo-absorption spectra for the one-dimensional model of the H atom and the stretched H_2 molecule of chapter 5. The spectra were obtained within an adiabatic TDDFT framework by the real-time propagation of the TDKS equations with the SCE potential. As the SCE functional is self-interaction free, the H spectrum shown is equal to the one from the time-propagation of the time-dependent Schrödinger equation. The CT peak for the electron hopping $HH \rightarrow H^+H^-$ in the H_2 spectra is at $\omega \approx 0.516\text{Ha}$.

Appendix A

PC Cell and Exchange-Correlation Hole for the Homogeneous Electron Gas

In this appendix we clarify the difference between the exchange-correlation hole and the point-charge plus continuum (PC) cell of chapter 3, by considering the homogeneous electron gas in the extreme low-density limit. Thus further extending the argument already given in the appendix of ref. [105].

More than seventy years ago Wigner [180, 289] pointed out that electrons embedded in a compensating uniformly charged background would crystallize at sufficiently low values of the density ρ . The SCE construction can be seen as nothing else than the Wigner idea generalized to a nonuniform density $\rho(\mathbf{r})$. Indeed, in ref. [102] the SCE formalism is presented as a “floating” Wigner crystal in a non-euclidean space, with the metric determined by the density $\rho(\mathbf{r})$.

In the case of the uniform electron gas the SCE co-motion functions are simply the positions of the bcc lattice points with origin fixed at the reference electron. Notice that the constraint of continuous density forces us to consider a “floating” Wigner crystal, which corresponds to the linear superposition of all the possible origins and orientations of the crystal, thus restoring the translational symmetry. The exchange-correlation hole $\rho(g(r) - 1)$, with $g(r)$ the pair-distribution function, can then be simply constructed by considering that the expected number of electrons in a spherical shell of radius r and thickness dr around the reference electron at the origin is given by

$$dN(r|0) = \rho g(r) 4\pi r^2 dr \quad (\text{A.1})$$

We can then place very narrow normalized gaussians (almost delta functions) at the bcc sites around the reference electron and take the spherical average. This way, we obtain the extreme low-density limit of $g(r)$. In figure A.1 we compare this low-density (or SCE) $g(r) - 1$ with the PC cell $c(r)$ in the same units, $c(r) = -\theta(r_s - r)$, with $\theta(x)$ the Heaviside step function. We see that the two are very different, except for

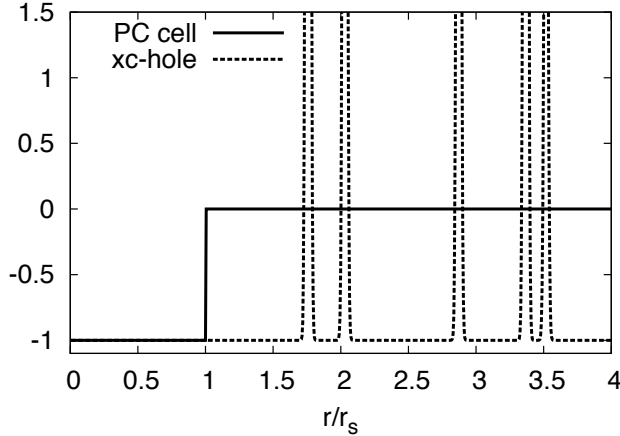


Figure A.1: PC cell divided by the density ρ (i.e. $c(r) = -\theta(r_s - r)$), and the pair-correlation function $g(r) - 1$, corresponding to the exchange-correlation hole divided by the density ρ , for the extreme low-density uniform electron gas.

$r/r_s \leq 1$. The exchange-correlation hole has positive peaks (indicating the positions of the other electrons) that extend to $r \rightarrow \infty$ (perfect long-range order). Notice that the exchange-correlation hole for the broken symmetry solution (without translational invariance) would be, instead, much less structured, but here we are interested in the solution constrained to the uniform density. The way the electrostatic energy is calculated from the PC cell and the exchange-correlation hole is also different [105]

$$w = \rho \int d\mathbf{r} \frac{g(r) - 1}{r} \quad (\text{A.2})$$

$$w = -\rho \int d\mathbf{r} \frac{c(r)}{r} + \frac{\rho^2}{2} \iint d\mathbf{r} d\mathbf{r}' \frac{c(r)c(r')}{|\mathbf{r} - \mathbf{r}'|} \quad (\text{A.3})$$

When we use the exchange-correlation hole (A.2) to evaluate the energy, we need to evaluate an infinite sum (all the peaks in figure A.1), which converges very badly (the Madelung sum), and that can be dealt with, e.g., the Ewald method. For the PC cell (A.3) we face two very simple, short-ranged, integrals [290]. The results from the two expressions differ only by 0.45%, as was already noted in ref. [291], where it was also proven that the PC value is a rigorous lower bound for the energy of the uniform electron gas.

Notice that if, instead, we consider the PC cell as a model for the exchange-correlation hole and we use $c(r)$ in (A.2) in place of $g(r) - 1$, we get a very poor result [105] with an error of $\sim 17\%$. The PC model does approximate the electrostatic potential of the exchange-correlation hole by constructing it in a different way.

Appendix B

KS-SCE Total Energies for Hooke's Atom

In table B.1 and figure B.1 we report ground state energies for the Hooke's atom, *i.e.* two electrons in the external harmonic potential

$$v_{ext}(r) = \frac{1}{2}\omega^2 r^2 \quad (\text{B.1})$$

Self-consistent solutions with the KS-SCE method of chapter 5 are compared to the accurate solutions of *ref.* [257]. In the low-density limit $\omega \rightarrow 0$ we see that KS-SCE approaches asymptotically the accurate solution.

ω	KS-SCE	accurate	error
0.00001	0.0005626	0.0005763	2.4%
0.0001	0.002665	0.002802	4.9%
0.0014	0.01647	0.01832	10.1%
0.01	0.06814	0.07921	14.0%
0.06	0.2813	0.3278	14.2%
0.1	0.4328	0.5	14.4%
0.3	1.135	1.276	11.1%
0.5	1.805	2.0	9.7%

Table B.1: Ground state energies for Hooke's atom at several spring constants ω of the self-consistent KS-SCE method compared with the accurate solution [257].

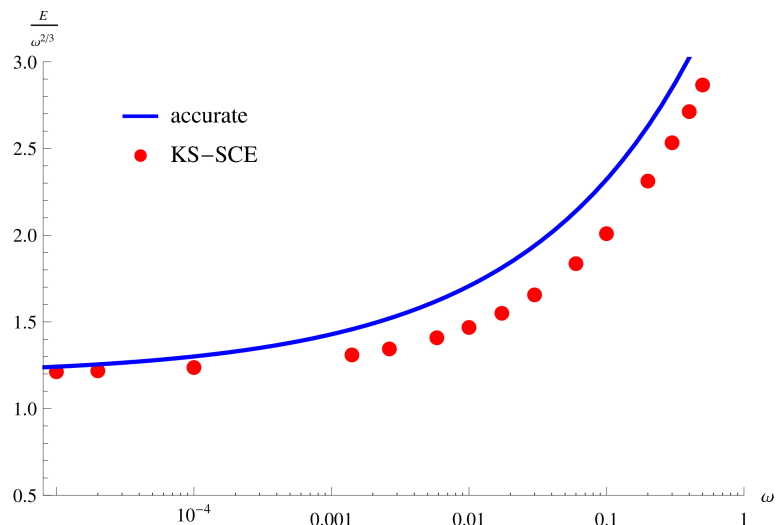


Figure B.1: Same as table B.1 graphically.

Samenvatting

In dit proefschrift worden nieuwe benaderingen voor dichtheidsfunktionalen afgeleid voor gebruik in dichtheidsfunktionaltheorie (DFT). Focus is hierbij op de beschrijving van sterke correlatie effecten zoals te zien bij micro-elektronica op de nano-meter schaal of chemisch reacties en die alleen maar moeilijk met traditionele dichtheidsfunktionalen te simuleren zijn.

Als uitgangspunt wordt het “strictly correlated electrons” (SCE) concept gebruikt. Door middel van een combinatie van het SCE referentiesysteem met het gebruikelijke Kohn-Sham (KS) referentiesysteem kunnen benaderingen opgesteld worden welke zowel het kwantummechanische karakter van het elektron als de klassieke Coulomb repulsie tussen meerdere elektronen weergeven maar nog altijd makkelijk op te lossen zijn. Hierbij worden empirische parameter in de afleiding voorkomen en de benaderingen worden puur formeel gemotiveerd in het kader van de *adiabatische connectie* van DFT.

Nadat in de eerste drie hoofdstukken een introductie en overzicht over de formele grondslagen gegeven wordt, stellen wij in hoofdstuk 4 als mogelijk fungtionaalbenadering een interpolatie voor tussen de KS en SCE referentiesystemen. Deze aanpak gaat uit van *lokale* energiedichthes en kan deze door onthouden van het SCE referentiesysteem nauwkeurig modelleren voor systemen met sterke correlatie. Wij laten aan hand van berekeningen voor kwantumpunten en atomen zien dat een nauwkeurige modellering van de fysische lokale energiedichtheid voor elk correlatieregime ook de tot nu toe onbekende eerste afgeleide van de lokale energiedichtheid in ten minste één van de twee referentiesystemen vereist. Aanvullend vergelijken wij de SCE lokale energiedichthes met lokale energiedichthes van het PC model en wij beschouwen in het gestrekte H₂ molecuul de toepasbaarheid van de Lieb-Oxford grens voor lokale energiedichthes.

In hoofdstuk 5 introduceren wij de KS-SCE methode welke de SCE *globale* energiedichtheid als benadering voor de fysische globale energiedichtheid gebruikt en een eerste afgeleide van de energiedichtheid vermindert. *Zelfconsistente* oplossingen van de *spinbeperkte* KS vergelijkingen met de SCE dichtheidsfunktional worden beschouwd voor sterk gecorreleerde kwantum draden en ééndimensionale modellen voor atomen en chemische bindingen. Wij laten zien dat de KS-SCE methode systemen met weinig en sterke correlatie goed beschrijft en dat er voor systemen tussen deze limieten correcties nodig zijn. Afsluitend worden correcties voorgesteld welke de eerste afgeleide van de globale energiedichtheid bijhalen en op *postfunctionaal* niveau gebruikt worden.

De afgeleiddiscontinuïteit van de SCE dichtheidsfunctionaal wordt in hoofdstuk 6 bekeken. In het algemeen stelt de afgeleiddiscontinuïteit een analytisch kenmerk van de exacte dichtheidsfunctionaal voor maar is niet gemodelleerd door traditionele dichtheidsfunctionalen. Omdat bekend is dat de SCE dichtheidsfunctionaal exact wordt voor systemen in de sterke correlatie limiet, beschouwen wij kwantumpunten en kwantumdraden in het regime van sterke correlatie. Daarbij wordt het SCE concept voor systemen met een gebroken aantal elektronen afgeleidt. Verder laten wij zien dat de SCE dichtheidsfunctionaal zelf in systemen buiten de sterke correlatie limiet een afgeleiddiscontinuïteit vertoont, hoewel deze minder op de exacte afgeleiddiscontinuïteit lijkt als het systeem ver van de limiet gaat liggen.

Onderzoekt aan de isoelektronische serie van helium stellen wij in hoofdstuk 7 voor. Wij tonen aan dat de KS-SCE methode in de anionen uit deze serie de binding van het tweede elektron aan de atoomkern sterk overschat, maar verbetering mogelijk is door correcties van de SCE lokale energiedichtheid. Deze correcties gaan uit van het homogene elektronen gas (HEG) en zijn makkelijk zelfconsistent op te lossen. Door de HEG correcties wordt een zelfinteractiefout geïntroduceerd, waarbij blijkt dat deze minder erg is dan bij traditionele dichtheidsfunctionalen.

Een samenvatting en vooruitzicht wordt in hoofdstuk 8 gegeven. Mogelijkheden ter voorkoming van de zelfinteractiefout in de HEG correcties van de SCE dichtheidsfunctionaal worden geïllustreerd en eerste resultaten voor de simulatie van ladingsoverdracht op lange afstand middels *time-dependent DFT* in en ééndimensionaal H_2 molecuul worden kort benadert.

Acknowledgment

The author thanks Robert van Leeuwen for sharing the program inverting the KS equations. I am grateful to Oleg Gritsenko and Łukaš Mentel for helpful assistance in developing the program for the calculation of the physical local energy density, and to Erik van Lenthe for his assistance with the ADF package. Evert Jan Baerends, Oleg Gritsenko, Angel Rubio, Michael Seidl, Giovanni Vignale, Robert van Leeuwen, Stefan Kurth, Klaas Giesbertz, Christian Mendl and Francesc Malet shall be acknowledged for many insightful discussions. For their warm hospitality in their research groups at the Pohang University of Science and Technology, South Korea, and the University of the Basque Country, San Sebastian, Spain, where parts of this work were done, I thank Evert Jan Baerends and Angel Rubio respectively.

Further I am indebted to Hester Zijstra, Mirko Franchini, Robert Rüger, Pier Philipsen and Evert Jan Baerends for the careful reading of the manuscript of this thesis. Ook wil ik graag Fritz van den Aerlenbeeck bedanken voor onze kritische discussies over het auteursrecht van dit werk.

For the nice atmosphere in our research department I would like to thank the members of the VU Theoretical Chemistry group. It was a great experience to join our forces in overcoming the struggles of the daily work life and in realizing our high aspirations of academia.

Paola, you were a splendid supervisor! Thanks a lot for your patience, honest criticism, professional and personal advice, and for all your trust. But the most grateful I am for the freedom you granted me, which made me truly enjoy my work.

Michael, dir danke ich für all die Liebe mit der du das Essen in der Kantine zubereitet hast. Ohne dich hätte es sicher nicht geschmeckt.

To all my friends in Amsterdam and allover the world a big shout out! I am a product of my environment and you are the bad influence my mother always warned me of.

Najwjeći džak pak słuše mojej swójbi, a wosebje mojimaj staršimaj. Hačrunješ so tu w dalojke cuzbje komdžu, sym wašu lubošć wsědnie čuw. Ja so wam džakwem za wšu podpěru, dobry rady a za wjele wjesoło hodžiny we waše zhromadnošći.

List of Publications

1. A. Mirtschink, M. Seidl and P. Gori-Giorgi
“*Energy densities in the strong-interaction limit of density functional theory*”
J. Chem. Theory Comput. **8**, 3097 (2012)
2. F. Malet, A. Mirtschink, J. C. Cremon, S. M. Reimann and P. Gori-Giorgi
“*Kohn-Sham density functional theory for quantum wires in arbitrary correlation regimes*”
Phys. Rev. B **87**, 115146 (2013)
3. A. Mirtschink, M. Seidl and P. Gori-Giorgi
“*The derivative discontinuity in the strong-interaction limit of density functional theory*”
Phys. Rev. Lett. **111**, 126402 (2013)
4. F. Malet, A. Mirtschink, K. J. H. Giesbertz, L. O. Wagner and P. Gori-Giorgi
“*Exchange-correlation functionals from the strongly interacting limit of DFT: Applications to model chemical systems*”
Phys. Chem. Chem. Phys. **16**, 14551 (2014)
5. A. Mirtschink, C. J. Umrigar, J. D. Morgan III and P. Gori-Giorgi
“*Energy density functionals from the strong-coupling limit applied to the anions of the He isoelectronic series*”
J. Chem. Phys. **140**, 18A532 (2014)
6. F. Malet, A. Mirtschink, K. J. H. Giesbertz and P. Gori-Giorgi
“*Density functional theory for strongly interacting electrons*”
in *Many-Electron Approaches in Physics, Chemistry and Mathematics*, 153, Springer International Publishing, Switzerland (2014)
7. F. Malet, A. Mirtschink, C. B. Mendl, J. Bjerlin, E. Karabulut, S. Reiman and P. Gori-Giorgi
“*Density functional theory for strongly correlated dipolar ultracold gases*”
to be submitted
8. A. Mirtschink, U. De Giovannini, A. Rubio and P. Gori-Giorgi
“*Pilot applications of the SCE functional for the long-range charge transfer description in adiabatic TDDFT*”
in preparation

9. G. Lani, A. Mirtschink, S. Kurth and P. Gori-Giorgi
“Time-dependent quantum transport within the strictly correlated electrons formalism”
in preparation
10. S. Vuckovic, L. O. Wagner, A. Mirtschink and P. Gori-Giorgi
“Hydrogen molecule dissociation curve in the strictly correlated regime of density functional theory”
in preparation

Bibliography

- [1] P. Hohenberg and W. Kohn, Phys. Rev. **136**, B 864 (1964).
- [2] D. R. Bowler and T. Miyazaki, J. Phys.: Condens. Matter **22**, 074207 (2012).
- [3] W. Kohn and L. J. Sham, Phys. Rev. A **140**, 1133 (1965).
- [4] U. von Barth and L. Hedin, J. Phys. C **5**, 1629 (1972).
- [5] F. Malet and P. Gori-Giorgi, Phys. Rev. Lett. **109**, 246402 (2012).
- [6] T. Helgaker et al., Chem. Rev. **112**, 543 (2012).
- [7] R. J. Bartlett, Ann. Rev. Phys. Chem. **32**, 359 (1981).
- [8] C. Angeli, M. Pastore and R. Cimiraglia, Theor. Chem. Acc. **117**, 743 (2007).
- [9] C. D. Sherrill and H. F. Schäfer III, Adv. Quantum Chem. **34**, 143 (1999).
- [10] P. G. Szalay, T. Müller, G. Gidofalvi, H. Lischka and R. Shepard, Chem. Rev. **112**, 108 (2012).
- [11] H. C. H. W. Lai and S. Shaik, J. Phys. Chem. **115**, 1721 (2011).
- [12] R. J. Bartlett and M. Musiał, Rev. Mod. Phys. **79**, 291 (2007).
- [13] D. I. Lyakh, M. Musiał, V. F. Lotrich and R. J. Bartlett, Chem. Rev. **112**, 182 (2012).
- [14] C. Háttig, W. Klopper, A. Köhn and D. P. Tew, Chem. Rev. **112**, 4 (2012).
- [15] L. Kong, F. A. Bischoff and E. F. Valeev, Chem. Rev. **112**, 75 (2012).
- [16] B. M. Austin, D. Y. Zubarev and W. A. Lester Jr., Chem. Rev. **112**, 263 (2012).
- [17] K. H. Marti and M. Reiher, Z. Phys. Chem. **224**, 583 (2010).
- [18] G. K. L. Chan and S. Sharma, Ann. Rev. Phys. Chem. **62**, 465 (2011).
- [19] A. J. Coleman and V. I. Yukalov, *Reduced Density Matrices: Coulson's Challenge*, Springer-Verlag, Berlin, 2000.
- [20] D. A. Mazziotti, Phys. Rev. Lett. **108**, 263002 (2012).
- [21] B. Verstichel, H. van Aggelen, D. Van Neck, P. W. Ayers and P. Bultinck, Phys. Rev. A **80**, 032508 (2009).
- [22] D. A. Mazziotti, Phys. Rev. Lett. **106**, 083001 (2011).
- [23] D. A. Mazziotti, Phys. Rev. A **81**, 062515 (2010).
- [24] A. M. Sand and D. A. Mazziotti, Comp. Theor. Chem. **1003**, 44 (2013).
- [25] F. Colmenero and C. Valdemoro, Phys. Rev. A **47**, 979 (1993).
- [26] H. . Nakatsuji and K. Yasuda, Phys. Rev. Lett. **76**, 1039 (1996).
- [27] D. A. Mazziotti, Chem. Rev. **112**, 224 (2012).
- [28] M. Higuchi and K. Higuchi, Comp. Theor. Chem. **1003**, 91 (2013).
- [29] P. W. Ayers and E. R. Davidson, Adv. Chem. Phys. **134**, 443 (2007).
- [30] M. E. Pistol, Phys. Rev. Lett. **449**, 208 (2007).

- [31] P. W. Ayers, J. Math. Phys.. **46**, 062107 (2005).
- [32] K. Higuchi and M. Higuchi, Phys. Rev. A **85**, 062508 (2012).
- [33] A. J. Coleman, Rev. Mod. Phys. **35**, 668 (1963).
- [34] M. Piris, Int. J. Quantum Chem. **113**, 620 (2013).
- [35] D. R. Rohr, K. Pernal, O. V. Gritsenko and E. J. Baerends, J. Chem. Phys. **129**, 164105 (2008).
- [36] L. M. Mentel, R. van Meer, O. V. Gritsenko and E. J. Baerends, J. Chem. Phys. **140**, 214105 (2014).
- [37] S. Sharma, J. K. Dewhurst, N. N. Lathiotakis and E. K. U. Gross, Phys. Rev. B **78**, 78 (2008).
- [38] A. D. Becke, J. Chem. Phys. **140**, 18A301 (2014).
- [39] R. M. Dreizler and E. K. U. Gross, *Density Functional Theory*, Springer-Verlag, Berlin, 1990.
- [40] M. Levy, Proc. Natl. Acad. Sci. U.S.A. **76**, 6062 (1979).
- [41] T. L. Gilbert, Phys. Rev. B **12**, 2111 (1975).
- [42] J. Harris and R. Jones, J. Phys. F **4**, 1170 (1974).
- [43] D. C. Langreth and J. P. Perdew, Solid State Commun. **17**, 1425 (1975).
- [44] O. Gunnarsson and B. I. Lundqvist, Phys. Rev. B **13**, 4274 (1976).
- [45] A. M. Teale, S. Coriani and T. Helgaker, J. Chem. Phys. **130**, 104111 (2009).
- [46] A. M. Teale, S. Coriani and T. Helgaker, J. Chem. Phys. **132**, 164115 (2010).
- [47] P. Dirac, Proc. Camb. Phil. Soc. **26**, 376 (1930).
- [48] J. C. Slater, Phys. Rev. **81**, 385 (1951).
- [49] S. J. Vosko, L. Wilk and M. Nusair, Can. J. Phys. **58**, 1200 (1980).
- [50] J. P. Perdew and Y. Wang, Phys. Rev. B **45**, 13244 (1992).
- [51] S.-K. Ma and K. A. Brueckner, Phys. Rev. **165**, 165 (1968).
- [52] J. P. Perdew, Phys. Rev. Lett. **55**, 1665 (1985).
- [53] J. P. Perdew and Y. Wang, Phys. Rev. B **33**, 8800 (1986).
- [54] Y. Wang, J. P. Perdew, J. A. Chevary, L. D. MacDonald and S. H. Vosko, Phys. Rev. A **41**, 78 (1990).
- [55] J. P. Perdew, K. Burke and Y. Wang, Phys. Rev. B **54**, 16533 (1996).
- [56] E. S. J. P. Perdew, L. A. Constantin and K. Burke, Phys. Rev. Lett. **97**, 223002 (2006).
- [57] D. C. Langreth and M. J. Mehl, Phys. Rev. B **28**, 1809 (1983).
- [58] J. P. Perdew, Phys. Rev. B **33**, 8822 (1986).
- [59] A. D. Becke, J. Chem. Phys. **84**, 4524 (1986).
- [60] A. D. Becke, Phys. Rev. A **38**, 3098 (1988).
- [61] C. Lee, W. Yang and R. G. Parr, Phys. Rev. B **37**, 785 (1988).
- [62] J. P. Perdew et al., Phys. Rev. B **46**, 6671 (1992).
- [63] J. P. Perdew, K. Burke and M. Ernzerhof, Phys. Rev. Lett. **77**, 3865 (1996).
- [64] A. D. Becke, Int. J. Quantum. Chem. **23**, 1915 (1983).
- [65] A. D. Becke, J. Chem. Phys. **109**, 2092 (1998).
- [66] A. D. Becke, The Journal of Chemical Physics **104** (1996).
- [67] E. I. Proynov, S. Sirois and D. H. Salahub, Int. J. Quantum Chem. **64**, 427 (1997).
- [68] T. van Voorhis and G. E. Scuseria, J. Chem. Phys. **109**, 400 (1998).
- [69] M. Filatov and W. Thiel, Phys. Rev. A **57**, 189 (1998).

- [70] J. B. Krieger, J. Chen, G. Iafrate and A. Savin, in *Electron Correlations and Materials Properties*, edited by A. Gonis and N. Kioussis, Plenum, New York, 1999.
- [71] J. P. Perdew, S. Kurth, A. Zupan and P. Blaha, Phys. Rev. Lett. **82**, 2544 (1999).
- [72] A. D. Becke and E. R. Johnson, J. Chem. Phys. **124**, 221101 (2006).
- [73] J. P. Perdew, A. Ruzsinszky, G. I. Csonka, L. A. Constantin and J. Sun, Phys. Rev. Lett. **103**, 026403 (2009).
- [74] J. B. Krieger, Y. Li and G. J. Iafrate, Phys. Lett. A **146**, 256 (1990).
- [75] S. Kümmel and J. P. Perdew, Phys. Rev. B **68**, 035103 (2003).
- [76] V. N. Staroverov, G. E. Scuseria and E. R. Davidson, J. Chem. Phys. **124**, 141103 (2006).
- [77] V. N. Staroverov, G. E. Scuseria and E. R. Davidson, J. Chem. Phys. **125**, 081104 (2006).
- [78] S. Kümmel and L. Kronik, Rev. Mod. Phys. **80**, 3 (2008).
- [79] F. Furche, Phys. Rev. B **64**, 195120 (2001).
- [80] H. V. Nguyen and S. de Gironcoli, Phys. Rev. B **79**, 205114 (2009).
- [81] A. D. Becke, J. Chem. Phys. **98**, 1372 (1993).
- [82] P. J. Stephens, F. J. Devlin, C. F. Chabalowski and M. J. Frisch, J. Phys. Chem. **98**, 11623 (1994).
- [83] J. P. Perdew, M. Ernzerhof and K. Burke, J. Chem. Phys. **105**, 9982 (1996).
- [84] S. Grimme, J. Chem. Phys. **124**, 034108 (2006).
- [85] K. Sharkas, J. Toulouse and A. Savin, J. Chem. Phys. **134**, 064113 (2011).
- [86] E. Brémond and C. Adamo, J. Chem. Phys. **135**, 024106 (2011).
- [87] J. Toulouse, K. Sharkas, E. Brémond and C. Adamo, J. Chem. Phys. **135**, 101102 (2011).
- [88] A. J. Cohen, P. Mori-Sánchez and W. Yang, Chem. Rev. **112**, 289 (2012).
- [89] K. Burke, J. Chem. Phys. **136**, 150901 (2012).
- [90] M. M. Pant and A. K. Rajagopal, Solid State Commun. **10**, 1157 (1972).
- [91] S. H. Vosko, J. P. Perdew and A. H. MacDonald, Phys. Rev. Lett. **35**, 1725 (1975).
- [92] W. Kohn and P. Vashishta, in *Theory of the Inhomogeneous Electron Gas*, edited by S. Lundqvist and N. H. March, page 79, Plenum, New York, 1983.
- [93] J. Sun, M. Marsman, A. Ruzsinszky, G. Kresse and J. P. Perdew, Phys. Rev. B **83**, 121410 (2011).
- [94] E. J. Baerends, O. V. Gritsenko and R. van Meer, Phys. Chem. Chem. Phys. **15**, 16408 (2013).
- [95] A. D. Becke, J. Chem. Phys. **98**, 5648 (1993).
- [96] J. Heyd, G. E. Scuseria and M. Ernzerhof, J. Chem. Phys. **118**, 8207 (2003).
- [97] K. Burke, M. Ernzerhof and J. P. Perdew, Chem. Phys. Lett. **265**, 115 (1997).
- [98] A. Görling and M. Levy, Phys. Rev. B **47**, 13105 (1993).
- [99] M. Ernzerhof, Chem. Phys. Lett. **263**, 499 (1996).
- [100] P. Mori-Sánchez, A. J. Cohen and W. T. Yang, J. Chem. Phys. **124**, 091102 (2006).
- [101] M. J. G. Peach, A. M. Teale and D. J. Tozer, J. Chem. Phys. **126**, 244104 (2007).
- [102] P. Gori-Giorgi, G. Vignale and M. Seidl, J. Chem. Theory Comput. **5**, 743 (2009).
- [103] M. Seidl, Phys. Rev. A **60**, 4387 (1999).
- [104] M. Seidl, J. P. Perdew and M. Levy, Phys. Rev. A **59**, 51 (1999).
- [105] M. Seidl, J. P. Perdew and S. Kurth, Phys. Rev. A **62**, 012502 (2000).
- [106] H. Stoll and A. Savin, in *Density Functional Methods in Physics*, page 177, Plenum, New York, 1985.

- [107] A. Savin, in *Recent Developments and Applications of Modern Density Functional Theory*, edited by J. M. Seminario, page 327, Elsevier, Amsterdam, 1996.
- [108] W. Yang, *J. Chem. Phys.* **109**, 10107 (1998).
- [109] A. M. Teale, S. Coriani and T. Helgaker, *J. Chem. Phys.* **133**, 164112 (2010).
- [110] T. Leininger, H. Stoll, H.-J. Werner and A. Savin, *Chem. Phys. Lett.* **275**, 151 (1997).
- [111] R. Pollet, A. Savin, T. Leininger and H. Stoll, *J. Chem. Phys.* **116**, 1250 (2002).
- [112] J. Toulouse, P. Gori-Giorgi and A. Savin, *Theor. Chem. Acc.* **114**, 305 (2005).
- [113] E. Fromager, J. Toulouse and H. J. A. Jensen, *J. Chem. Phys.* **126**, 074111 (2007).
- [114] A. Stoyanova, A. M. Teale, J. Toulouse, T. Helgaker and E. Fromager, *J. Chem. Phys.* **139**, 134113 (2013).
- [115] A. Savin, *J. Chem. Phys.* **140**, 18A509 (2014).
- [116] P. Gori-Giorgi and A. Savin, *Int. J. Quantum Chem.* **109**, 2410 (2009).
- [117] M. Seidl, P. Gori-Giorgi and A. Savin, *Phys. Rev. A* **75**, 042511 (2007).
- [118] P. Gori-Giorgi and M. Seidl, *Phys. Chem. Chem. Phys.* **12**, 14405 (2010).
- [119] E. Räsänen, M. Seidl and P. Gori-Giorgi, *Phys. Rev. B* **83**, 195111 (2011).
- [120] G. Buttazzo, L. De Pascale and P. Gori-Giorgi, *Phys. Rev. A* **85**, 062502 (2012).
- [121] C. Cotar, G. Friesecke and C. Klüppelberg, *Comm. Pure Appl. Math.* **66**, 548 (2013).
- [122] G. Friesecke, C. B. Mendl, B. Pass, C. Cotar and C. Klüppelberg, *J. Chem. Phys.* **139**, 164109 (2013).
- [123] C. B. Mendl and L. Lin, *Phys. Rev. B* **87**, 125106 (2013).
- [124] C. B. M. H. Chen, G. Friesecke, arXiv:1405.7026 (2014).
- [125] A. M. S. Vuckovic, L. O. Wagner and P. Gori-Giorgi, in preparation (2014).
- [126] P. Gori-Giorgi, M. Seidl and G. Vignale, *Phys. Rev. Lett.* **103**, 166402 (2009).
- [127] M. Colombo, L. De Pascale and S. Di Marino, *Canad. J. Math.* **11** (2014).
- [128] M. Seidl, J. P. Perdew and S. Kurth, *Phys. Rev. Lett.* **84**, 5070 (2000).
- [129] L. O. Wagner and P. Gori-Giorgi, arXiv:1408.5426 (2014).
- [130] P. Gori-Giorgi and A. Savin, *J. Phys.: Conf. Ser.* **117**, 012017 (2008).
- [131] A. Savin, *Chem. Phys.* **356**, 91 (2009).
- [132] W. Yang, Y. Zhang and P. W. Ayers, *Phys. Rev. Lett.* **84**, 5172 (2000).
- [133] A. J. Cohen, P. Mori-Sánchez and W. T. Yang, *Science* **321**, 792 (2008).
- [134] A. J. Cohen, P. Mori-Sánchez and W. T. Yang, *J. Chem. Phys.* **129**, 121104 (2008).
- [135] P. W. Ayers, *J. Math. Chem.* **43**, 285 (2008).
- [136] K. Burke, F. G. Cruz and K.-C. Lam, *J. Chem. Phys.* **109**, 8161 (1998).
- [137] L. Cohen, *J. Chem. Phys.* **70**, 788 (1979).
- [138] L. Cohen, *J. Chem. Phys.* **80**, 4277 (1996).
- [139] L. Cohen, *Phys. Lett. A* **212**, 315 (1996).
- [140] P. Ayers, R. G. Parr and A. Nagy, *Int. J. Quantum Chem.* **90**, 309 (2002).
- [141] A. D. Becke, *J. Chem. Phys.* **122**, 064101 (2005).
- [142] A. D. Becke and E. R. Johnson, *J. Chem. Phys.* **127**, 124108 (2007).
- [143] J. P. Perdew, , V. N. Staroverov, J. Tao and G. E. Scuseria, *Phys. Rev. A* **78**, 052513 (2008).
- [144] M. A. Buijse, E. J. Baerends and J. G. Snijders, *Phys. Rev. A* **40**, 4190 (1989).
- [145] A. D. Becke and M. R. Roussel, *Phys. Rev. A* **39**, 3761 (1989).
- [146] Y. Wang and R. G. Parr, *Phys. Rev. A* **47**, 1591 (1993).

- [147] R. van Leeuwen and E. J. Baerends, Phys. Rev. A **49**, 2421 (1994).
- [148] O. V. Gritsenko, R. van Leeuwen and E. J. Baerends, Phys. Rev. A **52**, 1870 (1995).
- [149] K. Peirs, D. van Neck and M. Waroquier, Phys. Rev. A **67**, 012505 (2003).
- [150] E. S. Kadantsev and M. J. Scott, Phys. Rev. A **69**, 012502 (2004).
- [151] R. Astala and M. J. Scott, Phys. Rev. B **73**, 115127 (2006).
- [152] E. H. Lieb, Int. J. Quantum. Chem. **24**, 24 (1983).
- [153] F. Colonna and A. Savin, J. Chem. Phys. **110**, 2828 (1999).
- [154] M. W. Schmidt et al., J. Comput. Chem. **14**, 1347 (1993).
- [155] Wolfram Research, Inc., Mathematica 9.0, Champaign, Illinois, 2012.
- [156] M. Taut, Phys. Rev. A **48**, 3561 (1993).
- [157] M. Ernzerhof, K. Burke and J. P. Perdew, J. Chem. Phys. **105**, 2798 (1996).
- [158] D. E. Freund, B. D. Huxtable and J. D. Morgan, Phys. Rev. A **29**, 980 (1984).
- [159] A. I. Al-Sharif, R. Resta and C. J. Umrigar, Phys. Rev. A **57**, 2466 (1998).
- [160] J. Toulouse, private communication. The sphericalized densities of the B and C atoms were obtained from variational Monte Carlo using accurate optimized wavefunctions as described in refs. [?, ?].
- [161] E. H. Lieb, Phys. Lett. **70A**, 444 (1979).
- [162] E. H. Lieb and S. Oxford, Int. J. Quantum. Chem. **19**, 427 (1981).
- [163] G. K.-L. Chan and N. C. Handy, Phys. Rev. A **59**, 3075 (1999).
- [164] J. P. Perdew, in *Electronic Structure of Solids '91*, edited by P. Ziesche and H. Eschrig, Akademie Verlag, Berlin, 1991.
- [165] E. Räsänen, S. Pittalis, K. Capelle and C. R. Proetto, Phys. Rev. Lett. **102**, 206406 (2009).
- [166] M. M. Odashima and K. Capelle, J. Chem. Phys. **127**, 05416 (2007).
- [167] M. Levy and J. P. Perdew, Phys. Rev. B **48**, 11638 (1993).
- [168] M. M. Odashima and K. Capelle, Phys. Rev. A **79**, 062515 (2009).
- [169] R. Haunschild, M. M. Odashima, G. E. Scuseria, J. P. Perdew and K. Capelle, J. Chem. Phys. **136**, 184102 (2012).
- [170] Y. Zhang and W. Yang, Phys. Rev. Lett. **80**, 890 (1998).
- [171] N. Helbig, I. V. Tokatly and A. Rubio, J. Chem. Phys. **131**, 224105 (2009).
- [172] P. Gori-Giorgi and J. P. Perdew, Phys. Rev. B **64**, 155102 (2001).
- [173] B. Davoudi, M. Polini, R. Asgari and M. P. Tosi, Phys. Rev. B **66**, 075110 (2002).
- [174] P. Gori-Giorgi and A. Savin, Phys. Rev. A **71**, 032513 (2005).
- [175] C.-O. Almbladh and U. von Barth, Phys. Rev. B **31**, 3231 (1985).
- [176] M. Levy, J. P. Perdew and V. Sahni, Phys. Rev. A **30**, 2745 (1984).
- [177] M. Levy and J. P. Perdew, Phys. Rev. A **32**, 2010 (1985).
- [178] Z. F. Liu and K. Burke, J. Chem. Phys. **131**, 124124 (2009).
- [179] P. Gori-Giorgi, private communication.
- [180] E. P. Wigner, Phys. Rev. **46**, 1002 (1934).
- [181] O. M. Auslaender et al., Science (New York, N.Y.) **308**, 88 (2005).
- [182] L. H. Kristinsdottir et al., Phys. Rev. B **83**, 041101 (2011).
- [183] N. Ziani, F. Cavaliere and M. Sassetti, Phys. Rev. B **86**, 125451 (2012).
- [184] V. V. Deshpande and M. Bockrath, Nature Phys. **4**, 314 (2008).
- [185] A. Secchi and M. Rontani, Phys. Rev. B **82**, 035417 (2010).
- [186] A. Secchi and M. Rontani, Phys. Rev. B **85**, 121410 (2012).

- [187] V. V. Deshpande, M. Bockrath, L. I. Glazman and A. Yacoby, *Nature (London)* **464**, 209 (2010).
- [188] J. M. Taylor and T. Calarco, *Phys. Rev. A* **78**, 062331 (2008).
- [189] C. E. Creffield, W. Hausler, J. H. Jefferson and S. Sarkar, *Phys. Rev. B* **59**, 10719 (1999).
- [190] R. Egger, W. Hausler, C. H. Mak and H. Grabert, *Phys. Rev. Lett.* **82**, 3320 (1999).
- [191] C. Yannouleas and U. Landman, *Phys. Rev. Lett.* **82**, 5325 (1999).
- [192] S. Reimann, M. Koskinen and M. Manninen, *Phys. Rev. B* **62**, 8108 (2000).
- [193] A. V. Filinov, M. Bonitz and Y. E. Lozovik, *Phys. Rev. Lett.* **86**, 3851 (2001).
- [194] A. Ghosal, A. D. Guclu, C. J. Umrigar, D. Ullmo and H. U. Baranger, *Phys. Rev. B* **76**, 085341 (2007).
- [195] F. Cavaliere, U. D. Giovannini, M. Sassetti and B. Kramer, *New J. Phys.* **11**, 123004 (2009).
- [196] C. Ellenberger et al., *Phys. Rev. Lett.* **96**, 126806 (2006).
- [197] A. Ghosal, A. D. Guclu, C. J. Umrigar, D. Ullmo and H. U. Baranger, *Nature Phys.* **2**, 336 (2006).
- [198] A. D. Guclu, A. Ghosal, C. J. Umrigar and H. U. Baranger, *Phys. Rev. B* **77**, 041301 (2008).
- [199] L. Shulenburger, M. Casula, G. Senatore and R. M. Martin, *Phys. Rev. B* **78**, 165303 (2008).
- [200] E. Stoudenmire, L. O. Wagner, S. R. White and K. Burke, *Phys. Rev. Lett.* **109**, 056402 (2012).
- [201] V. I. Anisimov, J. Zaanen and O. K. Andersen, *Phys. Rev. B* **44**, 943 (1991).
- [202] M. Grüning, O. V. Gritsenko and E. J. Baerends, *J. Chem. Phys.* **118**, 7183 (2003).
- [203] M. Borgh et al., *Int. J. Quantum Chem.* **105**, 817 (2005).
- [204] S. H. Abedinpour, M. Polini, G. Xianlong and M. P. Tosi, *Eur. Phys. J. B* **56**, 127 (2007).
- [205] J. P. Bergfield, Z.-F. Liu, K. Burke and C. A. Stafford, *Phys. Rev. Lett.* **108**, 066801 (2012).
- [206] C. Verdozzi, *Phys. Rev. Lett.* **101**, 166401 (2008).
- [207] D. G. Tempel, T. J. Martínez and N. T. Maitra, *J. Chem. Theory Comput.* **5**, 770 (2009).
- [208] S. Kurth, G. Stefanucci, E. Khosravi, C. Verdozzi and E. K. U. Gross, *Phys. Rev. Lett.* **104**, 236801 (2010).
- [209] G. Stefanucci and S. Kurth, *Phys. Rev. Lett.* **107**, 216401 (2011).
- [210] D. Karlsson, A. Privitera and C. Verdozzi, *Phys. Rev. Lett.* **106**, 166401 (2011).
- [211] J. D. Ramsden and R. W. Godby, *Phys. Rev. Lett.* **109**, 036402 (2012).
- [212] C. Filippi, C. J. Umrigar and M. Taut, *J. Chem. Phys.* **100**, 1290 (1994).
- [213] O. V. Gritsenko, R. van Leeuwen and E. J. Baerends, *J. Chem. Phys.* **104**, 8535 (1996).
- [214] P. Mori-Sánchez, A. J. Cohen and W. Yang, *Phys. Rev. Lett.* **102**, 066403 (2009).
- [215] D. Vieira, *Phys. Rev. B* **86**, 075132 (2012).
- [216] S. Bednarek, B. Szafran, T. Chwiej and J. Adamowski, *Phys. Rev. B* **68**, 045328 (2003).
- [217] L. Calmels and A. Gold, *Phys. Rev. B* **56**, 1762 (1997).
- [218] M. Rontani, C. Cavazzoni, D. Bellucci and G. Goldoni, *J. Chem. Phys.* **124**, 124102 (2006).
- [219] S. M. Reimann and M. Manninen, *Rev. Mod. Phys.* **74**, 1283 (2002).
- [220] G. F. Giuliani and G. Vignale, *Quantum Theory of the Electron Liquid*, Cambridge University Press, New York, 2005.

- [221] M. Casula, S. Sorella and G. Senatore, Phys. Rev. B **74**, 245427 (2006).
- [222] D. Vieira and K. Capelle, J. Chem. Theory Comput. **6**, 3319 (2010).
- [223] D. Vieira, arXiv:1212.3241 .
- [224] L. O. Wagner, E. M. Stoudenmire, K. Burke and S. R. White, Phys. Chem. Chem. Phys. **14**, 8581 (2012).
- [225] N. Helbig et al., Phys. Rev. A **83**, 032503 (2011).
- [226] F. Malet, A. Mirtschink, J. C. Cremon, S. M. Reimann and P. Gori-Giorgi, Phys. Rev. B **87**, 115146 (2013).
- [227] C. B. Mendl, F. Malet and P. Gori-Giorgi, Phys. Rev. B **89**, 125106 (2014).
- [228] J. P. Perdew, R. G. Parr, M. Levy and J. L. Balduz, Phys. Rev. Lett. **49**, 1691 (1982).
- [229] O. Gunnarsson and K. Schönhammer, Phys. Rev. Lett. **56**, 1968 (1986).
- [230] R. W. Godby, M. Schlüter and L. J. Sham, Phys. Rev. Lett. **56**, 2415 (1986).
- [231] L. Kleinman, Phys. Rev. B **56**, 12042 (1997).
- [232] J. P. Perdew and M. Levy, Phys. Rev. B **56**, 16021 (1997).
- [233] L. Kleinman, Phys. Rev. B **56**, 16029 (1997).
- [234] F. E. Zahariev and Y. A. Wang, Phys. Rev. A. **70**, 042503 (2004).
- [235] M. Grüning, A. Marini and A. Rubio, Phys. Rev. B **74**, 161103 (2006).
- [236] E. Sagvolden and J. P. Perdew, Phys. Rev. A **77**, 012517 (2008).
- [237] V. Broasco, Z. Ying and J. Lorenzana, Scientific Reports **3**, 2172 (2013).
- [238] J. P. Perdew and M. Levy, Phys. Rev. Lett. **51**, 1884 (1983).
- [239] L. J. Sham and M. Schlüter, Phys. Rev. Lett. **51**, 1888 (1983).
- [240] J. P. Perdew, Int. J. Quantum Chem. Symp. **19**, 497 (1986).
- [241] O. Gritsenko and E. J. Baerends, J. Chem. Phys. **121**, 655 (2005).
- [242] D. Vieira, K. Capelle and C. A. Ullrich, Phys. Chem. Chem. Phys. **11**, 4647 (2009).
- [243] M. Hellgren and E. K. U. Gross, Phys. Rev. A **85**, 022514 (2012).
- [244] C. Toher, A. Filippetti, S. Sanvito and K. Burke, Phys. Rev. Lett. **95**, 146402 (2005).
- [245] K. Capelle, M. Borgh, K. Kärkkäinen and S. M. Reimann, Phys. Rev. Lett. **99**, 010402 (2007).
- [246] S. Kurth and G. Stefanucci, Phys. Rev. Lett. **111**, 030601 (2013).
- [247] I. Dabo et al., Phys. Rev. B **82**, 115121 (2010).
- [248] S. Refaelly-Abramson et al., Phys. Rev. Lett. **109**, 226405 (2012).
- [249] L. Kronik, T. Stein, S. Refaelly-Abramson and R. Baer, J. Chem. Theory Comput. **8**, 1515 (2012).
- [250] E. Kraisler and L. Kronik, Phys. Rev. Lett. **110**, 126403 (2013).
- [251] J. P. Perdew et al., Phys. Rev. A **76**, 040501 (2007).
- [252] J. F. Janak, Phys. Rev. B **18**, 7165 (1978).
- [253] O. A. Vydrov, G. E. Scuseria and J. P. Perdew, J. Chem. Phys. **126**, 154109 (2007).
- [254] A. J. Cohen, P. Mori-Sánchez and W. Yang, Phys. Rev. B **77**, 115123 (2008).
- [255] A. P. Gaiduk, D. S. Firaha and V. N. Staroverov, Phys. Rev. Lett. **108**, 253005 (2012).
- [256] M. Taut, A. Ernst and H. Eschrig, J. Phys. B: At. Mol. Opt. Phys. **31**, 2689 (1998).
- [257] J. Cioslowski and K. Pernal, J. Chem. Phys. **113**, 8434 (2000).
- [258] G. Lani, A. Mirtschink, S. Kurth and P. Gori-Giorgi, in preparation .
- [259] A. Mirtschink, U. De Giovannini, A. Rubio and P. Gori-Giorgi, in preparation .
- [260] N. A. Lima, M. F. Silva, L. N. Oliveira and K. Capelle, Phys. Rev. Lett. **90**, 146402 (2003).

- [261] J. D. Baker, D. E. Freund, R. N. Hill and J. D. Morgan III, Phys. Rev. A **41**, 1247 (1990).
- [262] J. M. Galbraith and H. F. Schäfer III, J. Chem. Phys. **105**, 862 (1996).
- [263] N. Rösch and S. B. Trickey, J. Chem. Phys. **106**, 8940 (1997).
- [264] H. Hotop and W. C. Lineberger, J. Chem. Phys. Ref. Data **4**, 539 (1975).
- [265] J. P. Perdew, J. Tao, V. N. Staroverov and G. E. Scuseria, J. Chem. Phys. **120**, 6898 (2004).
- [266] C. J. Umrigar and X. Gonze, Phys. Rev. A **50**, 3827 (1994).
- [267] K. Frankowski and C. L. Pekeris, Phys. Rev. **146**, 46 (1966).
- [268] K. Frankowski, Phys. Rev. **160**, 1 (1967).
- [269] V. A. Fock, Izv. Akad. Nauk SSSR, Ser. Fiz. **18**, 161 (1954).
- [270] V. A. Fock, Det Kongelige Norske Videnskabers Selskabs Forhandlinger **31**, 138 (1958).
- [271] J. D. Morgan III, Theor. Chim. Acta **69**, 181 (1986).
- [272] J. Katriel and E. R. Davidson, Proc. Natl. Acad. Sci. USA **77**, 4403 (1980).
- [273] M. Hoffmann-Ostenhof, T. Hoffmann-Ostenhof and B. Simon, J. Phys. A **16**, 1125 (1983).
- [274] Z. Qian, Phys. Rev. B **75**, 193104 (2007).
- [275] Z. Qian and V. Sahni, Phys. Rev. A **75**, 032517 (2007).
- [276] G. te Velde et al., J. Comp. Chem. **22**, 931 (2001).
- [277] C. F. Guerra, J. G. Snijders, G. te Velde and E. J. Baerends, Theor. Chem. Acc. **99**, 391 (1998).
- [278] ADF2013, SCM, Theoretical Chemistry, Vrije Universiteit Amsterdam, The Netherlands, www.scm.com.
- [279] J. Tao, J. P. Perdew, V. N. Staroverov and G. E. Scuseria, Phys. Rev. Lett. **91**, 146401 (2003).
- [280] D. P. Chong, E. van Lenthe, S. J. A. van Gisbergen and E. J. Baerends, J. Comp. Chem. **25**, 1030 (2004).
- [281] M.-C. Kim, E. Sim and K. Burke, Phys. Rev. Lett. **111**, 073003 (2013).
- [282] D. Lee, F. Furche and K. Burke, J. Phys. Chem. Lett. **1**, 2124 (2010).
- [283] M.-C. Kim, E. Sim and K. Burke, J. Chem. Phys. **134**, 171103 (2011).
- [284] O. V. Gritsenko, R. van Leeuwen and E. J. Baerends, J. Chem. Phys. **104**, 8535 (1997).
- [285] A. Mirtschink, M. Seidl and P. Gori-Giorgi, Phys. Rev. Lett. **111**, 126402 (2013).
- [286] F. Malet, A. Mirtschink, K. J. H. Giesbertz, L. O. Wagner and P. Gori-Giorgi, Phys. Chem. Chem. Phys. **16**, 14551 (2014).
- [287] A. Mirtschink, M. Seidl and P. Gori-Giorgi, J. Chem. Theory Comput. **8**, 3097 (2012).
- [288] P. Bleiziffer, A. Heßelmann, C. J. Umrigar and A. Görling, Phys. Rev. A **88**, 042513 (2013).
- [289] E. P. Wigner, Trans. Faraday Soc. **34**, 678 (1938).
- [290] L. Onsager, J. Phys. Chem. **43**, 189 (1939).
- [291] E. H. Lieb and H. Narhofer, J. Stat. Phys. **12**, 291 (1975).